Dissertation

Submitted to the

Combined Faculty of Natural Sciences and Mathematics

Of the Ruprecht – Karl – University Heidelberg, Germany

For the degree of

Doctor of Natural Sciences

Presented by

M.Sc. Pavle Boskovic

Born in Jagodina, Serbia

Oral examination: 01.03.2023

THE DUAL ROLE OF BCAT1 IN GLIOBLASTOMA: A METABOLIC ENZYME WITH A TWIST

Referees:

Prof. Dr. Peter Angel

Prof. Dr. Peter Lichter

The work and results of the following dissertation were performed and obtained from October 2018 until November 2022 under the supervision of Dr Bernhard Radlwimmer and Prof Dr Peter Lichter in the Division of Molecular Genetics at the German Cancer Research Center (DKFZ), Heidelberg, Germany.

Declaration

I hereby declare that I have written the submitted dissertation “The Dual Role of BCAT1 in Glioblastoma: a Metabolic Enzyme With a Twist” myself and in the process have not used any other sources than those indicated.

I hereby declare that I have not applied to be examined at any other institution, nor have I used the dissertation in this or any other form at any other institution as an examination paper, nor submitted it to any other faculty as a dissertation

_____

Pavle Boskovic

Summary

Glioblastoma is the most common central nervous system malignancy in adults with a very poor outcome due to its invasiveness, intratumoral heterogeneity, poorly differentiated features, and immunosuppressive microenvironment. Previous work suggested that Branched-chain amino acid transaminase 1 (BCAT1) is often highly expressed in glioblastoma and multiple modes of action for its oncogenic potential have been proposed. In this thesis, I focus on investigating a novel role of BCAT1 in maintaining mitotic fidelity, and how it impacts the cellular plasticity of glioblastoma cells and the tumor immune microenvironment.

We have found that BCAT1 localizes to the key mitotic structures during cell division as well as in the nucleus during interphase. Using co-immunoprecipitation mass spectrometry, I showed that BCAT1 associates with many components of the mitotic spindle and the kinetochore during mitosis. Through proteomic and phosphoproteomic analysis I showed that the central kinases of the spindle assembly checkpoint, TTK and AURKB, showed significantly decreased activity during mitosis upon BCAT1-KO.

By analyzing the expression patterns of human and mouse glioblastoma cells and tumor samples of the TCGA-GBM cohort, I found that BCAT1 expression is strongly correlated with the cellular state of glioblastoma, with high expression being indicative of a mesenchymal phenotype and low or no expression with a neuronal cellular state. I further confirmed these observations through a series of differentiation experiments of murine glioblastoma stem cells where the Bcat1-KO showed a much higher tendency towards differentiation and lacked the plasticity of the control cells. Consistently, *in vivo* findings corroborated these results with a complete lack of tumor outgrowth of the Bcat1-KO cells in immunocompetent mice, and a significant growth delay in immunodeficient mice.

Lastly, I explored the impact of tumor BCAT1 expression on the immune microenvironment. I found that low BCAT1 expression was associated with a higher immune infiltration of both myeloid and T-cells in human tumor samples. These findings were additionally confirmed in *in vivo* experiments in immunocompetent mice. Furthermore, Bcat1-KO tumors did develop in the immunodeficient NSG and Rag2KO mouse models, highlighting the importance of the immune compartment in completely abrogating their growth.

In conclusion, the data presented here confirm the novel role of BCAT1 in maintaining mitotic fidelity of glioblastoma cells. Furthermore, it shows that BCAT1 expression is necessary for maintaining the plasticity of glioblastoma cells and an immunosuppressive tumor microenvironment.

Zusammenfassung

Das Glioblastom ist die häufigste bösartige Erkrankung des zentralen Nervensystems bei Erwachsenen und hat aufgrund der Invasivität, intratumoralen Heterogenität, geringen Differenzierung und immunsuppressiven Mikroumgebung eine sehr schlechte Prognose. Frühere Arbeiten haben gezeigt, dass die Branched-Chain Amino Acid Transaminase 1 (BCAT1) in Glioblastomen häufig stark exprimiert wird, und es wurden mehrere Wirkmechanismen für ihr onkogenes Potenzial vorgeschlagen. In dieser Arbeit beschreibe ich eine neuartige Rolle von BCAT1 in der Aufrechterhaltung der mitotischen Genauigkeit sowie in der Beeinflussung der zellulären Plastizität von Glioblastomzellen und der immunologische Mikroumgebung des Tumors.

Wir haben herausgefunden, dass BCAT1 während der Zellteilung an den mitotischen Schlüsselstrukturen und während der Interphase im Zellkern lokalisiert ist. Mit Hilfe von Co-Immunpräzipitation-Massenspektrometrie habe ich gezeigt, dass BCAT1 während der Mitose mit vielen Komponenten des mitotischen Spindelapparats und des Kinetochors assoziiert ist. Durch proteomische und phosphoproteomische Analysen konnte ich zeigen, dass die Spindelaufbaukontrollpunkts, TTK und AURKB, zeigten bei BCAT1-KO eine deutlich verringerte Aktivität während der Mitose. Diese in silico-Ergebnisse wurden von unserer Gruppe weiter validiert.

Durch die Analyse der Expressionsmuster von humanen und murinen Glioblastomzellen und Tumorproben der TCGA-GBM-Kohorte habe ich herausgefunden, dass die BCAT1-Expression stark mit dem zellulären Zustand des Glioblastoms korreliert, wobei eine hohe Expression auf einen mesenchymalen Phänotyp und eine niedrige oder fehlende Expression auf einen neuronalen zellulären Zustand hindeutet. Ich bestätigte diese Beobachtungen durch Differenzierungsexperimente mit murinen Glioblastom-Stammzellen , bei denen die Bcat1-KO-Zellen eine stärkere Tendenz zur Differenzierung zeigten und die Plastizität, die in Kontrollzellen beobachtet wurde, verloren ging. In vivo-Befunde bestätigten diese Ergebnisse, denn die Bcat1-KO-Zellen entwickelten keine Tumore in immunkompetenten Mäusen, und die Tumore in immundefizienten Mäusen wuchsen deutlich langsamer.

Schließlich untersuchte ich die Auswirkungen der BCAT1-Expression des Tumors auf die immunologische Mikroumgebung. Ich fand heraus, dass eine niedrige BCAT1-Expression mit einer höheren Immuninfiltration sowohl von myeloischen als auch von T-Zellen in menschlichen Tumorproben verbunden war. Diese Ergebnisse wurden zusätzlich in invivo-Experimenten an immunkompetenten Mäusen bestätigt. Darüber hinaus entwickelten sich Bcat1-KO-Tumore auch in den immundefizienten NSG- und Rag2KO-Mausmodellen, was die Bedeutung des Immunsystems für die vollständige Unterdrückung ihres Wachstums verdeutlicht.

Zusammenfassend bestätigen die hier vorgestellten Daten eine neue Rolle von BCAT1 bei der Aufrechterhaltung der mitotischen Prozesse von Glioblastomzellen. Außerdem zeigen sie, dass die BCAT1-Expression für die Aufrechterhaltung der Plastizität von Glioblastomzellen und einer immunsuppressiven Tumormikroumgebung notwendig ist.

List of Figures

List of Tables

Abbreviations

2-HG	2-hydroxygkutarate
a-KG	alpha – ketoglutarate
AML	acute myeloid leukemia
ANOVA	analysis of variance
APC	anaphase promoting complex
ATR	ataxia telangiectasia mutated and Rad3-related
AURKA	Aurora kinase A
AURKB	Aurora kinase B
BCAA	branched-chain amino acid
BCAT	branched chain amino acid transaminase
BCKA	branched chain keto acid
BER	base excision repair
BKO	BCAT1-knockout
BP	biological process
BSA	bovine serum albumin
CC	cellular component
CD	cluster of differentiation
CFP	cyan fluorescent protein
CNS	central nervous system
CPM	counts per million
CRISPR	clustered regularly interspaced short palindromic repeats
CSF	colony-stimulating factor
DAPI	4′,6-diamidino-2-phenylindole
DKFZ	Deutsches Krebsforschungszentrum
DMEM	Dulbecco's Modified Eagle Medium
DMSO	dimethyl sulfoxide
DNA	Deoxyribonucleic acid
DNMT	DNA methyl transferase
ECM	extracellular matrix
EDTA	ethylenediamineteraacetic acid
EGF	epidermal growth factor
EGFR	epidermal growth factor receptor
FACS	fluorescently activated cell sorting
FCS	fetal calf serum
FGF	fibroblast growth factor
GAM	glioma-associated myeloid cell

GFP	green fluorescent protein
GO	gene ontology
GSEA	gene set enrichment analysis
GSH	glutathione
HRP	horseradish peroxidase
IDH	isocytate dehydrogenase
IF	immunofluorescent
IL	interleukin
IQR	Interquartile range
IVIS	*in vivo* imaging system
KO	knockout
LB	lysogeny broth
LC-MS	liquid chromatography – mass spectrometry
LCPM	log-counts per million
LFQ	label free quantification
LUC	luciferase
MDS	multidimensional scaling
MF	molecular function
MGMT	O-6-methylguanine-DNA methyltransferase
MYC	MYC Proto-Oncogene, BHLH Transcription Factor
NES	normalized enrichment score
NOD/SCID	non-diabetic/severe combined immunodeficient
NSC	neural stem cell
NSG	non-diabetic/severe combined immunodeficient gamma
NT	non-targeting
OCT	optimal cutting temperature
OPC	oligodendrocyte precursor cell
PAGE	polyacrylamide gel electrophoresis
PBMC	peripheral blood monocytic cells
PCA	principal component analysis
PCR	polymerase chain reaction
PDAC	pancreatic ductal adenocarcinoma
PDGFR	platelet-derived growth factor receptor
PEI	polyethylenimin
PFA	paraformaldehyde
PGK	phosphoglycerate kinase
PLK1	polo-like kinase 1

PTEN	phosphatase and tensin homolog
PTM	post-translational modification
RAS	rat sarcoma virus
RNA	ribonucleic acid
ROS	reactive oxygen species
RTK	receptor tyrosine kinase
SAC	spindle assembly checkpoint
SAM	s-adenosylmethionine
SC	stem cell
SDS	sodium dodecyl sulfate
SGZ	subgranular zone
SVZ	subventricular zone
TBS	tris-buffer saline
TCGA-GBM	The Cancer Genome Atlas Project – Glioblastoma multiforme (the name of the dataset is used in full even though by new convention glioblastoma is no longer referred to as glioblastoma multiforme)
TDG	Thymine-DNA glycosylase
TET	ten-eleven translocation
TGF	tumor growth factor
TME	tumor microenvironment
TMZ	temozolomide
US	United States
UV	ultraviolet
WB	western blot
WHO	World Health Organization
WT	wildtype

Table of Contents

1. Introduction

1.1. Glioblastoma

1.1.1. Clinical and epidemiological aspects

Glioblastoma is a malignant tumor of the central nervous system (CNS) localized within the brain. According to the recent WHO (World Health Organization) classification of CNS tumors, glioblastomas are characterized as stage IV primary gliomas with a wildtype isocitrate dehydrogenase 1 (IDH1) gene (IDH^{WT}) (Louis et al. 2021).

Glioblastoma accounts for almost 50% of all CNS malignant tumors diagnosed in adults with an incidence of 3.2 per 100.000 within the US population and a mean age of diagnosis of 64 (Ostrom et al. 2013). It has a similar impact in both males and females, with a slightly higher incidence in men (Ostrom et al. 2018).

Glioblastomas are typically diagnosed through brain imaging after the onset of symptoms, at which point tumor development is usually advanced. Further characterization of the tumors and a final diagnosis is performed through molecular testing for markers such as epidermal growth factor receptor (EGFR) amplification, chromosome 7 gain and chromosome 10 loss, and others (Melhem et al. 2022). Even in case of the lack of typical histological features, a diffuse IDH^{WT} glioma can be classified as a glioblastoma by means of detailed molecular characterization (Brat et al. 2018).

Glioblastoma is an incurable malignancy with an extremely poor prognosis. Regardless of the mode of treatment, the 5-year survival rate post diagnosis remains below 5%, with a median survival of only 15 months (Tamimi and Juweid 2017; Koshy et al. 2012).

1.1.2. Treatment strategies and novel therapies

Currently, the first line treatment for glioblastoma entails an aggressive, trimodal approach of surgical resection, temozolomide (TMZ) administration and radiation. Maximal safe surgical resection remains the most effective way of treating glioblastoma (Molinaro et al. 2020). However, despite the aggressive approach, in most cases the tumors recur and become refractive to further treatment.

TMZ is a DNA-alkylating chemotherapeutic agent that was shown to provide some improvement in glioblastoma patient survival in comparison to radiation treatment alone (12.1 and 14.6 months median survival, respectively) (Stupp et al. 2005). However, even though statistically significant, this improvement was only marginal and did not affect the overall survival rates. One of the key confounding factors for determining the efficacy of TMZ treatment was the promotor methylation status of the MGMT (O-6-methylguanine-DNA methyltransferase) gene, with high promotor methylation associated with a better response (Esteller et al. 2000). Unfortunately, approaches of dose-dense and dose-intensive TMZ application did not contribute to an increased survival time, regardless of the MGMT promotor methylation status (Gilbert et al. 2013).

Lack of an efficient treatment of glioblastoma has prompted many clinical trials examining the efficacy of small molecule inhibitors, commonly based on personalized medicine approaches, or immunotherapeutic approaches which have shown promising results in some cancer entities.

Because of the high frequency of receptor tyrosine kinase (RTK) mutations (in particular EGFR, platelet-derived growth factor receptor (PDGFR) and vascular endothelial growth factor receptor (VEGFR)), glioblastoma was thought to be a good candidate entity for small kinase inhibitor treatments. However, multiple trials using different inhibitors have failed to show any improvement in patient survival, which was especially surprising for those targeting the EGFR receptor (Pollack et al. 2007; Peereboom et al. 2010).

Recently, immune checkpoint inhibitors, cell-based vaccines and other immuno-modulatory therapies have been tested in the context of glioblastoma in multiple clinical trials, however these attempts have also shown underwhelming results, likely due to the immunosuppressive nature of the tumors (for a detailed overview of conducted trials, see (Medikonda et al. 2021)).

1.1.3. Glioblastoma subtypes

Due to observations of consistent genomic aberrations on the level of individual genes or larger genomic regions, the question of associating glioblastoma characteristics with specific molecular markers became an important aspect of glioblastoma research. One of the first molecular classifications of glioblastoma derived from the TCGA-GBM database of sequenced tumors was performed by Verhaak et al (Verhaak et al. 2010). The authors used gene expression data to classify glioblastomas as neural, proneural, mesenchymal and classical. Based on the molecular classification proposed, some subtype-specific phenotypic characteristics could be observed, for

example proneural glioblastomas had an overall longer survival time, whereas the classical ones showed a better response to treatment. On the other hand, mesenchymal tumors were associated with poor survival, aggressive features, and an inflammatory response.

A few years later, Wang et al (Q. Wang et al. 2017) argued that only the proneural, classical and mesenchymal subtypes reflect the molecular characteristics of the tumor cells, and that the neural subtype is generally an artifact of bulk sequencing which includes a portion of the tumor microenvironment cells of neuronal origin.

More recently, advances in sequencing technologies, more detailed datasets including region specific samples and single cell sequencing techniques have blurred the line between the 3 canonical subtypes. Instead, new data points towards a high intratumoral heterogeneity with multiple molecular subtypes being detectable in a single tumor sample (Couturier et al. 2020) and common subtype switching upon treatment and resection (Phillips et al. 2006). Based on these findings, further attempts have been made to classify glioblastoma cells based on pathways and developmental programs to get a better understanding of the mechanisms driving glioblastoma development and progression (Neftel et al. 2019; Garofano et al. 2021).

1.1.4. Tumor microenvironment

It has been shown many times that studying cancer in a physiologically meaningful way requires the additional study of the non-malignant cellular populations that constitute the tumor microenvironment (TME) (Jin and Jin 2020). Throughout carcinogenesis, tumor cells co-opt the non-malignant cells of their environment into providing sustenance for growth and expansion such as growth factors, metabolites or even forming blood vessels (Baghban et al. 2020; Jin and Jin 2020; Farc and Cristea 2021).

Many studies have been published on the effects of tumor associated fibroblasts and their roles in promoting tumor growth of cancer entities such as liver cancer through paracrine signaling (Sahai et al. 2020). Furthermore, ongoing efforts into researching the mechanisms of tumor angiogenesis which depend on the interaction of tumor cells with endothelial cells, pericytes and other cell types, have resulted in novel anti-angiogenic therapies with promising outcomes in some cancer entities (De Palma, Biziato, and Petrova 2017; Lopes-Coelho et al. 2021).

Another major cellular population in the TME are the cells of the immune system. Namely, the components of the innate immune system, primarily the myeloid cells, are often found not only present, but actively expanded within different tumor entities (Binnewies et al. 2018). Commonly, the tumor cells reprogram myeloid cells of the TME into an immunosuppressive phenotype which promotes tumor growth and restricts the antigen presenting capacity of the innate immune system to the adaptive components such as effector T-cells (Noy and Pollard 2014; Xiang et al. 2021). Furthermore, the immunosuppressive myeloid cells of the microenvironment can prevent the activation and cause exhaustion of the tumor infiltrating T lymphocytes (TILs), hampering any immune regulation of the tumor cells even in the cases of antigen recognition and clonal expansion (Ravi et al. 2022).

Glioblastomas are tumors of the brain that do not disseminate to other parts of the body. That, together with the tight regulation of cell types present in the brain limits the diversity of cellular types of their TME. Novel studies exploring glioblastoma using single cell sequencing techniques often describe 5 populations of TME cells aside from the malignant cells: astrocytes, oligodendrocytes, neurons, myeloid cells and T-cells. Notably, smaller populations of neural stem cells (NSC) or oligodendrocyte-precursor cells (OPC) have also been reported (Couturier et al. 2020; Abdelfattah et al. 2022; Yeo et al. 2022).

Astrocytes are glial cells of the brain initially believed to simply form the parenchyma of the brain tissue. However, the role of astrocytes has been shown to be far more extensive, with involvement in mechanisms such as synaptic regulation, metabolic shuttling, synaptic transmission, injury response and inflammation and others (Liu et al. 2021; Schiweck et al. 2021; Perez-Catalan, Doe, and Ackerman 2021). Because of this, it is not surprising that astrocytic cells have a considerable impact on glioblastoma growth, likely through their paracrine influence of growth factor secretion, cytokine secretion and metabolic shuttling or even through promoting immunosuppression (Brandao et al. 2019; Henrik Heiland et al. 2019). Much less is known regarding the influence of neurons and oligodendrocytes in the glioblastoma microenvironment. However, there are studies showing that neuronal-cancer cell signaling promotes tumor growth and migration in glioblastoma (Venkatesh et al. 2019; Venkataramani et al. 2019).

1.1.5. Glioblastoma-associated myeloid cells and their role in immunosuppression

Myeloid cells, or more specifically glioblastoma-associated myeloid cells (GAM), constitute a large portion of the glioblastoma microenvironment, reported to account for 30% to 50% of all of the cells of the tumor mass (Rossi et al. 1987; Morantz et al. 1979). The origin of the GAMs is a highly contested topic. Namely, brain myeloid cells – microglia, are specialized macrophages that originate from the yolk sac and populate the brain during early development (Ginhoux et al. 2010). The microglial compartment was later shown to be self-sufficient in maintaining the innate immune system of the brain as little to no repopulation by blood-derived myeloid cells of the brain could be observed in homeostatic conditions (Huang et al. 2018). However, it is clear that in the context of the glioblastoma TME, the myeloid compartment is greatly expanded but the origin of GAMs remains a disputed topic with contradicting evidence implying a dominant microglial or monocyte-derived origin (Parney, Waldron, and Parsa 2009; A. Müller et al. 2015). Because of this, many studies refer to these cells as glioblastoma associated myeloid cells or simply macrophages.

Glioblastoma cells not only attract and promote the expansion of myeloid cells, but also promote their reprogramming to a highly immunosuppressive phenotype. Canonically, macrophage activation has been described as a transition to either pro-inflammatory M1 macrophages or immunosuppressive, alternative, M2 macrophages (Mantovani et al. 2002). Even though GAMs are generally described as M2 type macrophages due to their immunosuppressive capacity, their expressional profile does not fall clearly into the M1 - M2 polarization paradigm (Szulzewsky et al. 2015).

GAMs have been proposed to promote glioblastoma growth and progression through different mechanisms. Firstly, the immunosuppressive myeloid cells secret cytokines and growth factors related to wound healing cellular programs, such as transforming growth factor β (TGFβ) and many others (Feng et al. 2015; Coniglio et al. 2012; Markovic et al. 2009)(Figure 1). These factors can be used by glioblastoma cells to promote their survival, proliferation and invasion either through directly remodeling the extracellular matrix through metalloproteinases or through providing invasion-stimulating signaling (Markovic et al. 2009). Furthermore, the injury-based response of the microglia results in enhanced angiogenesis which is crucial for tumor growth and nutrient supply (Brandenburg et al. 2016).

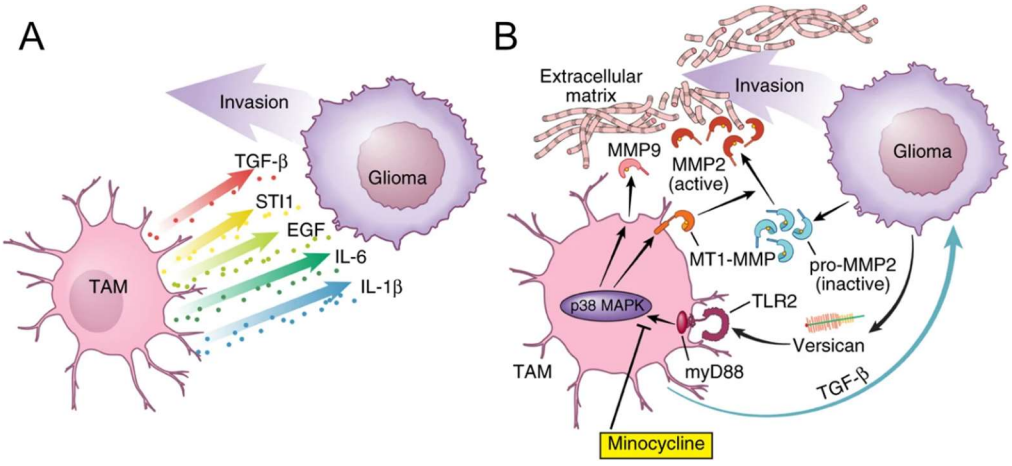

Figure 1 Example modes of action of macrophage-dependent glioblastoma growth. A) Tumor-associated macrophages (TAM) promote glioblastoma invasion and proliferation through the secretion of cytokines such as interleukin 6 (IL-6), interleukin 1b (IL-1b) and growth factors such as TGFβ. B) TAMs increase the invasive potential of glioblastoma cells through direct extracellular matrix (ECM) remodeling mediated by matrix metalloproteinases (MMPs) such as MMP9, MMP2, and others. Figure was adapted from (Hambardzumyan, Gutmann, and Kettenmann 2016)

1.1.6. T-cells in the glioblastoma microenvironment

Despite the considerable number of myeloid cells in the TME, glioblastomas are generally considered “immune cold” tumors. The main reason for this is the very low lymphoid and in particular T-cell infiltration (H. Wang et al. 2021).

T cells are the main effector cells of the adaptive immune system, and the $CD8^+$ T-cells are generally attributed with the role of immune surveillance and tumor cell clearance (Farhood, Najafi, and Mortezaee 2019, 8). Because of this, many of the novel strategies for treating cancer rely on immunotherapeutics that increase tumor T-cell infiltration, prevent T-cell exhaustion or interfere with their suppression by the tumor or myeloid cells through immune checkpoint blockade (Raskov et al. 2021).

Due to the severe immunosuppressive characteristics of the glioblastoma myeloid microenvironment, effector T-cell infiltration into these tumors is very low to begin with, and the T-cells which are present are often exhausted and unable to target tumor cells (Woroniecka and Fecci 2018). Attempts to enhance the T-cell response in glioblastoma through immune checkpoint blockade or various vaccination strategies have not shown promising results in clinical trials so far (Medikonda et al. 2021).

1.2. Cell division and cancer

1.2.1. The cell cycle in homeostasis

In order to maintain homeostasis, the tissues of the body are constantly replenished with new cells through cellular division, a process of a single somatic cell dividing into two daughter cells with near identical genetic material (Schafer 1998). However, poorly regulated cell division would quickly be detrimental for the body and result in neoplasm development (Matthews, Bertoli, and de Bruin 2022).

Simplified, the cell cycle consists of 2 phases termed the interphase (G1, S and G2) and the M phase. However, only a very small percentage of cells in the human body is capable of active division, whereas the large majority of the cells went through a process of terminal differentiation commonly referred to as the G0 phase (Nurse 2000; Matson and Cook 2017).

G1, or Gap 1 phase, is a phase of the cell cycle that directly follows cell division. During this phase the cell grows and acquires necessary nutrients and building blocks for further divisions. The S phase, or the synthesis phase, refers to a portion of the cell cycle in which the genetic material of the cell is duplicated (Nurse 2000). The G2, Gap 2, phase is another growth phase in which organelles of the cell and other supramolecular structures grow and increase in numbers to be subdivided into daughter cells. Finally, the M phase of the cell cycle, or mitosis, is the dynamic process of cellular division, in which one cell divides its genetic material, organelles and membranes (cytokinesis) into two daughter cells (Kapoor 2017).

1.2.2. Cell cycle regulation

It is imperative that cell division and by extension the cell cycle remains under tight control throughout life in order to avoid aberrant cell growth or an accelerated accumulation of division-related genomic alterations (Matthews, Bertoli, and de Bruin 2022). Because of this, the cell cycle is regulated at multiple stages often referred to as checkpoints, at which cell intrinsic and exogenous signals converge to indicate whether a cell can and should proceed through the further stages of the cell cycle (Sudakin, Chan, and Yen 2001).

The major cell cycle checkpoints described so far are the G1/S, S, G2/M and M checkpoints, referring to the stage of the cell cycle which they regulate.

G1/S checkpoint is mainly associated with cell growth and the availability of exogenous growth signals (Rubin, Sage, and Skotheim 2020). In non-dividing cell, a major S-phase inhibiting protein Rb (retinoblastoma protein) actively represses E2F (E2 factor)-mediated transcription. Once the cell receives sufficient pro-mitotic signals, a combination of Cyclin D (CycD) dependent kinases CDK2 and CDK4 will hyperphosphorylate and inhibit Rb, allowing the cell to continue through to S phase and DNA replication (Narasimha et al. 2014).

The S-phase checkpoint is a mechanism devoted to preventing cell division in case of excessive DNA damage. The S-phase checkpoint; unlike the rest of the cell cycle, is not directly mediated through Cyclins and CDKs, but rather DNA-damage-sensing kinases and proteins such as ATR (*Ataxia telangiectasia* and Rad3 related) and CHK2 (Checkpoint kinase 2) (Segurado and Tercero 2009). Upon detecting DNA damage or the lack of nucleotides for further DNA synthesis, a cascade of phosphorylation events culminating in the activation of CHK2 triggers the checkpoint response, preventing the cell from continuing through the cycle unless the damage is mediated (Alcasabas et al. 2001, 1).

The progression through G2 into M phase is regulated through the G2/M checkpoint. The main drivers of M-phase entry are CDK1 (cyclin dependent kinase 1) and a G2-specific cyclin, CycB (Gould and Nurse 1989, 2). Once CDK1 is activated by CycD, a series of phosphorylation events involving CDC25A-C (cell division cycle 25 A-C), AURKA (Aurora kinase A) and PLK1 (polo-like kinase 1) results in the transition into M-phase (Seki et al. 2008).

1.2.3. Mitosis

Mitosis is the process of cellular division in which the duplicated genomic DNA, all of the cellular organelles and membranes are divided into two new daughter cells. Even though it is a small part of the cell cycle, mitosis is an extremely complex process that can be further subdivided into prophase, prometaphase, metaphase, anaphase, telophase and cytokinesis (McIntosh 2016) (Figure 2)

During prophase, the chromosomes condense, facilitated through protein complexes such as condensins (Figure 2A) (Hudson, Marshall, and Earnshaw 2009). In prometaphase, the nuclear

envelope disintegrates by forming smaller vesicles (Cooper 2000) while the kinetochore microtubules organized at the centrosomes extend towards the condensed mitotic chromosomes and begin forming kinetochore structures at the centromeres (Santaguida and Musacchio 2009). The microtubule cytoskeletal machinery responsible for the further separation of the chromosomes throughout mitosis is referred to as the mitotic spindle (Walczak and Heald 2008). During metaphase, through a 'trial and error' mechanism, the microtubules of the mitotic spindle attach to all of the chromosomes and complete forming kinetochores, while aligning the chromosomes along the middle of the dividing cell (Kapoor 2017) (Figure 2E). Once the cell completes metaphase, the anaphase promoting complex (APC) ubiquitinates and thus promotes the degradation of the protein securin, which in term releases the separase protease from inhibition and initiates the separation of sister chromatids (identical DNA copies of each of the chromosomes) in anaphase (J.-M. Peters 2006) (Figure 2D). Once the sister chromatids are separated, they begin traveling to the opposite poles of the dividing cell through the activity of the mitotic spindle (Figure 2E). During telophase, the final stage of mitosis, the new daughter cells begin the process of cell membrane and cytosol separation – cytokinesis, while the chromosomal material decondensates and the nuclear envelopes reform (Figure 2F) (Barr and Gruneberg 2007).

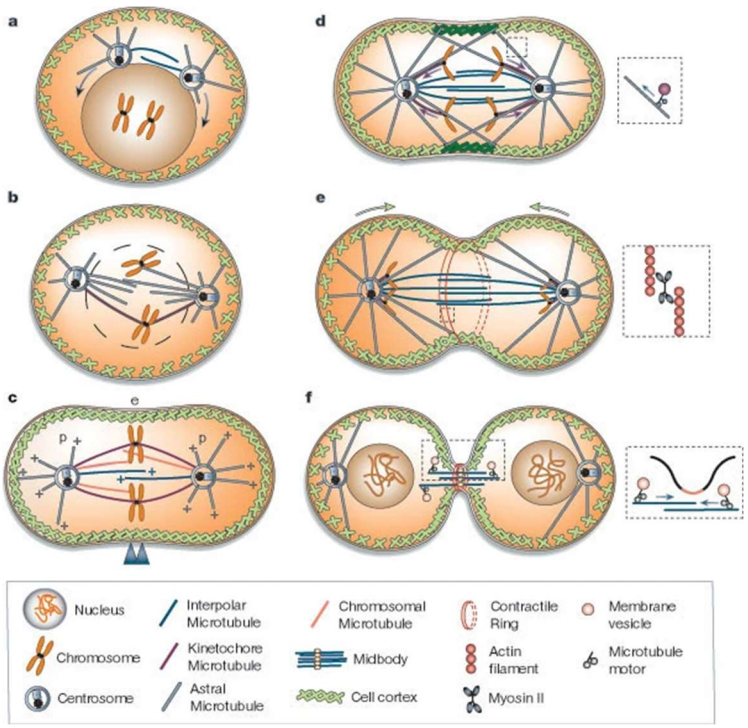

Figure 2 Schematic representation of the phases of mitosis. Chromosomes are represented with orange lines, interpolar and kinetochore microtubules with blue and red line, respectively. Dashed orange line represents the contractile cytokinetic ring. A) prophase, b) prometaphase, c) metaphase, d) and e) anaphase f) telophase. Figure adapted from (Scholey, Brust-Mascher, and Mogilner 2003)

1.2.4. Spindle assembly checkpoint (SAC)

The main regulatory point of progression through mitosis occurs during the metaphase and is referred to as the spindle-assembly checkpoint (SAC). SAC is a pathway which halts mitosis in case of incomplete or aberrant spindle formation(Musacchio and Hardwick 2002).

The SAC mainly functions through the mitotic checkpoint complex made out of MAD1 and MAD2 (mitotic arrest deficient 1 and 2), BUB1 (budding uninhibited by benzimidazole 1) BUB1B (BUB1 mitotic checkpoint serine/threonine kinase B) and BUB3 (BUB3 mitotic checkpoint protein). This complex acts on CDC20 to prevent it from activating the APC/C and thus keeping separase inactive and securin intact (Sudakin, Chan and Yen 2001). Once the chromosomes are bioriented and all of the kinetochores properly attached, the inhibition on APC/C is released and mitosis can continue.

The SAC includes other crucial kinases such as TTK1 (MPS1, multipolar spindle 1) and AURKB (Aurora kinase B). These kinases function as additional signal regulators of the SAC and their impairment leads to severe mitotic defects (Kallio et al. 2002; Morrow et al. 2005; Murata-Hori, Tatsuka, and Wang 2002; Abrieu et al. 2001, 1; E. Weiss and Winey 1996, 1).

1.2.5. Cell division in cancer

Cancer is a disease of aberrant cell growth and proliferation that relies on constant proliferative signaling facilitated intrinsically by the cancer cells or through the TME. Furthermore, cancer cells need ways of bypassing regulatory mechanisms and checkpoints of the cell cycle introduced in the previous sections. This is often achieved through mutations in key pathways regulating S phase, mitotic entry and mitotic exit (Sanchez-Vega et al. 2018; Lecona and Fernandez-Capetillo 2018; L. Wang et al. 2015, 20).

Even though proteins regulating cell cycle checkpoints are often found mutated in cancer (Figure 2, red), proteins that are related to mitotic stress response and the SAC, such as the APC /C complex and AURKB typically are not (Figure 2, blue). This is likely due to the high proliferative capacity of cancer cells. In this context, mutations of proteins regulating the spindle assembly and chromosome segregation would quickly lead to disastrous mitotic events which are not compatible with further growth. In fact, maintenance of spindle protein activity might be beneficial for tumor growth (Borah et al. 2021; J et al. 2019; Kallio et al. 2002).

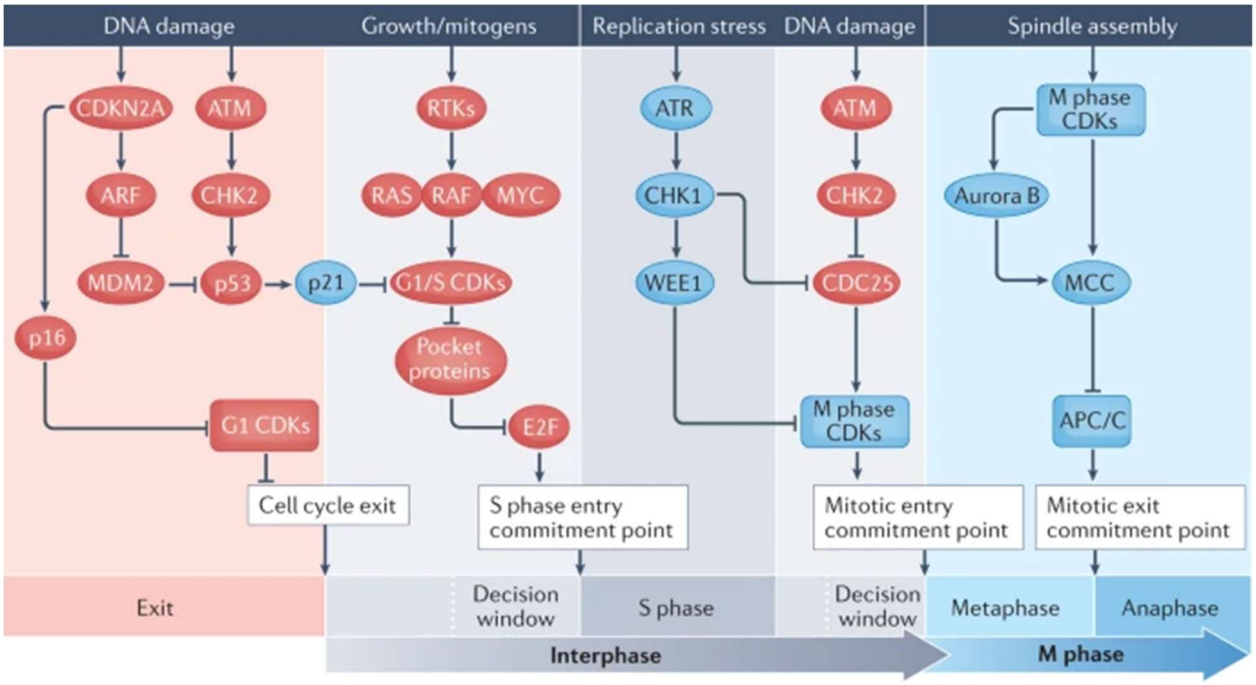

Figure 3 Overview of mitotic regulatory pathways affected in cancer. Proteins that are often mutated in cancer entities are shown in red, while proteins that are rarely mutated are shown in blue. The regulatory pathways of the proteins are shown below, while the main signaling contributing to checkpoint activation at each stage are shown on top of each pathway. Figure was adapted from (Matthews, Bertoli, and de Bruin 2022).

1.3. Cell differentiation in glioblastoma

1.3.1. Neural stem cell differentiation

Neural stem cells (NSCs) are a population of multipotent cells from which lineages of glial (oligodendrocytes and astrocytes) and neuronal cells can be derived (Ma et al. 2009). It was long thought that brain cells, primarily neurons, remain unchanged throughout life, and that most neurogenesis and gliogenesis occurs early during development (D. B. 1930). However, findings of NSCs in the adult human and mouse brain disputed these claims, and raised new questions about neuronal plasticity and regeneration (Gage 2000; Ming and Song 2005).

Currently, it is believed that adult NSCs localize to two specific regions of the brain: the subventricular zone (SVZ) of the lateral ventricles (Doetsch et al. 1999) and the subgranular zone (SGZ) of the *dentate gyrus* (Kuhn, Dickinson-Anson, and Gage 1996) (Figure 4A). Even though there have been studies showing successful isolation of NSCs from other brain regions, this has not been widely accepted (S. Weiss et al. 1996; Seri et al. 2006).

One of the defining features of adult NSCs is their ability to self-renew and differentiate in multiple lineages which they retain under *in vitro* conditions as well (Nurcombe et al. 1993). There are two current models for their differentiation, a hierarchical model of differentiation into lineage-restricted progenitors (Hack et al. 2005) and a single-lineage model of intrinsically diverse NSCs with different differentiation potentials (Merkle, Mirzadeh, and Alvarez-Buylla 2007) (Figure 4B and 4C).

Anatomically, NSCs of the SVZ and the SGZ reside in NSC-specific niches which promote the self-renewal and help maintain NSC pluripotency within the brain (Ma, Ming, and Song 2005). However, the capacity of these cells to self-renew and proliferate raises obvious questions about their potential to form tumors if the regulation of these processes is disrupted.

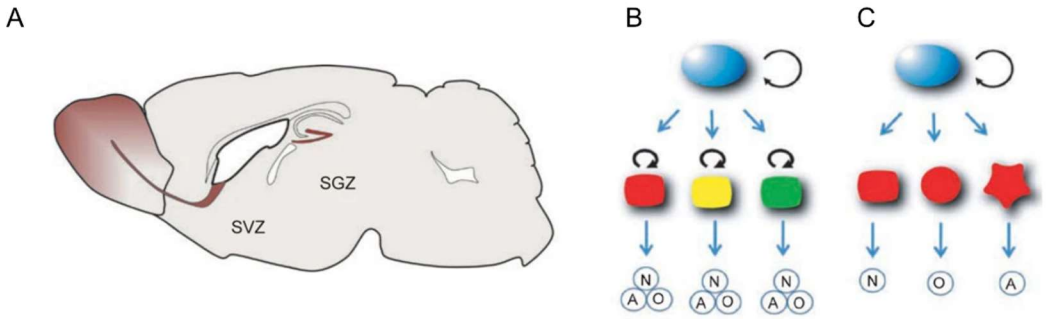

Figure 4 Neural Stem Cells in the Adult brain. A) Schematic localization of adult neural stem cells (NSCs) in the mouse brain subventricular zone (SVZ) and the subgranular zone (SGZ) B) Neural stem cell differentiation model of intrinsically diverse neural stem cells and C) lineage-restricted progenitors. Figure adapted from (Ma et al. 2009)

1.3.2. Glioblastoma cell of origin

The exact cell of origin in glioblastoma, i.e., the normal cell from which the tumor originates through genetic modifications, remains an important point of discussion today. To answer this question, multiple studies using lineage specific mouse models have been developed. In these models, cell type-specific promotors are used to knockout tumor suppressor genes which are commonly inactivated in glioblastoma: TP53 (tumor protein 53), PTEN (phosphatase and tensin homolog) and NF1 (neurofibromatosis type 1), in a temporally regulated lineage-specific manner (Körber et al. 2019).

Using nestin-creER (Cre recombinase estrogen receptor) mouse models, it was shown that the knockout of tumor suppressor genes in adult mouse NSCs results in the formation of glioblastomas (S. Alcantara Llaguno et al. 2009). Similarly, Ascl1-driven Cre recombinase expression (restricted to more committed CNS progenitors) also caused the formation of glioblastomas in mouse models (Galvao et al. 2014). However, even though the overall timeline of tumor formation in these models was similar, depending on whether the cell of origin was an adult neural stem cell or a committed progenitor, the resulting tumors showed different glioblastoma subtype expression patterns (S. R. Alcantara Llaguno et al. 2015). Much less is known on the ability of post-mitotic CNS cells to form glioblastoma.

These studies largely demonstrate that glioblastomas can form as a result of genetic alterations of different stem and progenitor cell populations of the brain, highlighting a possible mechanism for their overwhelming heterogeneity.

1.3.3. Cell differentiation in glioblastoma

Cell proliferation and poor differentiation are some of the main characteristics of high-grade cancers, certainly in glioblastoma. Because of this, potential strategies of inducing terminal differentiation of glioblastoma cells are highly sought for in current research (Fang et al. 2021; Ferrucci and Zollo 2016; Garnier et al. 2019).

Interestingly, some studies have shown that one of the potential mechanisms underlying IDH mutant glioma growth is through 2-hydroxyglutarate (2-HG, the metabolic product of mutated IDH) mediated prevention of differentiation. Furthermore, the inhibition of the mutated enzyme seems to cause terminal tumor cell differentiation (Turcan et al. 2013; Pusch et al. 2017).

Less research has been done on inducing glioblastoma cell differentiation outside of the context of IDH mutated tumors, however differentiation therapy either alone or as combination treatment remains a highly valuable area of research in glioblastoma and cancer biology in general.

1.3.4. DNA methylation as a mechanism of cellular differentiation

DNA methylation is an epigenetic mechanism of transcriptional silencing involving direct modification of cytosine residues by C5 methylation (5-mC). DNA methylation can occur throughout the entire genome, but it is highly enriched in regions rich in alternating cytosine and guanine residues referred to CpG islands (Sun et al. 2021). CpG islands are often found in promoter regions of genes, and their hypermethylation causes transcriptional repression.

DNA methylation is established by DNA methyltransferases (DNMTs) which transfer a methyl group form S-adenosyl-l-methionine (SAM) to the cytosine C5 (Goll and Bestor 2005). DNA demethylation is a more diverse process, which can occur passively, through the loss of 5-mC during cell divisions in the lack of DNMT activity (Bayraktar et al. 2020), or actively through enzyme-dependent DNA demethylation. Main mediators of active DNA demethylation are the α-ketoglutarate (αKG) dependent ten-eleven translocation (TET) methylcytosine dioxygenases (Pastor, Aravind, and Rao 2013). TETs oxidize 5-mC into 5-hmC (5-hydroxymethylcitosine) followed by 5-fC (5-formylcitosine) and 5-caC (5-carboxylcytosine). 5-caC is then removed from the genome through the activity of the thymine-DNA glycosylase (TDG) enzyme and base-excision repair (BER) (Figure 5) (Nakajima and Kunimoto 2014, 2).

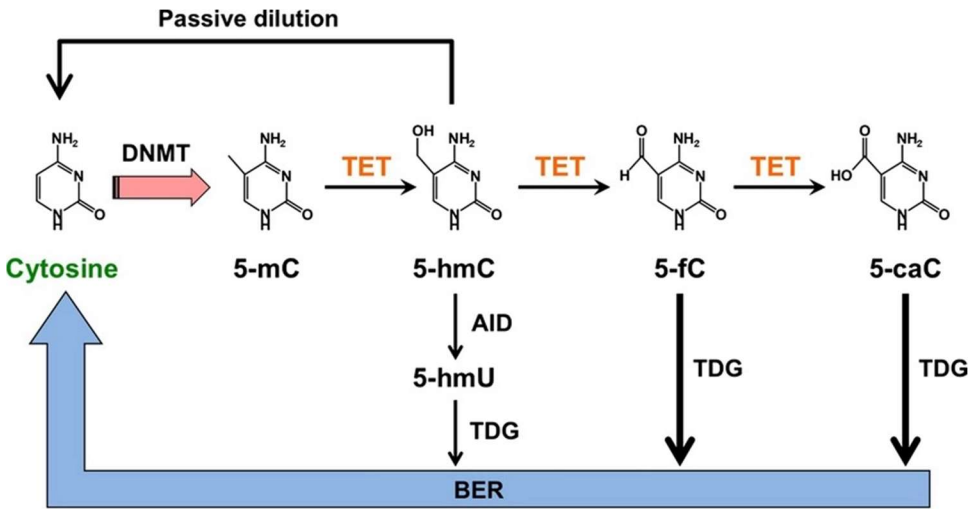

Figure 5 Schematic representation of the pathway of active DNA demethylation through the activity of the TET enzymes. DNMT – DNA methyltransferase; BER – base-excision repair; TET – ten-eleven translocation methyl dioxygenase; 5-mC – 5-methylcyosine; 5-fC – 5-formylcytosine; 5-caC – 5-carboxylcytosine. Figure adapted from (Nakajima and Kunimoto 2014, 2)

DNA methylation based repression of gene expression has long been known to define tissue and cell specific expressional patterns (Bird and Wolffe 1999). In particular, DNA methylation has been implicated in regulating fate specification and progenitor restriction in different neuronal and glial cell subpopulations (Stricker and Götz 2018; Takizawa et al. 2001).

1.3.5. DNA methylation and TET enzymes in glioblastoma

DNA methylation has long been a topic of research in brain cancers due to the discovery of IDH mutated gliomas (Nobusawa et al. 2009, 1). IDH mutations cause the accumulation of the oncometabolite 2-HG which is an effective αKG competitor and blocks the function of αKG-dependent dioxygenases such as TETs and histone demethylases (Xu et al. 2011) (Figure 6). This results in a genome-wide alteration of methylation patterns which have been shown to maintain the undifferentiated state of glioblastoma cells (Pusch et al. 2017; Turcan et al. 2013).

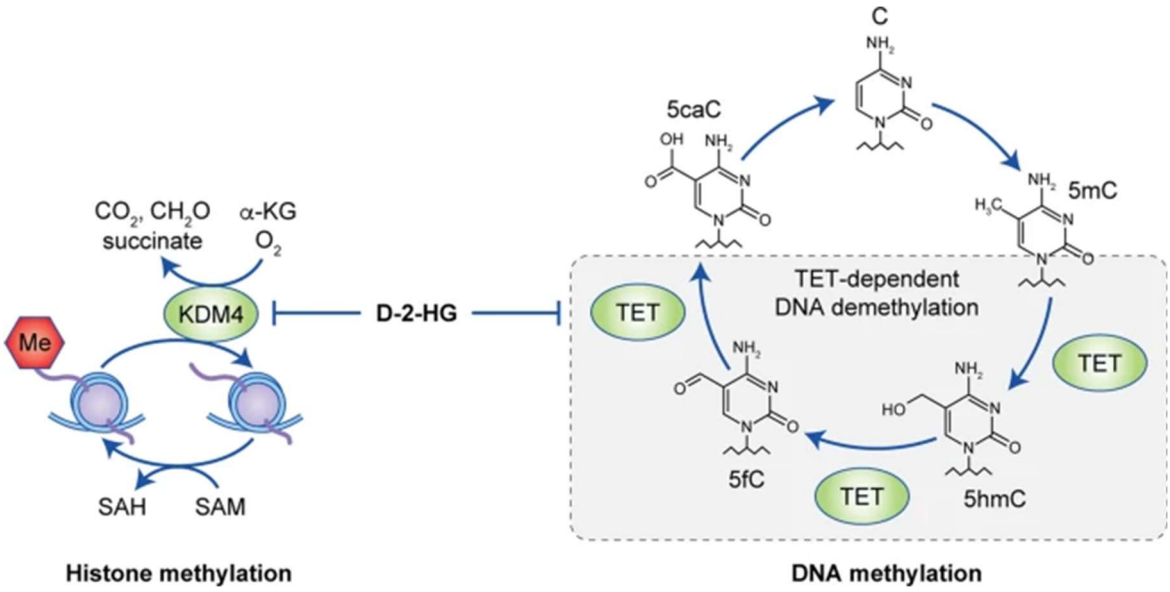

Figure 6 Mechanism of 2-hydroxygluterate-dependent epigenetic modifications. Figure adapted from (Han et al. 2020)

Even though glioblastomas do not have IDH mutations according to the most recent CNS tumor classification, the tumor cells remain poorly differentiated. Multiple studies have shown that TET enzymes restrict tumor growth through cellular differentiation, and mechanisms of how they can be downregulated or inactivated in tumors have been described (Bray et al. 2021). In glioblastomas, however, no consensus mechanism on TET inactivation has been found, even though some studies exploring individual TET enzymes have shown them to be capable of regulating glioblastoma differentiation when functional (García et al. 2018; T. Müller et al. 2012).

1.4. BCAT1 in homeostasis and cancer

1.4.1. Discovery and function

Branched chain amino acid transaminase 1 (BCAT1) is a metabolic, cytosolic enzyme with the function of catabolizing the branched chain amino acids (BCAA) valine, leucine and isoleucine into branched chain ketoacids (BCKA) α-ketoisovalerate, α-ketoisocaprotate and α-keto-b-methylvalerate, respectively (Figure 7). In doing so, BCAT1 transfers an amino-group equivalent from the BCAAs to αKG, producing glutamate. BCAT1 was initially described as a c-Myc response gene in fibroblasts (Evan et al. 1992) and later found to be conserved across eukaryotic species and implicated in the regulation of the cell cycle in yeast (Schuldiner et al. 1996, 39).

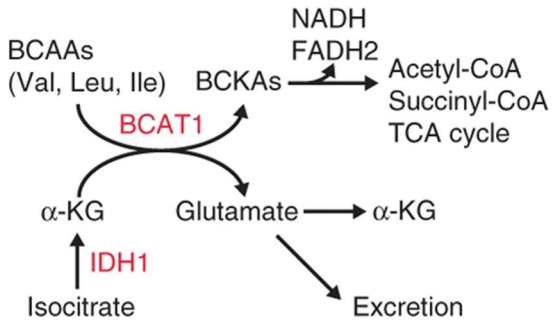

Figure 7 The metabolic function of BCAT1. BCAT1 converts branched chain amino acids (BCAAs) into branched chain keto acids (CKAs) thought transamination, exhausting cellular α-ketoglutarate (αKG) and producing glutamate. Figure adapted from (Tönjes et al. 2013)

BCAT is present in 2 isoforms, BCAT1 and BCAT2. BCAT1 expression is restricted to a few adult tissues such as the brain, ovaries and the placenta (Sweatt et al. 2004). Interestingly, BCAT1 expression is high during early embryonic development throughout the embryo as a consequence of c-Myc expression during these stages of development, and c-Myc overexpression in embryonic stem cells prevents the downregulation of BCAT1 upon their differentiation (Benvenisty et al. 1992). Unlike BCAT1, BCAT2 is a mitochondrial protein, constituent of a metabolic complex that processes BCAAs. BCAT2 is expressed ubiquitously throughout tissues and does not seem to be c-MYC regulated (Dhanani, Mann, and Adegoke 2019, 2).

The tissue specificity of BCAT1-expression raised questions regarding its function, in particular in the context of brain tissue and neurons. BCAT1 has been successfully isolated from rat and mouse brains (Hall et al. 1993) and shown to be specifically expressed in neurons, and in

particular glutaminergic neurons (Hull et al. 2015; 2012). Glutamate is a key neurotransmitter and it is hypothesized that BCAT1-derived glutamate maintains constant levels of brain glutamate through the metabolic shuttling between neurons that express BCAT1 and neighboring astrocytes (Hull et al. 2012) (Figure 8). This is further facilitated by the finding that most of the neuronal culture glutamate can be labeled through labeling the BCAAs (Yudkoff et al. 1993; 1994).

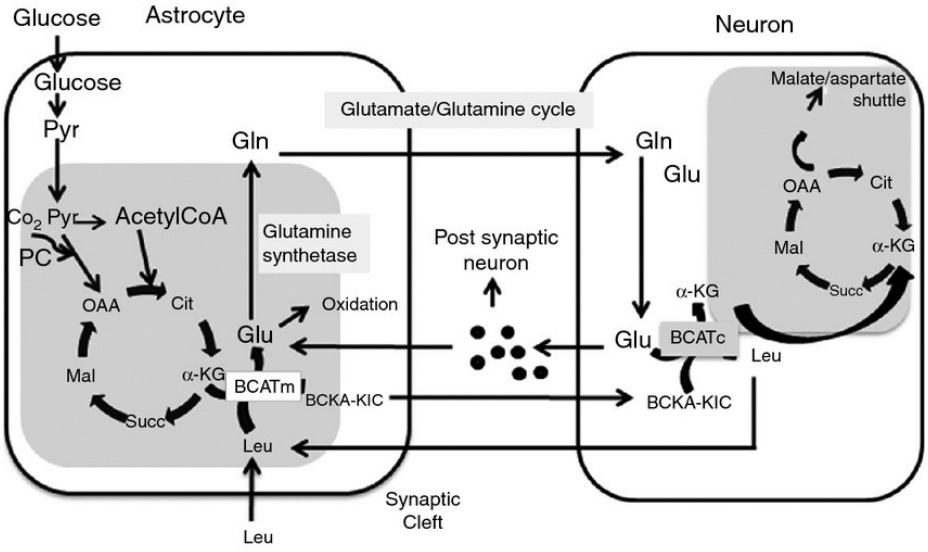

Figure 8 Metabolic shuttling cycle of glutamate (Glu) in the brain. The importance of BCAT1 (BCATc) expressed in glutaminergic neurons in ensuring proper synaptic signaling through metabolite shuttling with the surrounding astrocytes. Figure adapted from (Hull et al. 2012)

Recently, new insights into BCAT1's function independent of its metabolic activity have been proposed (Hillier et al. 2022; Ko et al. 2020). Namely, the BCAT1 protein contains a highly evolutionarily conserved, redox-active CxxC (Cysteine-X-X-Cysteine) motif which is commonly found in redox-regulating proteins (Fomenko and Gladyshev 2003). Biochemical assays and cell-culture experiments have shown that the CxxC motif can potentially play a role in redox equivalent transfer, similar to other redox proteins such as thioredoxin (Trx) (Myra E. Conway et al. 2008; Hillier et al. 2022). In our own work, we have shown that the CxxC motif of BCAT1 maintains the proper functioning of the SAC during mitosis in multiple models of human and mouse cancer and non-malignant cells (Francois et al. 2022).

1.4.2. BCAT1 in cancer

As BCAT1 is regulated by the oncogene c-MYC, it is not surprising that its expression is increased in many different cancer entities including glioblastoma, breast cancer, acute myeloid lymphoma (AML) and others (Tönjes et al. 2013, 1; Luo et al. 2021, 1; Raffel et al. 2017). However, different roles of BCAT1 and mechanisms for its oncogenic potential have been proposed for various tumor entities.

So far, the majority of the studies have focused on the catabolic role of BCAT1 in cancer, and how the balance of BCAAs/BCKAs and the byproducts αKG/glutamate influence tumor growth and development. BCAT1 is highly expressed in glioblastoma (Figure 9A) (Tönjes et al. 2013). In addition, high BCAT1 expression is related to poor survival in the TCGA-GBM dataset (Figure 9B). This was associated with the increased glutamate production and subsequent secretion from the overexpressing cells (Tönjes et al. 2013). Similarly, BCAT1 expression was found to be crucial for the growth of breast cancer (Thewes et al. 2017). Interestingly, Wang et al. found that BCAT1 promotes EGFR inhibitor resistance in lung carcinoma cell lines (Y. Wang et al. 2019). These findings consolidate the importance of BCAT1's metabolic function but through a different mechanism involving glutamate-derived glutathione (GSH) and reactive oxygen species (ROS) protection.

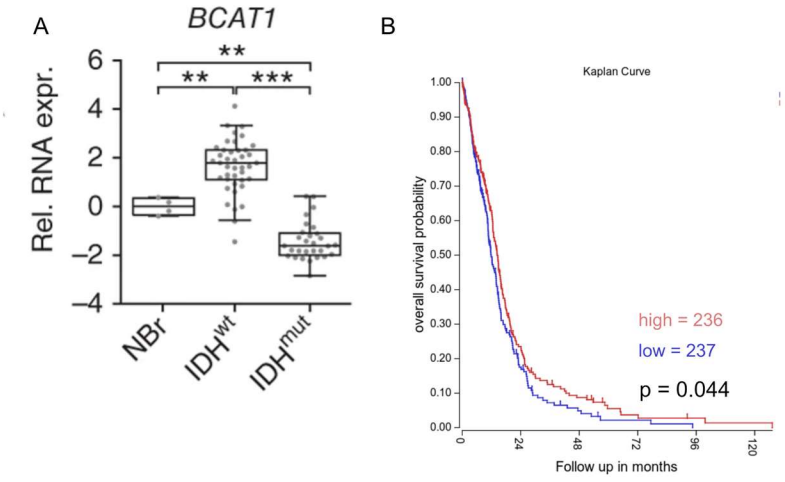

Figure 9 Expression of BCAT1 in glioblastoma. A) BCAT1 overexpression was evident in IDH^{WT} glioblastomas when compared to IDH^{mut} tumors, normalized to the expression in normal brain tissue (NBr). Adapted from (Tönjes et al. 2013). B) Glioblastoma patient overall survival from the TCGA-GBM dataset, stratified as $BCAT1^{high}$ (blue) and $BCTA1^{low}$ (red) according to the median expression. The graph was made using the R2: Genomics Analysis and Visualization Platform (http://r2.amc.nl).

Aside from catabolizing BCAAs and producing glutamate, BCAT1 exhausts cellular αKG. As αKG is a major regulator of DNA methylation and the hypoxia-induced factor 1a (HIF1a). Our group previously explored whether BCAT1 overexpression could potentially influence these pathways in AML (Raffel et al. 2017) and showed that BCAT1 does in fact restrict intracellular αKG levels which in turn mimics the IDH1 mutant AML in which 2-HG acts as a competitive inhibitor of αKG instead.

Finally, BCAT1 expression in cancer has been shown to influence the TME, as well. Preliminary work has shown that the products of BCAT1's catabolic reactions, BCKAs, can be secreted by tumor cells and modify the polarization phenotype of the surrounding macrophages (Silva et al. 2017, 1). Conversely, the expression of BCAT1 in the cells of the TME itself, not the tumor cells specifically, has also been shown to modify tumor growth in a pancreatic ductal adenocarcinoma (PDAC) model (Zhu et al. 2020).

1.4.3. BCAT1 in cellular differentiation

BCAT1 expression is high and ubiquitous during early embryonic development, as well in embryonic and induced pluripotent stem cells (Benvenisty et al. 1992; Francois et al. 2022). This, together with the fact that it modifies some of the key differentiation pathways through αKG, has prompted studies of the function of BCAT1 in cellular differentiation (Chen et al. 2020; Go et al. 2022).

So far, BCAT1 has been found to modulate cellular differentiation via the same mechanisms as in cancer cells. Namely, Chen et al. found that BCAT1 expression in mouse embryonic stem cells maintains their pluripotency through regulating DNA methylation and in particular the expression of RAS protein activator like 1 (RASAL1) (Chen et al. 2020). Interestingly, in stem cells lacking BCAT1, the authors describe a tendency towards spontaneous differentiation.

2. Aims of the Study

In this thesis, I aimed to study two novel roles of BCAT1. In the first part, I used unbiased proteomics approaches to

- elucidate the redox-dependent mechanism of BCAT1 in maintaining faithful mitosis.

In the second part, I explored the role of BCAT1 in an immunocompetent environment and aimed to:

1. Describe the function of BCAT1 expression in glioblastoma cells and its association with glioblastoma molecular subtypes
2. Characterize in detail the role of Bcat1 expression in glioblastoma in an in vivo, immunocompetent mouse model
3. Determine the importance of individual immune cell populations on the development and growth of glioblastoma cells in the context of Bcat1 knockout

3. Materials and Methods

3.1. Materials

3.1.1. Antibodies

Table 1 List of primary antibodies

Antibody	Distributor	Dilution
Anti-5-hydroxymethylcitosyne	Active Motif (39770)	IF:1:250
Anti-alphaTubulin	Sigma-Aldrich (T9025)	WB: 1:5000
Anti-Bcat1	Abcam (ab232700)	WB: 1:1000
Anti-BCAT1	BD Biosciences (611271)1	WB: 1:1000
Anti-Cas9	Cell Signaling Technology (14697T)	WB: 1:1000
Anti-CD8a	R&D Systems (NBP2-52659)	IF: 1:100
Anti-GFP	Abcam (ab13970)	IF: 1:500
Anti-GFP	Biocat (AB011-EV)	IF: 1:500 WB: 1:1000
Anti-Iba1	FUJIFILM Wako Chemicals Europe (019-1971)	IF: 1:250
Anti-Ki67	Abcam (ab15580)	IF: 1:250
Anti-TUBB31	Biolegend (MMS-435)	IF: 1:100
Anti-V5-tag	Cell Signaling Technology (13202S)	WB: 1:1000

Table 2 List of secondary antibodies

Antibody	Distributor	Dilution
Donkey anti-Chicken(H+L) CF488A	Sigma (SAB4600031-250ul)	IF:1:1000
Donkey anti-Chicken(H+L) CF633	Sigma (SAB4600127-50ul)	IF: 1:1000
Donkey anti-Goat(H+L) CF555	Sigma (SAB4600059-250ul)	IF: 1:1000
Donkey anti-Rabbit(H+L) CF647	Sigma (SAB4600177-250ul)	IF:1:1000
Goat anti-Mouse (H+L) AF647	ThermoFisher Scientific (A3272)	IF: 1:1000
Goat anti-Mouse AF488	ThermoFisher Scientific (A32723)	IF: 1:1000
Goat anti-Rabbit AF555	ThermoFisher Scientific (A21428)	IF: 1:1000
HRP anti-Mouse	Cell Signaling Technology (7076S)	WB: 1:2500
HRP anti-Rabbit	Cell Signaling Technology (7074S)	WB: 1:2500

3.1.2. Buffers and solutions

Table 3 List of Buffers used and their respective recipes

Buffer	Composition
Blocking buffer	5% BSA, 0.02% NaN_3,0.5% TritonX-100 in PBS
Blotting Buffer	25mM Tris, 200mM glycine, 20% methanol
LB Agar	1.6% (w/V) Agar in LB medium
LB medium	2.5% (w/V) Lauria Bertani powdered medium
Phosphate-buffer saline (PBS)	137mM NaCl, 2.7mM KCl, 10mM Na_2HPO_4, 1.8mM KH_2PO_4
Tris-buffer saline (TBS)	150mM NaCl, 10mM Tris, pH=7.4

3.1.3. Cell culture

Table 4 >List of cell culture media and reagents

Name	Distributor
Accutase	Sigma Aldrich, Munich, Germany
B27 Supplement	Life Technologies, GmbH, Carlsbad, CA, USA
Dimethyl Sulfoxide	Sigma Aldrich, Munich, Germany
Dulbecco's Modified Eagle's Medium (DMEM) – low glucose	Sigma Aldrich, Munich, Germany
Dulbecco's Modified Eagle's Medium / F12 Nutrient Mixture (DMEM/F12)	Life Technologies, GmbH, Carlsbad, CA, USA
Fetal Calf Serum (FCS)	Merck Millipore, Germany
Human EGF	Life Technologies, GmbH, Carlsbad, CA, USA
Human M-CSF	Miltenyi biotec, Bergisch Gladbach, Germany
Human recombinant FGFb	PreproTech, 100-18-100
Iscove's Modified Dulbecco's Medium (IMDM)	Life Technologies, GmbH, Carlsbad, CA, USA
N2 supplement	Life Technologies, GmbH, Carlsbad, CA, USA
OptiMEM	ThermoFisher Scientific, Waltham, MA, USA
Penicillin/Streptomycin (Penstrep)	ThermoFisher Scientific, Waltham, MA, USA
Polyethyleneimine	Polysciences Europe GmbH
Stem cell qualified ECM gel	Sigma Aldrich, Munich, Germany
Trypsin-EDTA (0.5%)	ThermoFisher Scientific, Waltham, MA, USA

3.1.4. Cell lines and bacteria

Table 5 List of animal, human and bacterial cell lines

Cells	Distributor
HEK293T	ATCC, Manassas, VA, USA
mGB2	Provided by the lab of Prof Peter Angel (DKFZ)
One Shot Stbl3 Chemically Competent *E. Coli*	Life Technologies GmbH
U251-MG	ATCC, Manassas, VA, USA

3.1.5. Mice

Strain	Source
Non-Obese Diabetic/Severe Combined Immunodeficiency (NSG)	Janvier Labs, Le Genest-Saint-Isle, France
C57BL/6J	Janvier Labs, Le Genest-Saint-Isle, France
C57BL/6NRj-Rag2^{tm1Ciphe}/Rj (Rag2KO)	Janvier Labs, Le Genest-Saint-Isle, France

3.1.6. Kits

Table 6 List of commercial Kits

Kit	Distributor
DNeasy Blood & Tissue Kits	Qiagen, Hilden, Germany
FastDigest (FD)	ThermoFischer Scientific, Waltham, MA, USA
Pierce BCA Protein Assay	ThermoFischer Scientific, Waltham, MA, USA
Pierce™ ECL Western Blotting-Substrat	ThermoFischer Scientific, Waltham, MA, USA
Protoscript II Reverse Transcription Kit	New England Biolabs, Ipswich, MA, USA
QIAGEN Plasmid Maxi Kit	Qiagen, Hilden, Germany
QIAGEN Plasmid Mini Kit	Qiagen, Hilden, Germany
QIAquick Gel extraction Kit	Qiagen, Hilden, Germany
QIAquick PCR Purification Kit	Qiagen, Hilden, Germany
Quick Ligation Kit	New England Biolabs, Ipswich, MA, USA
RNase-Free DNase Kit	Qiagen, Hilden, Germany
RNeasy Mini Kit	Qiagen, Hilden, Germany

3.1.7. Plasmids

Table 7 List of commercially available plasmids

Plasmid	Distributor
pLenti PGK V5-LUC Neo	#21471 ,Addgene, Cambridge, USA
pMD2.G	#12259 ,Addgene, Cambridge, USA
psPAX2	#12250 ,Addgene, Cambridge, USA
TLCv2	#87360 ,Addgene, Cambridge, USA

Table 8 List of plasmids created during the thesis work

Plasmid	Modification
TLCv2_sgRNA_Bcat1	Cloned in Bcat1 targeting sgRNA oligo
TLCv2_sgRNA_NT	Cloned in non-targeting sgRNA oligo

3.1.8. Primers and oligos

Table 9 List of oligonucleotides used for RT-qPCR experiments. Each primer is named based on the gene probed and the direction of the primer (forward and reverse). The sequences are always given in the 5'-3' direction

Oligo	Sequence
mAqp4 forward	ATCAGCATCGCTAAGTCCGTC
mAqp4 reverse	GAGGTGTGACCAGGTAGAGGA
mBcat1 forward	GAAGTGGCGGAGACTTTTAGG
mBcat1 reverse	TGGTCAGTAAACGTAGCTCCA
mCspg4 forward	GCTGTCTGTTGACGGAGTGTT
mCspg4 reverse	CGGCTGATTCCCTTCAGGTAAG
mGfap forward	CGGAGACGCATCACCTCTG
mGfap reverse	CGGAGACGCATCACCTCTG
mMap2 forward	GCCAGCCTCGGAACAAACA
mMap2 reverse	GCTCAGCGAATGAGGAAGGA
mPostn forward	TGGTATCAAGGTGCTATCTGCG
mPostn reverse	AATGCCCAGCGTGCCATAA

mS100b forward	TGGTTGCCCTCATTGATGTCT
mS100b reverse	CCCATCCCCATCTTCGTCC
mTbp forward	ATGATGCCTTACGGCACAGG
mTbp reverse	GTTGCTGAGATGTTGATTGCTG
mTubb3 forward	TAGACCCCAGCGGCAACTAT
mTubb3 reverse	GTTCCAGGTTCCAAGTCCACC

Table 10 List of oligonucleotides used for cloning experiments. The sequences are always given in the 5'-3' direction

Oligo	Sequence
sgRNA_Bcat1 forward	CACCGGCTGACCACATGCTGACG
sgRNA_Bcat1 reverse	AAACCGTCAGCATGTGGTCAGCC
sgRNA_NT forward	CACCGGTATTACTGATATTGGTGGG
sgRNA_NT reverse	AAACCCCACCAATATCAGTAATACC

3.1.9. Reagents and other materials

Table 11 List of consumables

Consumable	Distributor
0.22 µm Millex 4mm Durapore PVDF filters	Merck Millipore, Darmstadt, Germany
0.45 µm Millex 4mm Durapore PVDF filters	Merck Millipore, Darmstadt, Germany
96-well plate black	Greiner Bio-One GmbH, Kremsmünster, Austria
96-well plate white	Greiner Bio-One GmbH, Kremsmünster, Austria
Cell culture flasks and multi-well plates	Sarstedt GmbH, Nürnbrecht, Germany
Cell culture flasks and multi-well plates for adherent cells	BD Biosciences, Heidelberg, Germany
Eppendorf Safe-Lock microcentrifuge tubes (1.5 mL, 2.0 mL)	Eppendorf, Hamburg, Germany
FACS tubes	Becton, Dickinson and Company (BD), Franklin Lakes, NJ, USA
Falcon tubes (50 and 15 mL)	BD Biosciences, Heidelberg, Germany
Nunc Cryo tubes	Sigma Aldrich, Munich, Germany
Pipette tips (10 µl, 20 µl, 100 µl, 200 µl, 1000 µl)	VWR International GmbH, Darmstadt, Germany

Polyvinylidene fluoride (PVDF) transfer membrane	Merck Millipore, Darmstadt, Germany
Superfrost PLUS slides	Thermo Fisher Scientific, Waltham, MA, USA
Ultracentrifuge tubes 14,0 ml	Herolab, Heidelberg, Germany

Table 12 List of Chemicals

Chemical	Distributor
Ampicillin	Carl Roth, Karlsruhe, Germany
Bepanthen	Bayer, Leverkusen, Germany
Carprofen	
D-Luciferin, potassium salt	BIOZOL, Echnig, Germany
Doxycycline	Thermo Fisher Scientific, Waltham, MA, USA
Geneticin (G418 Sulfate)	Thermo Fisher Scientific, Waltham, MA, USA
Isoflurane	
Isopropanol	Thermo Fisher Scientific, Waltham, MA, USA
Methanol	Thermo Fisher Scientific, Waltham, MA, USA
NuPAGE 4-12 % bis-Tris 1.5 mm x 10-well	Life Technologies GmbH, Carlsbad, CA, USA
NuPAGE 4-12 % bis-Tris 1.5 mm x 15-well	Life Technologies GmbH, Carlsbad, CA, USA
NuPAGE 4X LDS sample buffer	Life Technologies GmbH, Carlsbad, CA, USA
NuPAGE MOPS SDS Running Buffer 20X	Life Technologies GmbH, Carlsbad, CA, USA
NuPAGE Sample Reducing Agent (10X)	Life Technologies GmbH, Carlsbad, CA, USA
Optimal cutting temperature compound (OCT)	Leica Microsystems, Wetzlar, Germany
Paraformaldehyde (PFA)	Sigma-Aldrich, Munich, Germany
primaQUANT cybr 2X SYBRGreen Mastermix	Steinbrenner Laborsysteme GmbH, Wiesenbach, Germany
ProLong Gold antifade mounting	Thermo Fisher Scientific, Waltham, MA, USA
Puromycin	Merck Millipore Darmstadt, Germany
Spectra Multicolor Broad Range Protein Ladder	Thermo Fisher Scientific, Waltham, MA, USA
Spectra Multicolor High Range Protein Ladder	Thermo Fisher Scientific, Waltham, MA, USA
Sucrose	Sigma-Aldrich, Munich Germany
T4 PNK	New England Biolabs, Ipswich, MA, USA
Triton X-100	Sigma Aldrich, Munich, Germany
Whole milk powder	Carl Roth, Karlsruhe, Germany

3.1.10. Equipment

Table 13 List of instruments

Instrument	Distributor
10 µL, Model 701 RN SYR, Small Removable NDL, 32 ga	Hamilton Company, Reno, NA, USA
BD FACS Aria Fusion-3	BD Biosciences, Heidelberg, Germany
BD FACS Canto TM II	BD Biosciences, Heidelberg, Germany
BD FACS LSR Fortessa	BD Biosciences, Heidelberg, Germany
Beckman Ultracentrifuge with SW41 rotor	Beckman Coulter GmbH, Krefeld, Germany
Centrifuge Heraeus Sepatech Varifuge 3.0R	M&S Laborgeräte GmbH, Wiesloch, Germany
Eppendorf Thermomixer comfort	Eppendorf, Hamburg, Germany
EZ-155 Stand-Alone Vaporizer	E-Z Systems,
Forma Steri-Cycle CO2 incubator	ThermoFisher Scientific, Waltham, MA, USA
HiSeq 2000 v4	Illumina Inc., San Diego, CA, USA
iNTAS imager	INTAS Science Imaging Instruments GmbH, Göttingen, Germany
IVIS Lumina LT Series III	Perkin Elmer, Waltham, MA, USA
Leica CM1860 UV	Leica Microsystems, Wetzlar, Germany
Leica TCS SP8 confocal microscope	Leica Microsystems, Wetzlar, Germany
MasterCycler EP Gradient S	Eppendorf, Hamburg, Germany
Mithras LB 940 plate reader	Berthold Technologies, Bad Wildbad, Germany
NanoDrop ND-2000c spectrometer	NanoDrop, Wilmington, NC, USA
Novaseq 6000 SP	Illumina Inc., San Diego, CA, USA
Pipettes (2 µl, 20 µl, 100 µl, 200 µl, 1000 µl)	STARLAB International GmbH, Hamburg, Germany
Quantstudio5	Thermo Fisher Scientific, Waltham, MA, USA
Sky Line Orbital Shaker	ELMI North America, Newbury Park, CA, USA
Stereotact	
Tube Roller	STARLAB International GmbH, Hamburg, Germany
Vi-CELL XR 2.03	Beckman Coulter GmbH, Krefeld, Germany
Zeiss Axioscan 7	Carl Zeiss AG, Jena, Germany

3.1.11. Software

Table 14 List of Software

Software	Distributor
Affinity Designer	Serif (Europe) Ltd., Nottingham, United Kingdom
FACS Diva	BD Biosciences, San Jose, USA
FlowJo	FlowJo, LLC., Ashland, USA
GraphPad Prism 9.0	GraphPad Software, San Diego, USA
ImageJ	Open Source, National Institute of Health, Bethesda, USA
INTAS ChemoStar	INTAS Science Imaging Instruments GmbH, Göttingen, Germany
Living Image	PerkinElmer, Waltham, MA, USA
Microsoft Office 365	Microsoft, Redmond, USA
QuantStudio Design and Analysis	ThermoFisher Scientific, Waltham, MA, USA
R 3.6	Open Source, R Foundation
R Studio	Open Source, R Foundation
SnapGene	GSL Biotech LLC, San Diego, USA
Zotero	Roy Rosenzweig Center for History and New Media, Fairfax, VA, USA

3.1.12. R packages

Table 15 List of R packages

Package	Reference/Link
DESeq2	(Love, Huber, and Anders 2014)
DMRcate	(T. J. Peters et al. 2021)
dplyr	https://dplyr.tidyverse.org
enrichplot	https://www.bioconductor.org/packages/release/bioc/html/enrichplot.html
fgsea	(Korotkevich et al. 2021)
ggplot2	(Wickham 2009)
goseq	(Young et al. 2010)
IlluminaMouseMethylationmanifest	https://github.com/chiaraherzog/IlluminaMouseMethylationmanifest
knitr	("Dynamic Documents with R and Knitr" n.d.)
limma	(Ritchie et al. 2015)
Matrix	https://cran.r-project.org/web/packages/Matrix/index.html

minfi	(Aryee et al. 2014)
missMethyl	(Phipson, Maksimovic, and Oshlack 2016)
org.Hs.eg.db	https://bioconductor.org/packages/release/data/annotation/html/org.Hs.eg.db.html
org.Mm.eg.db	https://bioconductor.org/packages/release/data/annotation/html/org.Mm.eg.db.html
PhosR	(Kim et al. 2021)
plotly	https://plotly.com/r/
preprocessCore	https://github.com/bmbolstad/preprocessCore
RColorBrewer	https://cran.r-project.org/web/packages/RColorBrewer/index.html
stringr	http://stringr.tidyverse.org
vsn	(Huber et al. 2002)

3.2. Bioinformatics Methods

All bioinformatics presented in this thesis was performed using R and RStudio software. For a detailed list of packages used in this thesis see Table 15.

3.2.1. Proteomics and phospoprotomics

All of the proteomics and phosphoproteomics samples used for this thesis were prepared and processed by L. Francois and the Proteomics Core Facility of the DKFZ. All of the analysis was performed using the label-free quantification (LFQ) values. The analysis was performed in the same way (described below) for all of the datasets in order to keep the results consistent. The majority of the analysis was done using modified or original functions of the *PhosR* package (Kim et al. 2021).

First, all potential contaminants and samples which showed significantly less detected peptides than the rest were removed from any downstream analysis. Data was transformed to logarithmic data and filtered stringently. During the filtering, all unique proteins which were not detected in at least half of the replicates in at least one of the groups were removed form downstream processing. Data was normalized using variance-stabilizing normalization (*vsn* R package, (Huber et al. 2002)). Imputation was performed using site- and condition- specific imputation (scImp) followed by paired-tail imputation (ptImp) to account for technically and biologically missing values, respectively. For the scImp, proteins with 50% or more detections in a group were considered. For the ptImp, the random drawing was done from a normal distribution mean-left-shifted by a factor of 2.2 standard deviations and a new standard deviation 30% of the original. The imputation methods were previously described and modified from the *PhosR* package.

PCA analysis was performed using the predefined function ‘plotQC’. Differential expression was determined using the *limma* R package. Briefly, the data was fit using a model matrix defined only by the group the samples belong to and every possible contrast was made.

3.2.2. RoKAI analysis

The RoKAI analysis was performed using the freely available online RoKAI tool (Yılmaz et al. 2021). All of the analysis was performed using the default settings of the application with both PSP and Singor databases.

3.2.3. GSEA, ssGSEA and GO-term enrichment

GO-term enrichment was analyzed using the *goseq* R package. Gene IDs were obtained through the *org.Hs.eg.db* or *org.Mm.eg.db* packages for human and mouse, respectively. Upregulated and downregulated differentially expressed genes with p-value<0.05 were selected for the enrichment analysis. The enrichment was evaluated against the Biological Process (BP), Cellular Component (CC) and Molecular Function (MF) terms.

The pre-ranked GSEA analysis was performed using the *fgsea* R package. Pre ranked gene lists were constructed from the differential expression analysis, ranked based on Log Fold Change. The analysis was performed with 1000 permutations against the specified genets. For the pre-ranked analysis involving glioblastoma molecular signatures, the signature genests were defined based on relevant publications (Verhaak et al. 2010; Q. Wang et al. 2017; Richards et al. 2021; Neftel et al. 2019; Garofano et al. 2021).

The single sample GSEA analysis (ssGSEA) was performed using the freely available ssGSEA2.0 for R. The analysis was done on normalized log(LFQ) values for the proteomics data and CPM values for RNA sequencing data, against the MSigDb genesets (Subramanian et al. 2005; Liberzon et al. 2015) or the curated post-translational modification (PTMSigDB) database (Krug et al. 2019b). Results are presented as signature-wise normalized z-score heatmaps or group-based mean normalized enrichment scores (NES).

3.2.4. TCGA data preparation and analysis

The TCGA-GBM data was obtained through the *TCGAbiolinks* R package, and the data was queried and processed using *TCGAWorkflow* and *TCGAWorkflowData*. For the analysis, legacy data was used to obtain raw count values for the patients with available Ilumina HiSeq RNA sequencing data. IDH mutated samples were excluded based on the reported IDH status and the remaining samples were normalized and processed according to the RNA sequencing protocol detailed below.

For the CIBERSORTx analysis, a web-based tool was used (Newman et al. 2019). A previously published signature of glioblastoma cell types was used as a gene-expression matrix (Mehani et al. 2022)

3.2.5. RNA sequencing data preparation and analysis

All RNA sequencing samples in this thesis were total cellular RNA pre-treated with on-column digestion of genomic DNA. Library preparation and sequencing was performed by the DKFZ Genomics and Proteomics core facility. Alignment of the rads was performed by the DKFZ Omics core facility (ODCF). U251-MG cells were sequenced using the HiSeq4000 instrument with read length of 50bp. mGB2 mouse cells were sequenced using the NovaSeq 6000 SP with read length of 150bp.

RNA sequencing processing was performed using R packages *limma* and *DEseq2*. Briefly, raw counts were filtered so that all genes with less than 10 counts per group were omitted from downstream analysis. Normalization was performed using variance stabilizing normalization, CPM, and log(CPM) (LCPM) values were calculated based on the normalized values Further filtering was performed based on the LCPM values to avoid overrepresentation of genes with low expression. Differential expression analysis was done with model fitting of a group-based model matrix.

3.2.6. Mouse methylation array analysis

For the mouse methylation array, DNA was collected from the mGB2 cells and isolated using the Qiagen DNA extraction kit. The sample preparation and chip measurements were performed by the DKFZ Genomics and Proteomics core facility using the Infinitum Methylation Mouse BeadChip.

Analysis was performed using the raw idt values provided by the facility. For the analysis, R packages originally designed for the human methylation array analysis *minfi*, *knitr*, *DMRcate* were modified to fit with mouse methylation data by utilizing the mouse-specific array annotation and manifest packages: *IlluminaMouseMethylationanno.12.v1.mm10* and *IlluminaMouseMethylationmanifest*.

The quality of the samples was checked by assessing average p-values for all probes across each sample. Probes with low quality detection were excluded from downstream analysis. Methylated and unmethylated data was normalized using quantile normalization. Differential methylation was calculated based on M-values using the same method as for differential expression specified in section 2.2.4.

Correlation of expression and methylation data was performed on significantly differentially expressed and significantly differentially methylated genes using spearman's ranked correlation analysis.

3.3. Laboratory Methods

3.3.1. Cell culturing and conditions

Human glioblastoma cells U251-MG were cultured in DMEM (low glucose) medium containing 10% FCS and 1% Penstrep. The cells were propagated as adherent cultures in 10% CO_2 conditions at 37°. After reaching confluence, cells were washed once with PBS and detached using Trypsin. Cells were either passaged for further culturing or seeded for experiments after counting using the ViCell automated cell counter.

Mouse glioblastoma cell line mGB2 was cultured in DMEM/F12 medium with the addition of 1% Penstrep, 1% B27 supplement, 1% N2 supplement, 10ng/mL hEGF and 10ng/mL rhFGF. The cells were cultured as neurospheres with 5% CO_2 at 37°C. Medium was exchanged every two days during culturing. Once the neurospheres reached 200-300um in diameter, the cells were transferred to a 15mL conical tube, and the spheroids were allowed to settle. The spheres were dissociated in 300-500ul Accutase with mild agitation and washed using DMEM/F12 medium without the added growth factors. The cells were either passaged for further culturing or counted and seeded for experiments using the ViCell cell counter.

3.3.2. *In vitro* cell differentiation

For the mGB2 cell differentiation experiments, the mGB2 cell line was first attached to the culturing plates. Culture dishes were coated using 10 times diluted ECM in cold DMEM/F12 medium for 1h at 37°C. When cells were cultured on cover slips, the coverslips were placed in a 24-well plate and sterilized under UV light for 1h prior to coating. Following the incubation, the appropriate number of cells for the experiment was seeded directly after removing the coating medium.

For the stem cell (SC) condition, the DMEM/F12 medium containing growth factors described in 2.3.1. was used. For the differentiating condition, DMEM/F12 was supplemented with 1% Penstrep and 5% fetal calf serum (FCS). For all differentiation experiments, the cells were cultured for 8 days unless otherwise specified, with passaging after 4 days of culture and medium exchanges every 2 days.

3.3.3. *In vitro* human macrophage differentiation

For the human macrophage and conditioned medium experiments, the conditioned medium was collected form cultured U251 cells. Once the cells reached confluency, they were washed once and cultured with fresh medium for an additional 24h. The conditioned medium was then collected, spun down at 2000rpm for 10min, filtered through a 0.22um filter and frozen at -80°C until use.

Human buffy coats were ordered from the Mannheim blood bank and kept at room temperature until isolation. The isolation of peripheral blood monocytes (PBMC) was performed using ficol gradient centrifugation. Once isolated, PBMCs were washed with PBS and seeded in serum free medium at a density of 300.000 cells/cm^2. The PBMCs were left in a 5% CO_2 incubator at 37°C for 3h until the monocytes attached to the dish. The dishes were then washed multiple times with serum free medium and cultured with either control or conditioned DMEM glucose low medium with 10% FCS, 1% Penstrep and 25ng/mL human recombinant M-CSF. The medium was replaced after 2 days after seeding and then every 3 days during the culturing.

3.3.4. Lentiviral production and transduction

For lentiviral production, the second-generation packaging system was used with plasmids psPAX.2 and pMD2.G. Virus production was performed using the HEK293T cell line. HEK293T cells were seeded 1 day prior to transfection at a density of 5 million cells per 10cm dish. The next day, the cells were transfected with a combination of the two packaging plasmids and the appropriate vector (2ug, 2ug and 4ug, respectively) and PEI (1mg/ml) in a ratio of DNA:PEI=1:3 in OptiMEM. The following day the medium was exchanged for fresh medium and collected again after 48h for ultracentrifugation (90min, 25.000 rpm at 4°C). The virus was resuspended in 100ul of OptiMEM over night, aliquoted and stored at -80°C until use.

For all transductions, lentiviruses were used at a 1:1000 dilution. The cells were transduced over night and the medium exchanged the following day. Cell selection and other experiments were performed 2 days after viral transduction.

3.3.5. CRISPR/Cas9 editing and Bcat1 knockout

CRISPR/Cas9 editing was used to knockout the Bcat1 gene from the mGB2 cell line. The cells were transduced with a lentivirus carrying inducible Cas9 expression and a puromycin resistance cassette (TLCv2) and the single-guide RNA (sgRNA) targeting Bcat1 or a non-targeting control (NT). 2 days after transduction, cells were selected using puromycin (1µg/mL) until all of the untransduced cells were dead. Once recovered, Cas9 expression was induced in the cells with doxycycline (1µg/mL) for 48h prior to single-cell seeding. The cells were seeded at a density of 0.5 cells/well in a 96-well U-bottom plate for single cell cloning. The medium was refreshed or changed in the following 2 weeks, or until the single-cells grew enough to be expanded into 24-well plates. Bcat1-KO screening was performed via western blots and a minimum of 5 knockout clones further expanded and cryopreserved. In the cells transduced with a non-targeting sgRNA, a random selection of 5 clones was made. Lack of Cas9 expression without doxycycline was confirmed via Westernblot against the Cas9 protein.

The expanded control and Bcat1-KO mGB2 clones were transduced with a lentivirus containing the PGK-Neo-V5-Luc construct expressing luciferase and a neomycin resistance cassette. The transduced cells were selected using geneticin (50µg/mL) until the untransduced controls were dead. V5-tagged Luciferase expression was confirmed using western blotting against the V5-tag.

3.3.6. Immunofluorescent staining procedures

Immunofluorescent stainings on mouse tissue sections or cover slips was done in a similar fashion after initial sample preparation. Mouse tissue cryosections on SuperFrost Plus slides was rehydrated in PBS at 37°C for 10min. Individual tissue sections were circled with the PAP pen and further staining procedures were performed in the same way as for cover slips.

For cells cultured on cover slips, the growth medium was washed with PBS, and the cells were fixed using 4% PFA at room temperature for 15min. Following fixation, the cover slips were washed in PBS and the staining procedure was done on parafilm in a humid chamber.

First, samples were permeabilized and unspecific binding was blocked using the blocking buffer (PBS, 5% BSA, 0.5% TritonX-100, 0.02% Sodium-azide) for 1h at room temperature. Samples were incubated with the primary antibody immediately after washing in 5x diluted blocking buffer

in PBS (the antibody concentrations can be found in Table 1) over night at 4°C. The samples were washed 3 times in PBS and incubated with the appropriate secondary antibodies in 5x diluted blocking buffer in PBS for 1h at room temperature (secondary antibody concentrations in Table 2). Samples were washed in PBS 3 times for 5min and mounted with DAPI-containing mounting medium with coverslips for mouse tissue slides or by inverting the cover slips with cultured cells onto slides. The slides were incubated at room temperature for 15min and stored at 4°C until imaged.

3.3.7. Confocal microscopy

Confocal microscopy was performed using the Leica SP8 confocal microscope. The majority of confocal imaging was performed using the 40x objective, aside from high-resolution cell morphology images which were obtained using the 63x objective. Both objectives were used with immersion oil. Laser intensities, gain and offset were kept consistent between samples for each individual staining. All image processing was performed using ImageJ.

3.3.8. Whole-slide fluorescent microscopy

Whole brain-slice imaging was performed using the Axioscan 7. DAPI was used for defining coarse and fine focus and all imaging was performed using the 40x objective. All channel settings were kept consistent for a single imaging session across the samples with the same stainings. All image processing was performed using ImageJ.

3.3.9. Immunoblotting procedures

Samples for immunoblotting were collected by lysing cell pellets in RIPA buffer containing protease and phosphatase inhibitors. Samples were incubated on ice for 15min and spun at 13.000rpm for 25min at 4°C in a tabletop centrifuge. Supernatants from each sample were transferred to a fresh tube.

Protein concentration was measured using a BCA assay. Briefly, a standard curve was constructed using samples containing 2, 1, 0.5, 0.25 0.125 and 0 mg/mL BSA. Using the BCA

reagents, the absorbance value for all samples was measured in triplicates and protein concentrations were calculated based on the standard curve.

20ug of protein were loaded on a pre-cast SDS-PAGE gel (4-12% gradient) per well and samples were run at 100V in MOPS running buffer until reaching the bottom of the gel. Proteins were transferred to a methanol activated PVDF membrane in Blotting buffer at 120V for 1.5h on ice. Membranes were blocked in TBS-T (TBS, 0.1% Tween20) buffer with 5% milk for 1h at room temperature and incubated with the primary antibody diluted in 5% milk TBS-T (for specific dilutions see Table 1) at 4°C over night. Membranes were washed in TBS-T 3 times for 10 min and incubated with an HRP-linked secondary antibody for 1h at room temperature in 5% milk TBS-T. After washing 3 times in TBS-T for 5min, the western blots were developed using ECL and the Intas imaging system.

3.3.10. Real time quantitative PCR (RT-qPCR)

RNA was extracted from tissues and cell pellets using the RNeasy Qiagen kit according to the manufacturer instructions. During extraction, on-column genomic DNA digestion was performed using Qiagen DNase A. RNA concentration was measured using Nanodrop.

cDNA synthesis was performed using the protoscript II kit. Briefly, 500-1000ng of RNA per reaction was used with 10uM Random hexanucleotide primers, 0.5uM of each dNTP and the reaction buffer and DMSO according to manufacturer instructions. cDNA was synthesized for 1h at 42°C, followed by a 20min enzyme inactivation at 65°C. cDNA was diluted to a final concentration of 6.25ng/ul (according to starting RNA amount).

RT-qPCR was performed using the 2x SYBRGreen PCR mix. Per reaction, 12.5ng of cDNA was used and forward and reverse primers with a final concentration of 0.5uM each. After the initial heating step for 3min at 93°C, the PCR was performed in 40cycles according to the SYBRGreen manual using QuantStudio 5. Threshold values for each gene were automatically determined using the QuantStudio software and expression fold changes were determined with the ddCt method.

3.3.11. Click-iT EdU assay

The Click-iT EdU assay for flow cytometry was performed following manufacturer instructions. Briefly, cells were incubated with EdU at a 10uM concentration for 1h unless otherwise specified.

Following the incubation, cells were detached, spun down and fixed in 4% PFA for 15min at room temperature. After a PBS washing step, the cells were permeabilized in 70ul PBS-T (PBS, 0.1% TritonX-100) for 30min at room temperature. The cells were washed in PBS 1% BSA and resuspended in 100ul of the Click-iT reaction cocktail with AF647-conjugated azide (prepared according to manufacturer instructions). The cells were incubated for 30min at room temperature protected from light and washed with PBS 1% BSA. Cells were resuspended in 200ul of PBS 1%BSA and 1 drop of the NucBlue dye was added. Cell positivity was assessed using flow cytometry.

3.4. Mouse procedures

All mice used in this study were acquired from Janvier labs (Table 6). All animal experiments were performed according to welfare regulations and were approved by the authorities under the approval number G314-19. During the experimental duration, the mice were housed in a dedicated mouse room with 12h day-night cycles and regulated temperature.

3.4.1. Cell preparation and intracranial injection

For all transplantation experiments, the mouse mGB2 line was used expressing GFP and V5-tagged Luciferase. The cells were collected through spheroid sedimentation and the neurospheres were dissociated using accutase with mild agitation at 37°C. Cells were counted and washed with PBS. Unless otherwise specified, the cells were resuspended in PBS at a final concentration of 200.000 cells/ul and kept on ice during the injection procedure.

Prior to the injection and 48h following the transplantation, analgesia was administered as defined in the animal protocol G314-19. Mice were anesthetized prior to the procedure with 2.5% Isoflurane in air and kept under anesthesia during the procedure with 1.5% isoflurane in air. The transplantation procedure was performed using the stereotactic injector. Mouse skull was exposed in the area of the bregma, and a small opening was made 2mm left of the bregma. Injection of the cells was done 3mm deep into the brain tissue, corresponding to the subventricular region. 2ul of the cells was injected over 10min, after which the syringe was slowly removed. The head wound was stitched, and the mice were left to recover.

3.4.2. In vivo bioluminescent imaging

Bioluminescent imaging of the tumors was performed using the IVIS measuring system. The mice were anesthetized with 2.5% isoflurane in air and kept under anesthesia with 1.5% isoflurane in air. Luciferin was injected at a concentration of 5mg/kg (15mg/mL stock solution in saline) to each mouse. Measurements were made 10min after the luciferin injection with a 3min exposure time

3.4.3. Brain collection and cryopreservation

Upon reaching end criteria or a pre-determined experimental endpoint, mice were sacrificed using CO_2 and the brain was quickly extracted. The entire brain, or just the injected hemisphere was fixed in 4% PFA in PBS for 24h at 4°C. Following the fixation, the brains were washed in PBS and cryoprotected in 30% Sucrose until sinking in the solution. Brains were frozen in cryomolds in Optimal cutting temperature compound (OCT) on dry ice and stored at -80°C until sectioned.

Sectioning was performed on a Leica CM1869 cryostat at-20°C. Brains were trimmed until reaching the tumor region (determined through GFP observation) and serial sections were collected (6-10um thickness) on Superfrost PLUS slides. Sections were dried 1h at room temperature and kept at -20°C until further processing

4. Results

4.1. The role of BCAT1 in the maintenance of mitotic fidelity

This first section of my doctoral thesis will refer to the study of the function of BCAT1 in mitosis, first identified by Liliana Francois (L. Francois) a PhD and postdoc in our lab (Division of Molecular Genetics at the DKFZ). Here I present the data that I generated, which resulted in a shared first authorship on the paper “BCAT1 redox function maintains mitotic fidelity” published in Cell Reports in October 2022 (Francois et al. 2022).

4.1.1. Combined site- and condition-specific and paired tail imputation result in clear sample separation of proteomic and phosphoproteomic LN229 and U251 data

The role of BCAT1 in mitosis was proposed after observations of BCAT1 knockout (BCAT1-KO) causing severe mitotic abnormalities in glioblastoma and other non-malignant cells. To explore the effects of BCAT1-KO in mitosis of U251 and LN229 glioblastoma cell lines, I analyzed LC-MS² (liguid chromatography mass spectrometry) datasets of unsynchronized and nocodazole-mitotically synchronized cells on the level of the whole proteome and the phosphoproteome. The samples for analysis were prepared by L. Francois and phosphopeptide enrichment by the Mass Spectrometry core facility of the DKFZ. The analysis was performed on the obtained label-free quantification (LFQ) values.

To avoid false positive findings, I used stringent filtering which resulted in the retention of approximately 3500-4500 peptides and more than 10000 phosphopeptides per sample (Figure 10A and 10B, Supplementary Figure 1A and 1B). As expected, the proteomic profiles of the two cell lines diverged significantly, overwhelming any effects of the BCAT1 status (NT vs KO) (data not shown). Because of this, I analyzed the data from the two cell lines separately for any downstream purpose.

Applying variance stabilizing normalization across the datasets was sufficient to obtain a clear separation of the U251 samples in a PCA (principal component analysis) (Supplementary Figure 1C and 1D, Unprocessed and normalized LFQ values). However, the normalization alone did not result in clear separation of the LN229 samples (Figure 10C and 10D, Unprocessed and normalized LFQ values). I used site- and condition-specific imputation (Kim et al. 2021) to impute missing values attributed to technical effects which only marginally improved sample separation (Figure 10C and 10D, scImp LFQ values). Finally, in order to impute the missing values attributable to biological effects, I used modified paired tail imputation (ptImp, (Kim et al. 2021)). Following this imputation method, the sample separation became clear in both the U251 and LN229 samples in a PCA (Figure 10C and 10D and Supplementary Figure 1C and D, ptImp LFQ values) and the data could be used for further downstream processing.

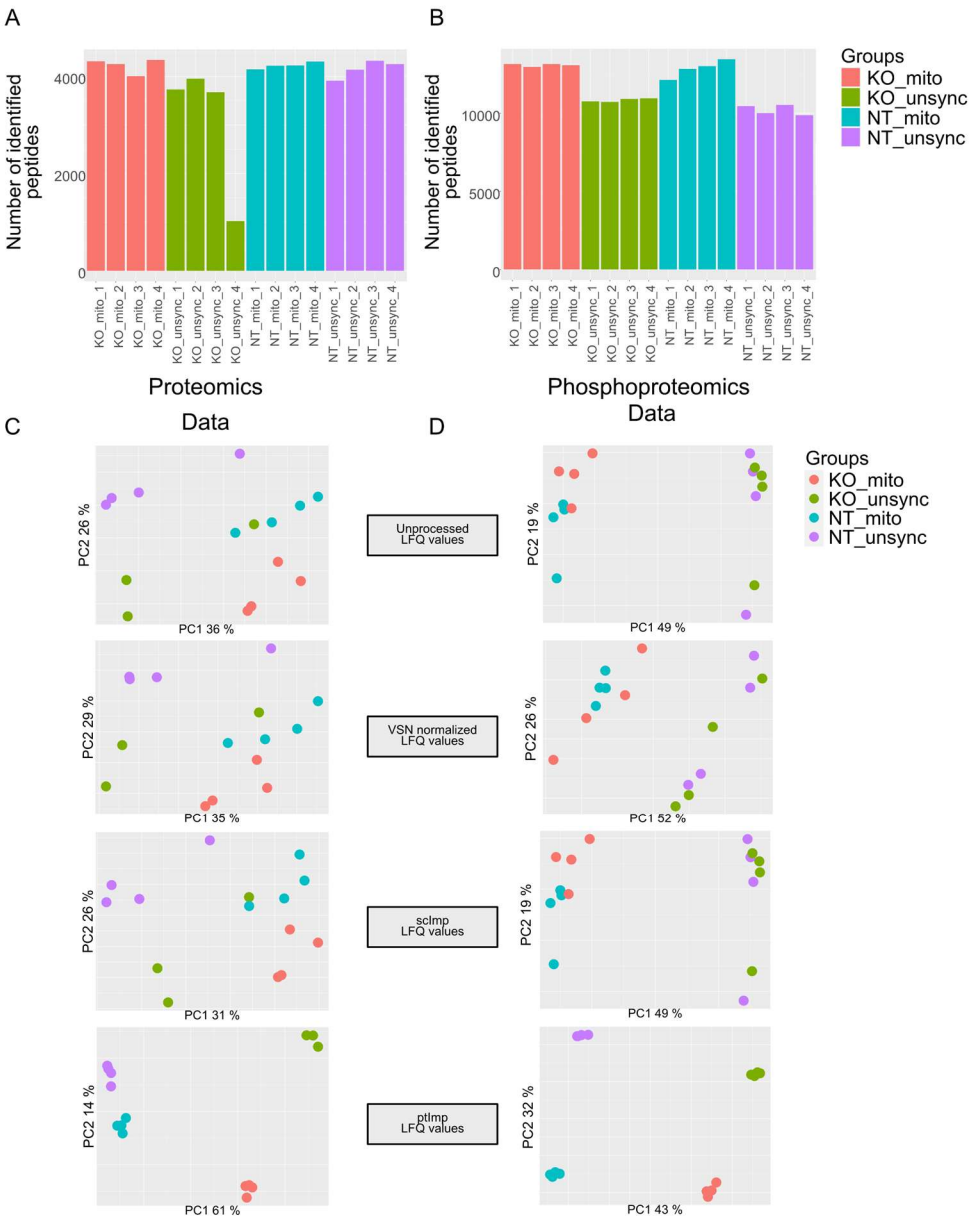

Figure 10 Proteomic and phosphoproteomic data preparation of LN229 control (NT) and BCAT1-KO (KO) mitotic (mito) and unsynchronized (unsync) samples. A) Number of identified peptides and B) phosphopeptides in the respective samples following stringent filtering for low-detection proteins. C) Principal component analysis of proteomic and D) phosphoproteomic datasets in different stages of data pre-processing: vsn normalization, site- and condition-specific imputation (scImp) and paired tail imputation (ptImp).

4.1.2. GO-Term enrichment confirms mitotic enrichment of the samples

In order to confirm that the mitotic synchronization with nocodazole treatment performed by L. Francois resulted in samples sufficiently enriched in mitotic cells, I modeled differential protein expression between the unsynchronized and mitotically synchronized U251 and LN229 whole proteome samples.

Using the differentially expressed proteins and the *goseq* R package (Young et al. 2010), I determined GO-term enrichment for Cellular Compartment (CC) and Biological Process (BP) terms restricting the analysis to proteins which were significantly differentially expressed (adjusted p-value <0.05) with a minimum log fold change difference of 1. Figure11A-D illustrates top enriched BP and CC terms in the mitotic samples of control (Figure 11A and 11C) and BCAT1-KO (Figure 11B and 11D) cells. The majority of the enriched terms were specific for the mitotic machinery or cellular division, indicating that both the control and BCAT1-KO samples were highly enriched for mitotic cells through the synchronization treatment.

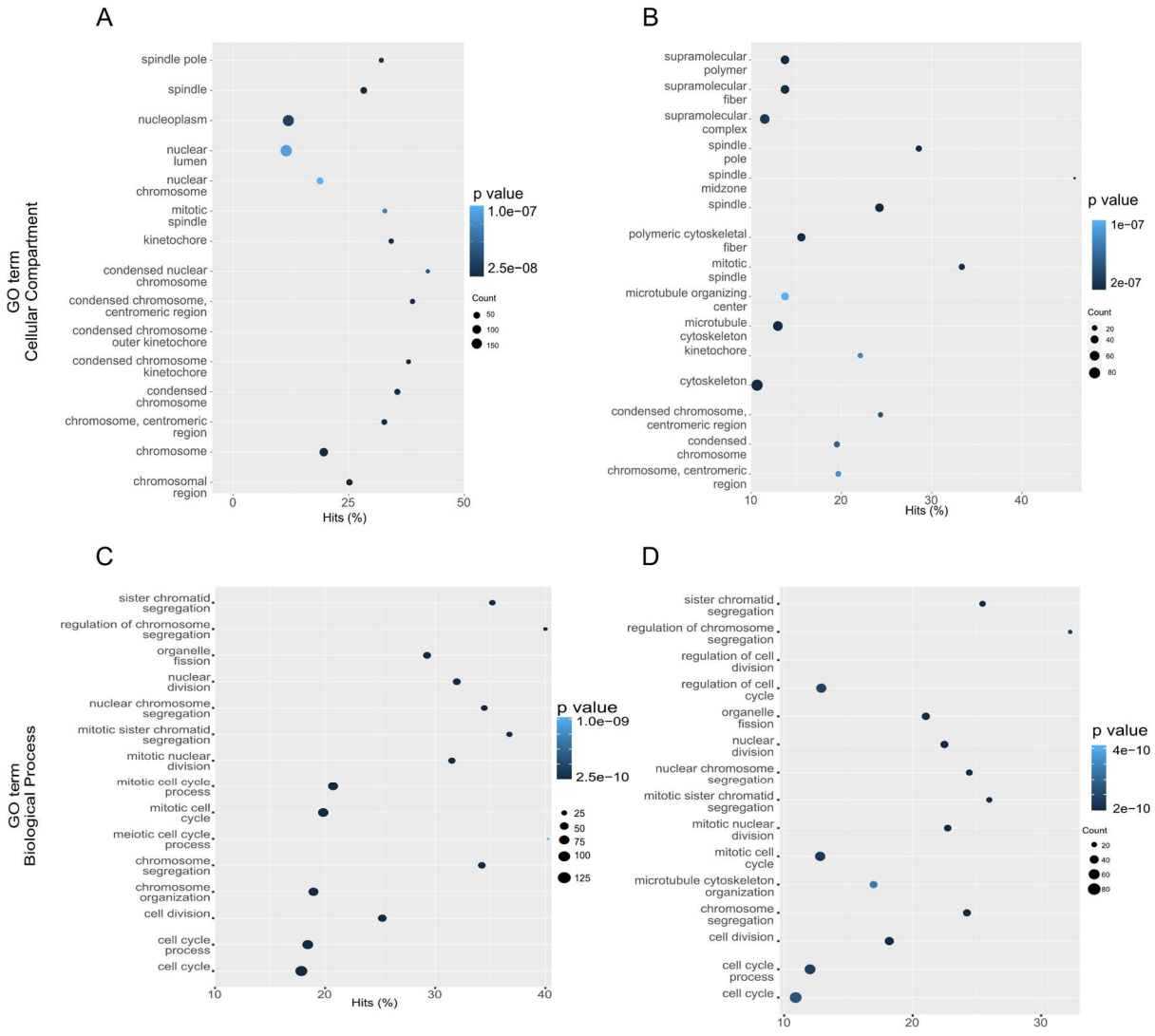

Figure 11 Biological Process (BP) and Cellular Component (CC) GO-term enrichment analysis of the U251 control and BCAT1-KO proteomes. A) Top BP-enriched terms in mitotic control and B) BCAT1-KO cells in comparison to the unsynchronized samples. C) Top CC-enriched terms in mitotic control and D) BCAT1-KO cells in comparison to the unsynchronized samples. Only proteins with differential expression of fold change higher than 1 and adjusted p-values lower than 0.05 were considered for this analysis. Sizes of data points correspond with gene counts and the color scale with the significance (p-value) of each term enrichment.

4.1.3. Robust interference of kinase activity and post-translational modification signatures confirm the mitotic enrichment through the activity of canonical mitotic kinases and related pathways

Cellular division is a tightly regulated process orchestrated through the activation and trans-localization of different mitotic kinases such as TTK, PLK1, BUB1, AURKA, AURKB and many others (McIntosh 2016; Gould and Nurse 1989; Alcasabas et al. 2001; Seki et al. 2008). A common method for determining kinase activity in phosphoproteomic datasets is Kinase-Substrate enrichment analysis (KSEA). However, due to the limitation of sample preparation, and in particular the phosphopeptide enrichment, our dataset does not contain phospho-tyrosine sites which could interfere with kinase enrichment inference. To test whether our dataset nevertheless can be used for kinase and pathway analysis, I used robust interference of kinase activity (RoKAI) (Yılmaz et al. 2021) on mitotic and unsynchronized phosphoproteome samples.

First, I determined differentially phosphorylated sites using differential expression modeling between the phosphoproteome data of unsynchronized and mitotically synchronized U251 and LN229 cells. With the differential phosphorylation log-fold change, I computed the kinase enrichment scores for the mitotic and unsynchronized U251 and LN229 control (Figure 12A and Supplementary Figure 2A) and BCAT1-KO (Figure 12B and Supplementary Figure 2B) cells. This analysis showed a strong enrichment score for the activity of mitotic kinases such as AURKB, TTK, AURKA, PLK1 and others, in the synchronized samples.

These results further confirm the mitotic enrichment of the synchronized samples and facilitate the possibility of inferring kinase activity using our phosphoproteomic dataset even in the lack of tyrosine-phosphorylation sites.

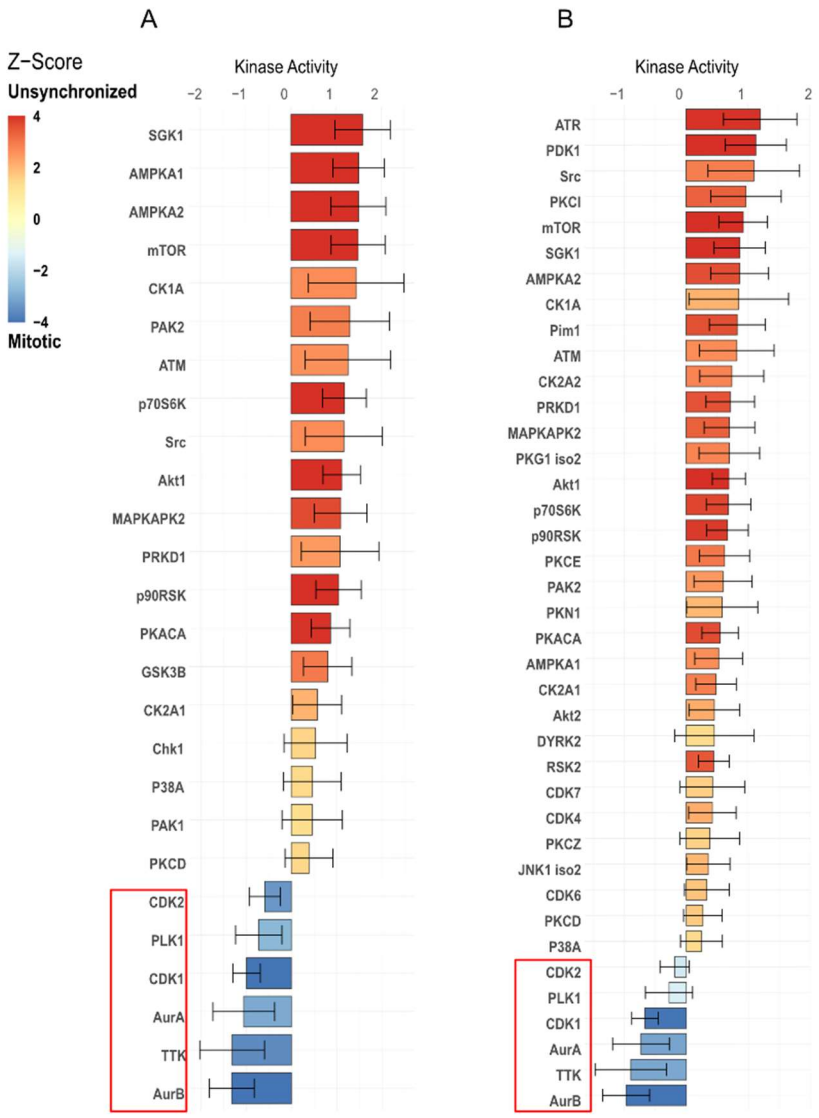

Figure 12 RoKAI Kinase Substrate enrichment analysis of U251 mitotic vs unsynchronized A) control and B) BCAT1-KO cells. The x-axis represents kinase activity scores with the positive scores corresponding to kinases with enriched activity in Unsynchronized samples and the negative to the enriched activity of the kinases in the Mitotic samples. The color scale denotes the z-score value of the inferred kinase activity in red (Unsynchronized) or blue (Mitotic). The graph was produced using the web-based tool http://rokai.io

Finally, I decided to test our data using the post-translational modification (PTM) signatures database (PTMSigDB) which contains not only kinase specific substrates but also phosphosite-specific up- and down-regulation signatures relating to biological pathways and inhibitor perturbations (Krug et al. 2019a). Using the normalized and imputed LFQ values I determined significantly enriched pathways in the mitotic control (Figure 13A and Supplementary figure 2C) and BCAT1-KO samples (Figure 13C and Supplementary Figure 2D). Single sample gene set enrichment analysis (ssGSEA) using the PTMSigDB shows a clear mitotic enrichment in both cell lines and both control and BCAT1-KO cells through the significant enrichment of pathways associated with mitotic kinases such as AURKA (Figure 13B and 13D, Supplementary Figure 2E and 2F), and perturbation pathways such as nocodazole treatment-associated signatures (Figure 13A and 13C, highlighted pathways).

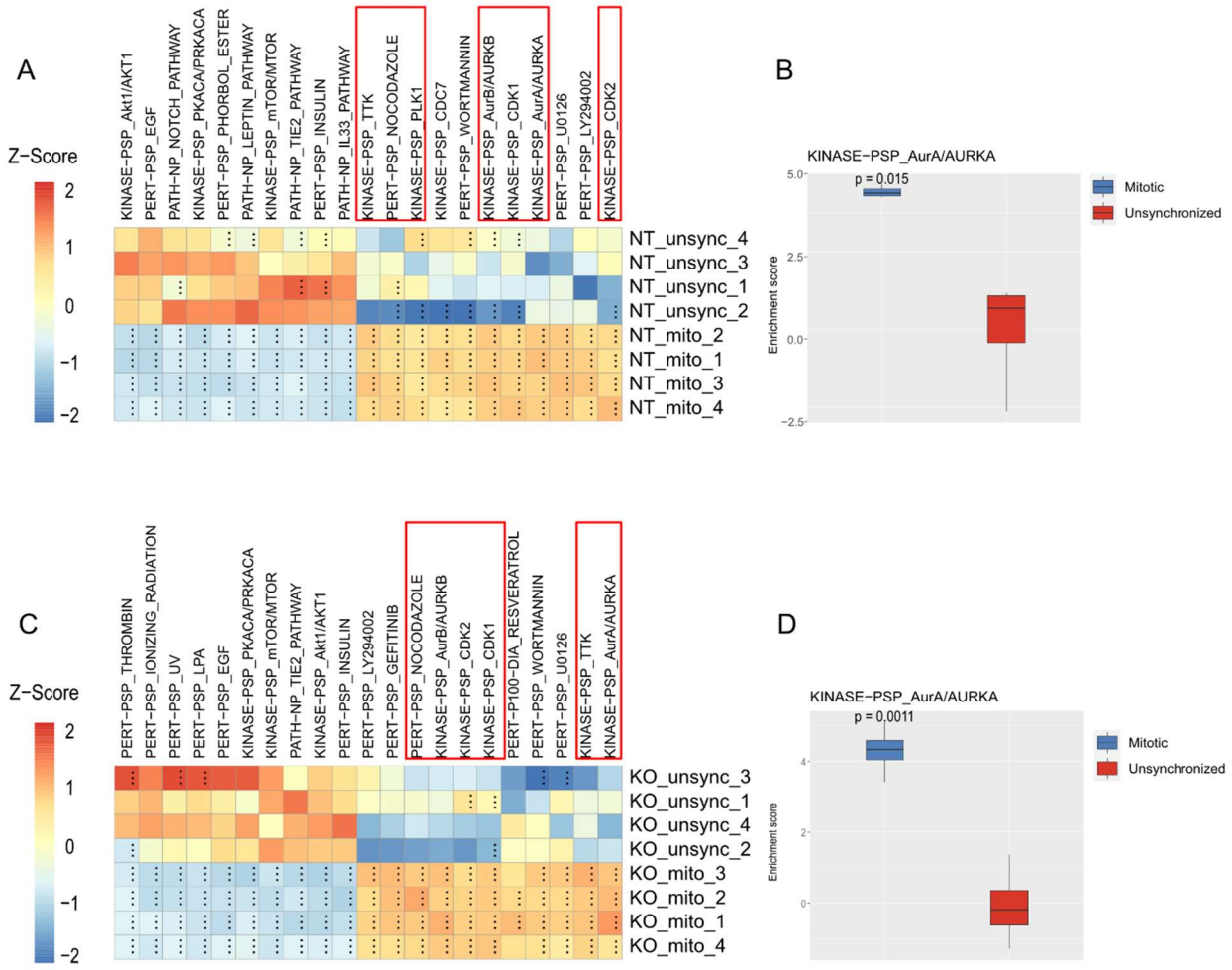

Figure 13 ssGSEA of PTMSigDB signature enrichment in U251 cells. A) Z-score normalized heat map of signatures positively (red) and negatively (blue) enriched in control (NT) and C) BCAT1-KO (KO) mitotic (mito) and unsynchronized (unsync), with noticeable mitotic signatures highlighted with red rectangles. B) Tukey plots of average normalized enrichment score (NES) across the 4 mitotic (blue) and unsynchronized (red) samples for the AURKA signaling signature in control and D) BCAT1-KO cells. Statistically significantly enriched signatures (adjusted p-value<0.05) are denoted with "…" in panels A) and C). Statistical significance of the NES difference in panels B) and D) was determined using an unpaired two-tailed student's t-test. Whiskers represent 1.5IQR (Interquartile range)

4.1.4. BCACT1 interacts with many components of the mitotic machinery during cell division

Following the observations of L. Francois that BCAT1 localizes to the nucleus and the mitotic spindle, we wanted to confirm interactions with the mitotic machinery with a LC-MS² approach. BCAT1-HA (HA-tagged BACT1) or CFP-HA (HA-tagged Cerulean Fluorescent Protein) were overexpressed in U251 BCAT1-KO cells, which were then synchronized in mitosis and subjected to HA-tag co-immunoprecipitation (co-IP). The co-IPed proteins and the input proteomes were submitted to the Mass Spectrometry core facility of the DKFZ for the LC-MS² analysis.

After filtering, the number of peptides pulled down with the CFP-HA coIP control was minimal (Figure 14A, control IP), confirming a specific coIP protocol. To analyze the data, I assigned a positive LFQ value to all peptides detected in the coIP samples and negative LFQ values to the peptides present in the input but not co-IPed with BCAT1-HA. Using these values, I performed a pre-ranked GSEA against the Hallmarks dataset (MSigDb database). I found that the top significantly enriched (adjusted p-value<0.01) signatures in the BCAT1-HA bound fraction correspond to the Mitotic Spindle (NES=2) and the G2M checkpoint (NES=2.3) signatures (Figure 14B). Furthermore, upon visualization of the proteins involved in mitosis, the organization of the mitotic spindle and the kinetochore (Figure 14C), the enrichment of those proteins in the BCAT1-HA coIP sample becomes exceedingly clear.

To exclude unspecific findings, the same GSEA analysis was performed using the proteins bound by CFP-HA and no statistically significant enrichment could be found (Supplementary Figure 3A), which was also confirmed upon mitotic network visualization (Supplementary Figure 3B).

This data indicates that BCAT1 binds to a large number of mitotic regulatory and structural components.

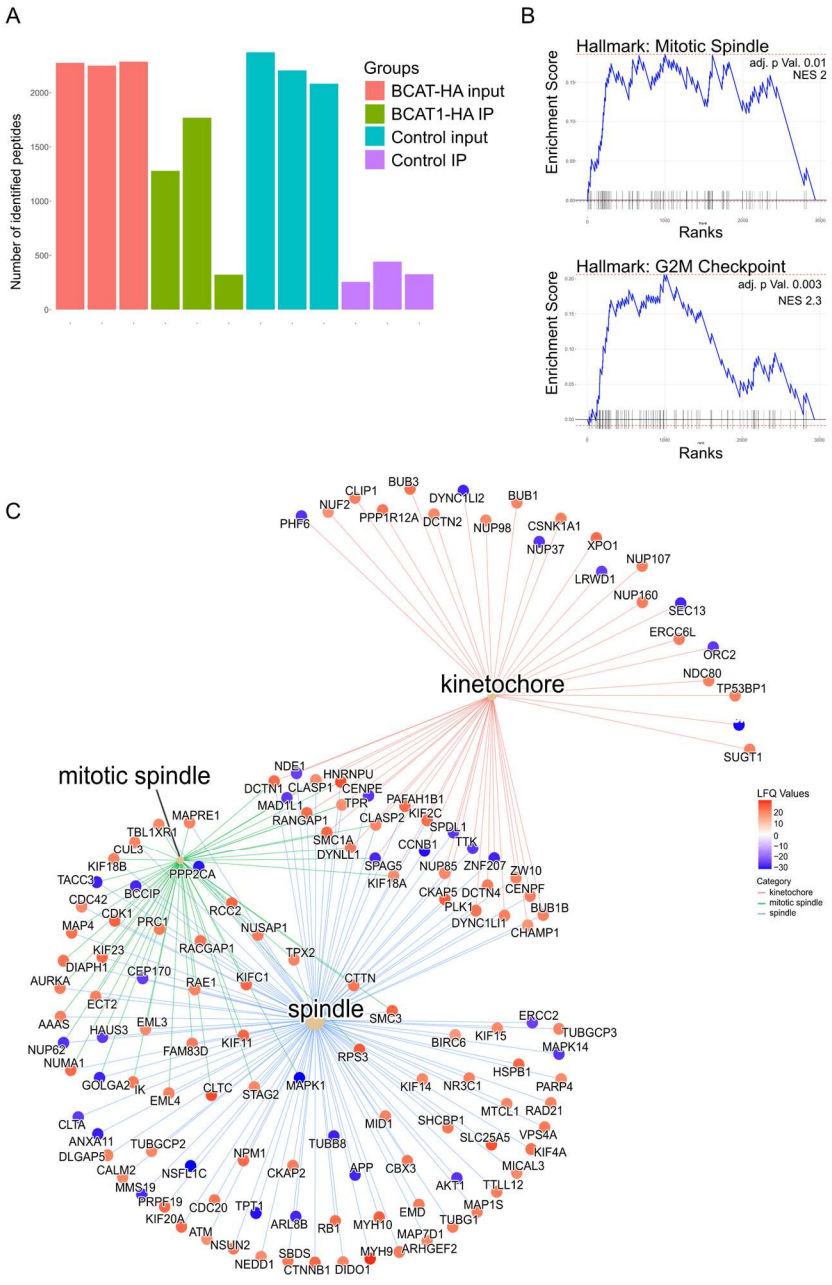

Figure 14 BCAT1-HA co-immunoprecipitation of mitotic proteins in synchronized U251 BCAT1-KO cells. A) Quantification of proteins found in the BCAT1-HA and CFP-HA co-immunoprecipitation samples (BCAT1_IP1-3 and ControlIP1-3, respectively) and their respective inputs. B) pre-Ranked GSEA analysis of proteins detected in the BCAT1-HA co-IP fraction (positive values) against the non-bound proteins detected in the input (negative values) according to the Hallmark MSigDb signature sets Mitotic spindle (NES=2, adjusted p-value=0.01) and G2M Checkpoint (NES=2.3, adjusted p-value=0.003). C) mitotic spindle and kinetochore protein networks with BACT1-HA-bound peptides represented as red and the un-bound proteins identified in the input represented as blue nodes.

4.1.5. Protein-level analysis indicates a potential decreased function of the key SAC regulator TTK, but does not explain the full extent of the mitotic defects

Live cell microscopy on LN229 and U251 cells performed by L. Francois indicated that the severe mitotic defects in BCAT1-KO cells could be attributed to an aberrant function of the spindle assembly checkpoint (SAC). To gain more mechanistic insight of this phenomenon, I used the proteomic and phosphoproteomic datasets described previously, comparing mitotic control and BCAT1-KO U251 and LN229 cells.

First, I looked at the protein expression of the well-known central SAC proteins in the two cell lines (Figure 15A). Interestingly, the only protein showing a considerable difference in expression between the mitotic control and BCAT1-KO cells was BUB1B in the U251 cell line (Figure 15A, upper panel). The remaining SAC proteins were expressed at similar levels. As the mitotic defects were observed in both cell lines and that the BUB1B expression was modified only in the U251 cells, I considered this not to be the causal event of the mitotic aberrations.

Mitotic kinases of the SAC are themselves regulated by phosphorylation (Seki et al. 2008; Morrow et al. 2005; Abrieu et al. 2001, 1). Since AURKB and TTK are the two important kinases that regulate the activity of the SAC, I looked at the phosphorylation state of these two proteins in the mitotic control and BCAT1-KO cells. After correcting the differential phosphorylation for differences in protein expression, there were no large differences in AURKB phosphorylation between the control and BCAT1-KO cells (Figure 15B, upper panel U251, lower panel LN229). Similarly, only a few phosphosites of TTK were found to be differentially regulated in the two cell lines (Figure 15C). Interestingly, T360 (Threonine 360) showed increased phosphorylation in both the LN229 and U251 control cells in comparison to the BCAT1-KO. This residue was found on the same peptide as the S362 and S363 (Serine 362 and 363) and all three have been reported as TTK autophosphorylation sites which can potentially regulate its function and kinetochore localization. These results indicate a possible impairment of the autophosphorylation function of the key SAC enzyme TTK, however, they do not account for the large-scale aberrations observed.

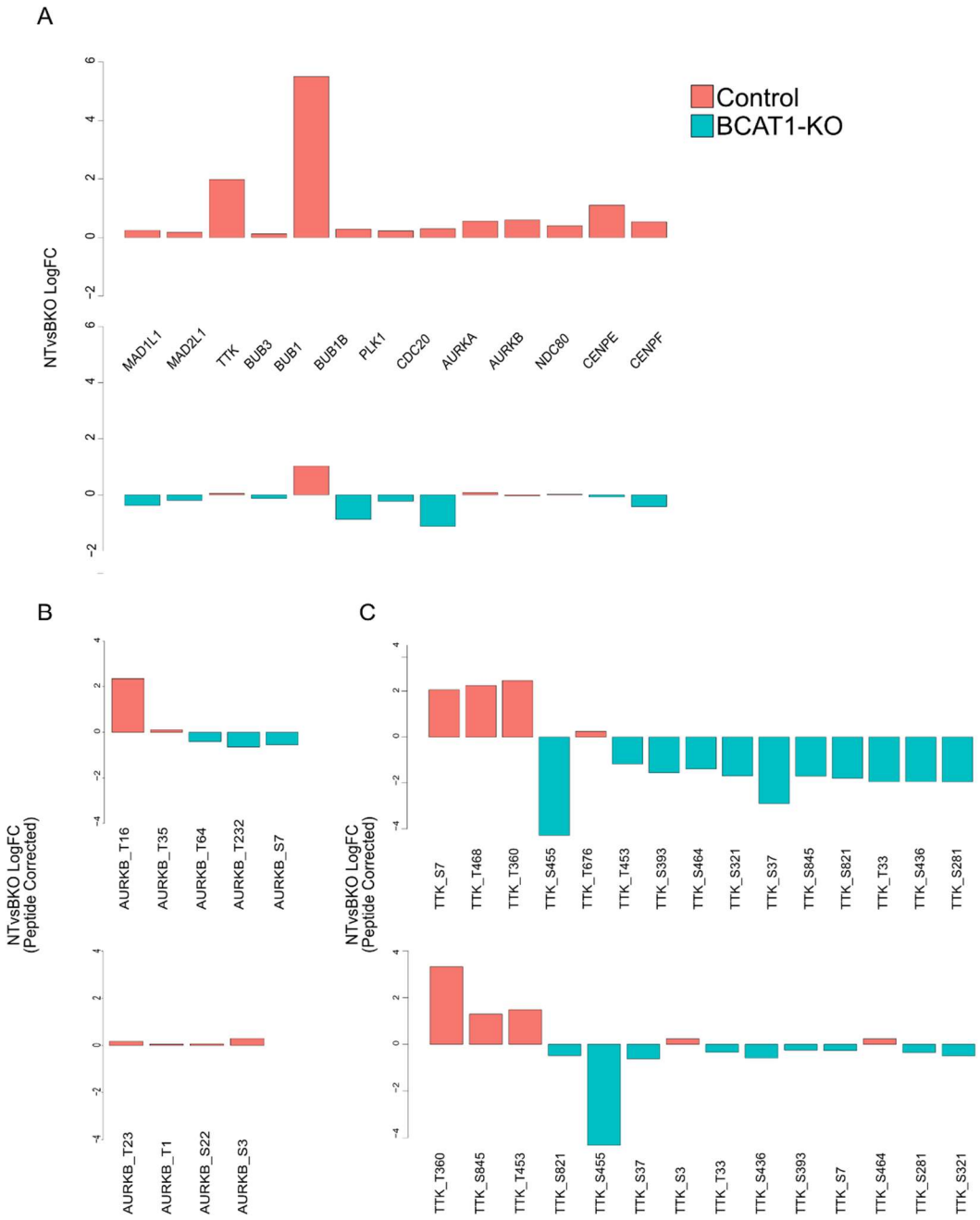

Figure 15 Expression and phosphorylation status of key SAC proteins. A) Protein expression of key SAC regulator proteins with log-foldchange of mitotic control (NT) vs BCAT1-KO (BKO) samples represented on the y-axis. The top panel refers to the U251 and the lower panel to the LN229 cell line. B) Differential phosphorylation of identified phosphosites of AURKB in U251 (top) and LN229 (bottom) mitotic vs control cells, corrected for the differences in AURKB expression. C) Differential phosphorylation of identified phosphosites of TTK in U251 (top) and LN229 (bottom) mitotic control (NT) vs BCAT1-KO (BKO) cells, corrected for the differences in TTK expression.

4.1.6. RoKAI and PTM ssGSEA analysis indicate a reduced function of the key SAC kinases AURKB and TTK in BCAT1-KO LN229 and U251 cells

As the observed mitotic aberrations cannot be readily explained on the level of individual protein expression and phosphorylation, I resorted to an unbiased approach to assess potential differences between control and BCAT1-KO mitotic cells.

Using differentially phosphorylated sites as input for the RoKAI analysis, as described previously, I computed kinase enrichment scores for the control and BCAT1-KO mitotic U251 and LN229 cells (Figure 16A and 16B, respectively). The analysis showed a clear increase in the activity of SAC kinases TTK, PLK1 and BUB1 in the LN229 control mitotic cells in comparison to the BCAT1-KO (Figure 16A, highlighted kinases). In the U251 cells, only an enrichment in the activity of TTK could be observed (Figure 16B, highlighted kinase) using this analysis.

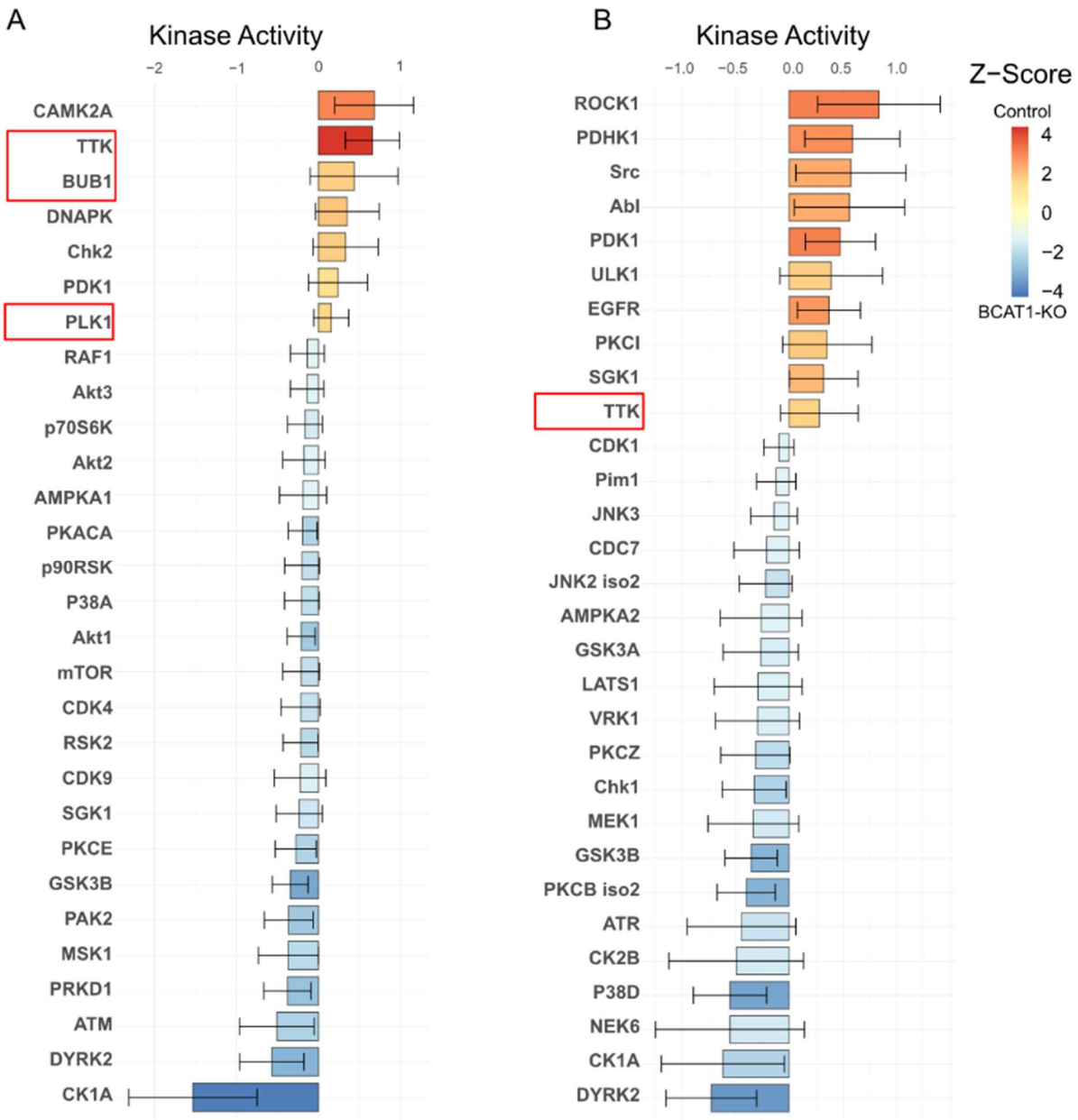

Figure 16 RoKAI analysis of the mitotic control and BCAT1-KO cells. A) RoKAI analysis performed on differentially phosphorylated sites between control and BCAt1-KO LN229 and B) U251 cells with a cutoff of minimum 3 substrates per kinase and an absolute z-score of 1.5

To further confirm these results, I used the same dataset to perform a PTM signature enrichment analysis on both cell lines and represented the results as z-score heatmaps of signatures with a highest median NES difference between control and BCAT1-KO cells (Figure 17A and 17C, U251 and LN229 cell lines, respectively). The results show that both the U251 and LN229 control cells have a higher enrichment score of the pathways associated with AURKB and TTK (Figure 17A and 17C, highlighted pathways). The average NES for both kinases was significantly higher in the control cells in comparison to the BCAT1-KO ones (Figure 17B and 17D).

Combined, these results indicate a reduction in the activity of two of the main SAC kinases responsible for regulating kinetochore assembly and proper microtubule attachment in the BCAT1-KO cells. Deficiencies in these pathways can readily explain the observed mitotic aberrations.

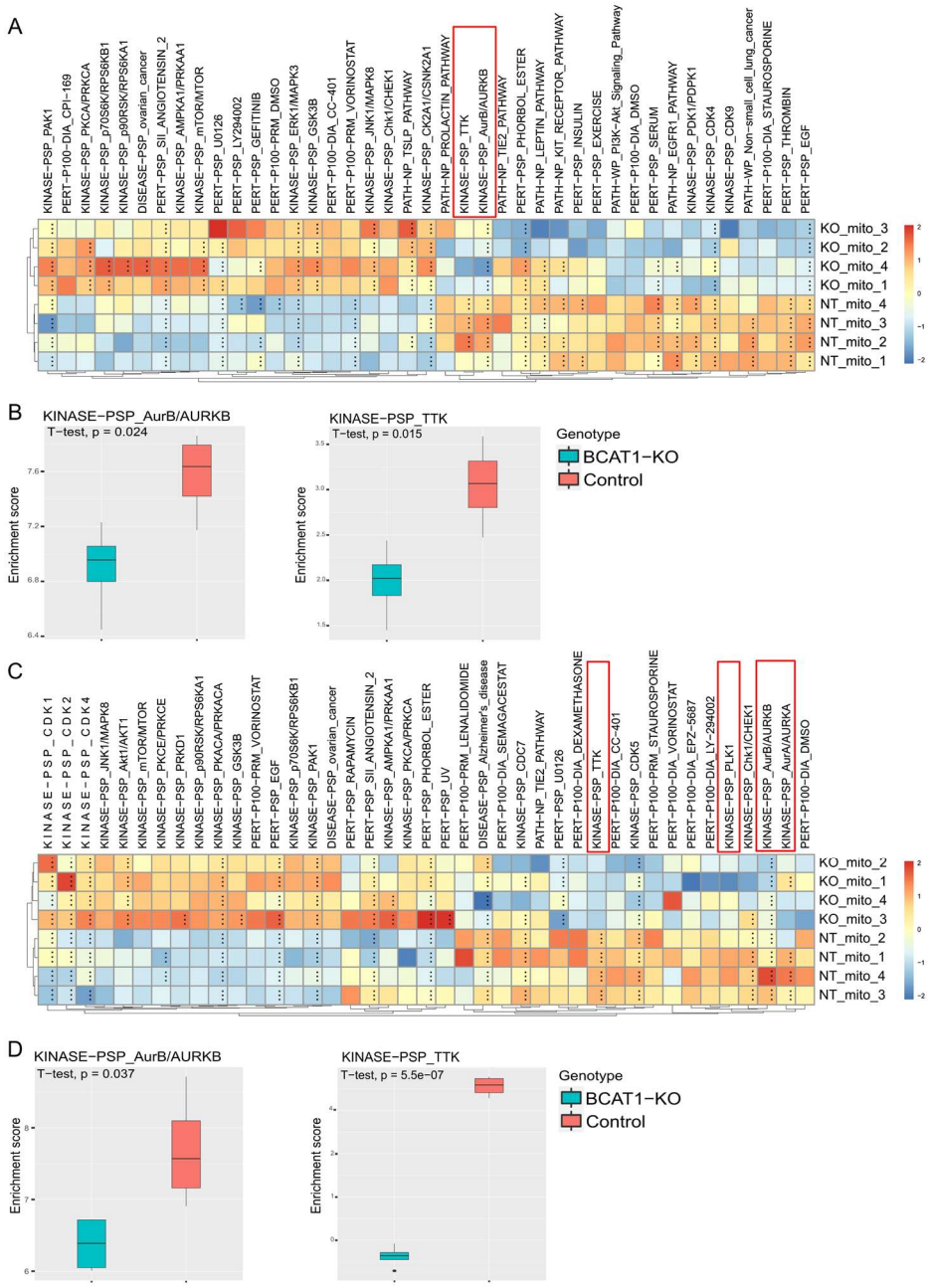

Figure 17 PTM ssGSEA analysis of mitotic control (NT) vs BCAT1-KO (KO) cells. A) z-score heat map of post-translational signature ssGSEA analysis, representing pathways with highest median NES difference between the control and BCAT1-KO U251 and C) LN229 mitotic cells. The color gradient corresponds to the z-score values of NES, the '…' denotes statistically significant enrichment with adjusted p-value < 0.05. Signatures corresponding to well-known mitotic kinases are highlighted with red rectangles. B) Average NES of 4 control (blue) and BCAT1-KO (red) replicates of mitotic U251 and D) LN229 cells corresponding to the AurB (left) and TTK (right) PTM signatures. Statistical significance was determined using a student's t-test and represented in the top left of each plot; error bars signify 1.5 IQR values

4.2. The role of BCAT1 in regulating glioblastoma cell differentiation

The second part of my doctoral thesis consisted of investigating an additional function of BCAT1 in glioblastoma unrelated to mitosis. In these next sections of the results, I will present the role of BCAT1 in differentiation of glioblastoma in human and mouse *in vitro* and *in vivo* model systems.

4.2.1. BCAT1 low-expressing glioblastomas show a predominantly neuronal expressional profile

Recent studies have described many novel molecular subtypes of glioblastoma cells (Q. Wang et al. 2017; Neftel et al. 2019; Garofano et al. 2021; Richards et al. 2021). To begin exploring the role of BCAT1 in glioblastoma, I used the publicly available TCGA-GBM dataset and assessed the correlation between the expression of BCAT1 and various molecular markers in the primary tumors.

I analyzed gene expression in 141 glioblastoma samples. Following the pre-processing, I quantified BCAT1 expression in each of the samples and the 20 highest expressing samples were grouped as BCAT1-high ($BCAT1^{H}$), and the 20 lowest as BCAT1-low ($BCAT1^{L}$) (Figure 18A). A multidimensional scaling (MDS) analysis showed that the $BCAT1^{H}$ and $BCAT1^{L}$ groups clustered distinctly, indicating divergent expressional patterns of the tumors based on BCAT1 expression levels (Figure 18B).

Next, I used the BCAT1 status to determine differential gene expression between the $BCAT^{H}$ and $BCAT1^{L}$ glioblastomas samples. Using the differentially expressed genes (DEG) I performed a pre-ranked GSEA with curated gene signatures from the above mentioned studies describing glioblastoma subtypes (Figure 18C). The $BCAT1^{H}$ tumors show statistically significantly enriched mesenchymal signatures, including those described by Wang et al, Verhaak *et al* and Neftel *et al* (Verhaak et al. 2010; Q. Wang et al. 2017; Neftel et al. 2019)(Figure 18C, Positive NES). On the other hand, the $BCAT1^{L}$ tumors showed a strong enrichment of signatures associated with a more differentiated phenotype, such as the proneural signature described by Wang *et al*, and the neural signatures described by Neftel *et al* and Garofano *et al* (Figure 18C, Negative NES). In fact, when I performed ssGSEA using these signatures and compared the mean NES, I could see a similar trend with a significantly higher mesenchymal enrichment in $BCAT1^{H}$ tumors, and neuronal-like signatures in $BCAT1^{L}$ tumors (Figure 18D).

These results suggest that $BCAT1^{L}$ tumors exhibit a more differentiated state, which could potentially explain the increased survival rate associated with lower BCAT1 expression (Figure 9B).

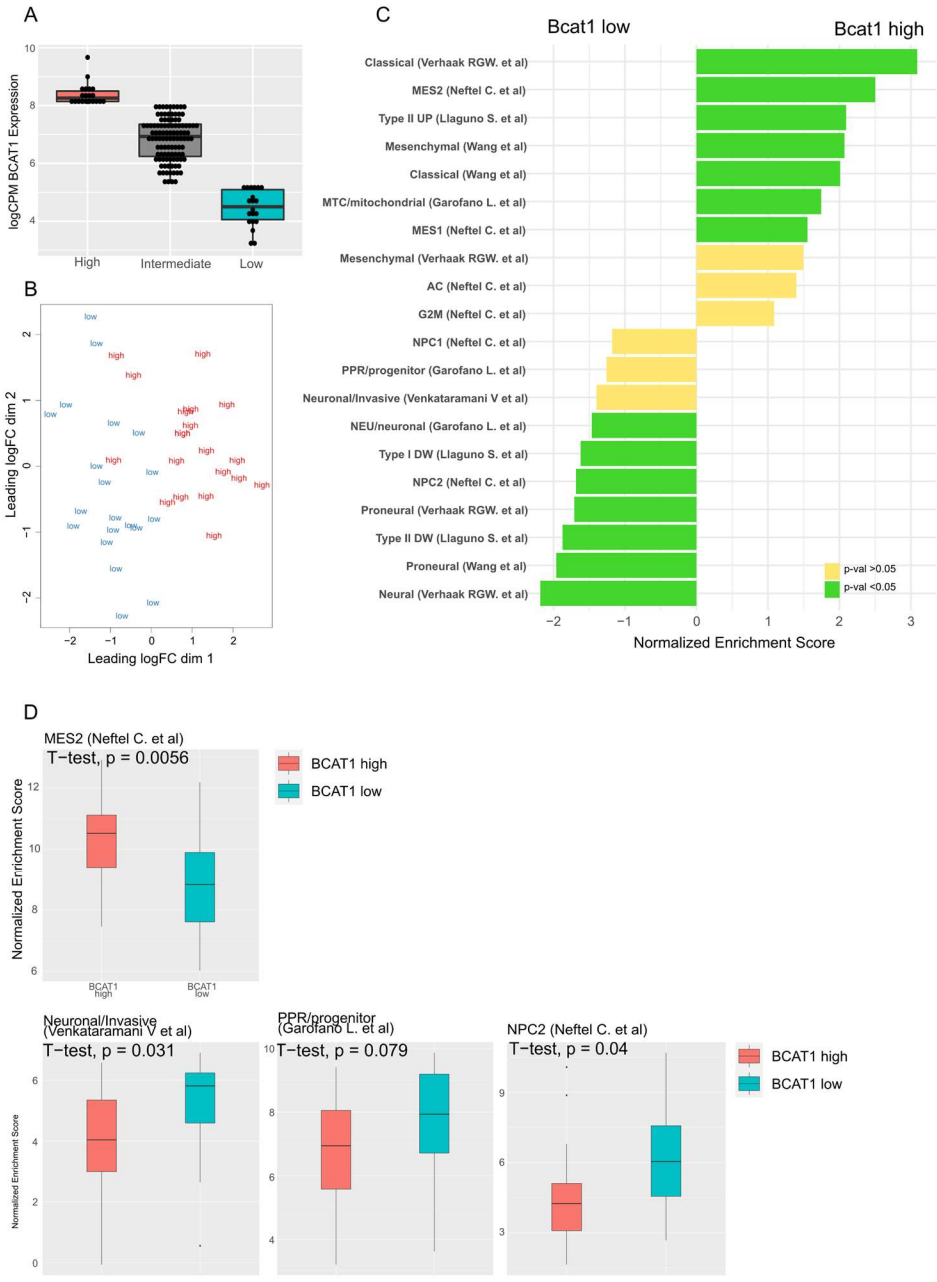

Figure 18 TCGA-GBM patient stratification based on BCAT1 expression levels. A) The expression of BCAT1 was determined for 141 IDH1^{WT} glioblastoma patients with available Illumina Sequencing data based on the log(CPM) values. Top and bottom 20 samples based on BCAT1 expression were chosen for the BCAT1 High (red) and BCAT1 Low (blue) groups. B) MDS analysis using top 500 genes with highest variability in the TCGA BCAT1H and BCAT1L dataset. C) Pre-ranked GSEA analysis using the curated glioblastoma molecular subtype gene signature set comparing BCAT1^{H} vs BCAT1^{L} cells. Statistically significantly enriched signatures (adjusted p-value < 0.05) are shown in green. D) Comparison of ssGSEA NES average scores of the 20 BCAT1^{H} (red) and the 20 BCAT1^{L} (blue) samples for representative glioblastoma molecular subtype gene signatures. Statistical significance was tested using an unpaired student's t-test and noted at the top of each plot. Error bars represent 1.5 IQR values.

4.2.2. BCAT1-KO U251 glioblastoma cells show a more differentiated, neuronal-like expressional profile

The TCGA data analysis provided insight into a possible correlation of BCAT1 expression and the differentiation states of glioblastomas. To address the question of a causal role, I performed RNA sequencing of the control and BCAT1-KO U251 human glioblastoma cells

MDS analysis of the sequenced U251 control and BCAT1-KO CRISPR clones showed a clear separation of samples along the BCAT1-dependent axis (Figure 19A, dim1), and minimal clonal variability (Figure 19A, dim2). Next, I used the glioblastoma subtype signatures to assess the cellular state of the cells in a pre-ranked GSEA (Figure 19B). Interestingly, the results matched those obtained using $BCAT1^{H}$ and $BCAT1^{L}$ TCGA samples. Specifically, the BCAT1-KO U251 cells show a high enrichment in signatures associated with neuronal development and differentiation such as the developmental signature described by Richards et al. (Richards et al. 2021), the NPC1 signature from Neftel et al (Neftel et al. 2019) and others (Figure 19B, Negative NES). Conversely, the U251 control cells show a strong enrichment of mesenchymal-associated signatures such as the MES1 and MES2 and the injury response signature which the authors associated primarily with mesenchymal glioblastoma (Richards et al. 2021) (Figure 19B, Positive NES)

To characterize the biological processes underlying the transcriptional differences, I performed a GO-term enrichment analysis using the differentially expressed genes. Consistently, the most strongly enriched terms in BCTA1-KO U251 cells in the cellular component (Figure 19C) and molecular function (Figure 19D) datasets were associated with neuronal and synaptic processes typical of neural development and signaling.

In summary, these results show a more differentiated, neuronal expressional pattern in the BCAT1-KO U251 cells that matches the expression profile of the TCGA $BCAT1^{L}$ tumor samples. These data suggest a potential causal relationship between BCAT1 expression and the differentiation status of glioblastoma cells.

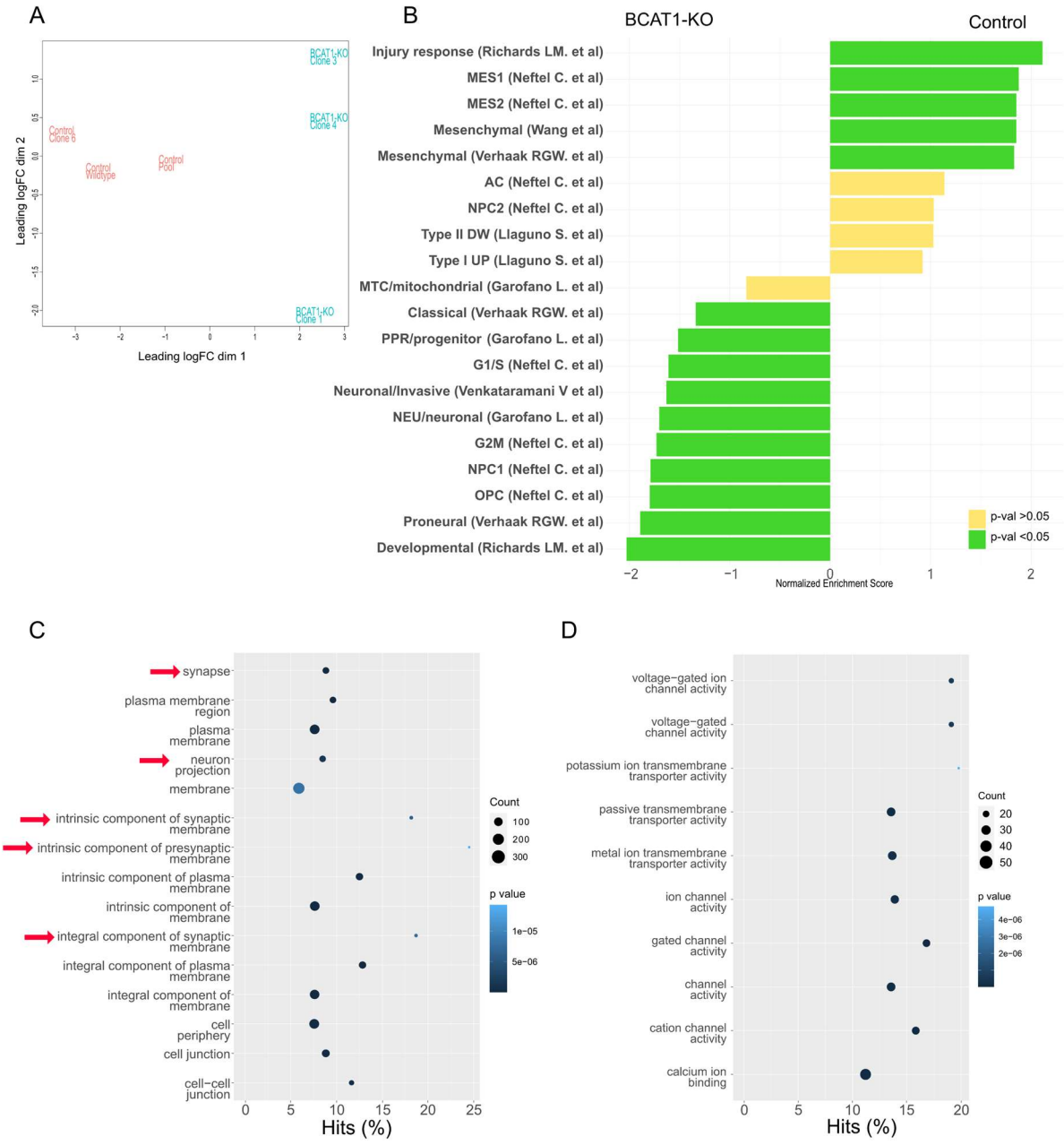

Figure 19 U251 control and BCAT1-KO RNA Sequencing analysis. A) MDS plot based on top 500 variable genes in the expression dataset of U251 control cells (control, Wildtype and Pool, red) and BCAT1-KO cells (Clone 1, Clone 3 and Clone 4. Blue). B) Pre-ranked GSEA using the curated glioblastoma molecular subtype gene signature set comparing control and BCAT1-KO U251 cells. Statistically significantly enriched signatures (adjusted p-value < 0.05) are shown in green. C) GO-term enrichment analysis using genes overexpressed in the BCAT1-KO cells against the cellular component and D) molecular function datasets. The size of each datapoint corresponds to the number of genes identified in the overexpression and its color to the p-value of the enrichment for the respective term.

4.2.3. Primary mouse glioblastoma cell lines recapitulate the TCGA and U251 differentiation expressional phenotype upon BCAT1-KO

The next part of my doctoral thesis entails *in vivo* experiments and the analysis of Bcat1-dependent cell differentiation in an *in vivo* environment. For this purpose, I worked with previously described primary mouse glioblastoma stem cells established in the lab of Prof. Angel (Costa et al. 2021) (Figure 20A). For my thesis, I decided on using the last *in vivo* passage of these cells referred to as mGB2. This cell line showed highly invasive and mesenchymal subtype glioblastoma features (Costa et al. 2021).

I performed CRISPR/Cas9-mediated knockout of Bcat1 in the mGB2 cell line and confirmed the knockout as well as Luciferase expression with a western blot analysis (Figure 20B). I proceeded with RNA collection and sequencing of the control and Bcat1-KO cells. Some of the sample processing for these experiments was performed together with Nathalie Wilke who completed her master thesis under my supervision at the division of Molecular Genetics.

In line with previous observations in the TCGA dataset and the U251 cells, I found a high enrichment of signatures associated with neuronal-like glioblastoma cells in the Bcat1-KO cells in a pre-ranked GSEA, whereas the control cells showed a high enrichment of mesenchymal-associated signatures (Figure 20C). Furthermore, when testing for enrichment of GO-terms, I observed a strong tendency towards neural-like biological processes in the Bcat1-KO cells (Figure 20D).

Upon examination of the top differentially expressed genes, I observed a strong overexpression of the transcription factor neurogenic differentiation 1 (NeuroD1) in the Bcat1-KO cells. This is a neuronal development-specific transcription factor known to be one of the drivers of a neurodevelopmental program when overexpressed in mouse NSCs (Pataskar et al. 2016). Using the genes directly regulated by NeuroD1, I could show that the expression of its targets is highly enriched in the Bcat1-KO cells (Figure 20E) strongly implying a neuronal-like expressional pattern.

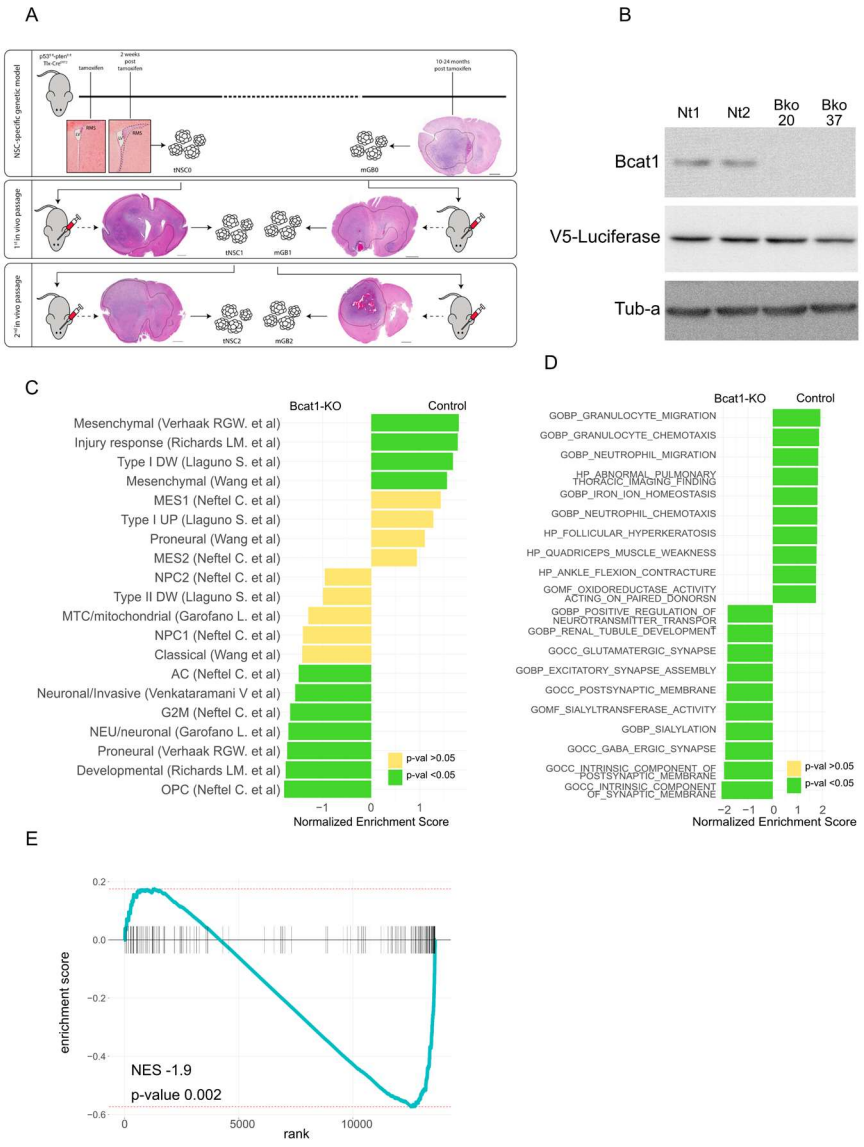

Figure 20 Primary mouse glioblastoma mGB2 cell RNA sequencing analysis. A) A schematic representation of the mouse model used to derive the mGB2 glioblastoma cell line (adapted from (Costa et al. 2021)). B) Immunoblot analysis of Bcat1 expression and V5-Luciferase expression in 2 CRISPR clones of control (non-targeting, Nt) and Bcat1-KO (Bko) cells. Tubulin was used as a loading control. C) pre-ranked GSEA using differentially expressed genes between control and Bcat1-KO mGB2 cells against the glioblastoma molecular subtype geneset. Positive NES corresponds to signatures enriched in control cells and negative in the Bcat1-KO cells. Signatures with p-value <0.05 are shown in green and p-value > 0.05 shown in yellow. D) pre-ranked GSEA using the curated C5 MSigDb genest covering the GO-terms with the same expression comparison as in C). Signatures with p-value <0.05 are shown in green .E) Pre-ranked GSEA using a geneset derived from known direct targets of NeuroD1 in mouse NSCs (Pataskar et al. 2016) using the differentially expressed control vs Bcat1-KO genes showing enrichment in the Bcat1-KO cells (NES=-1.9, p-value = 0.002).

4.2.4. Human U251 and mouse mGB2 glioblastoma cells show a significant overlap in BCAT1-dependent gene expression

The similarities in transcriptional profiles of the human and mouse glioblastoma cells prompted me to explore commonly between them upon BCAT1-KO. Despite expected variation between the models, 729 genes were found to be co-regulated (Figure 21A, 'co-regulated'). As this is a surprisingly large overlap, I used the commonly regulated genes to perform a pre-ranked GSEA analysis against the glioblastoma molecular subtype geneset and observed that the coregulated genes are sufficient to distinguish the control and BCAT1-KO cells along the mesenchymal-neuronal glioblastoma axis (Figure 21B).

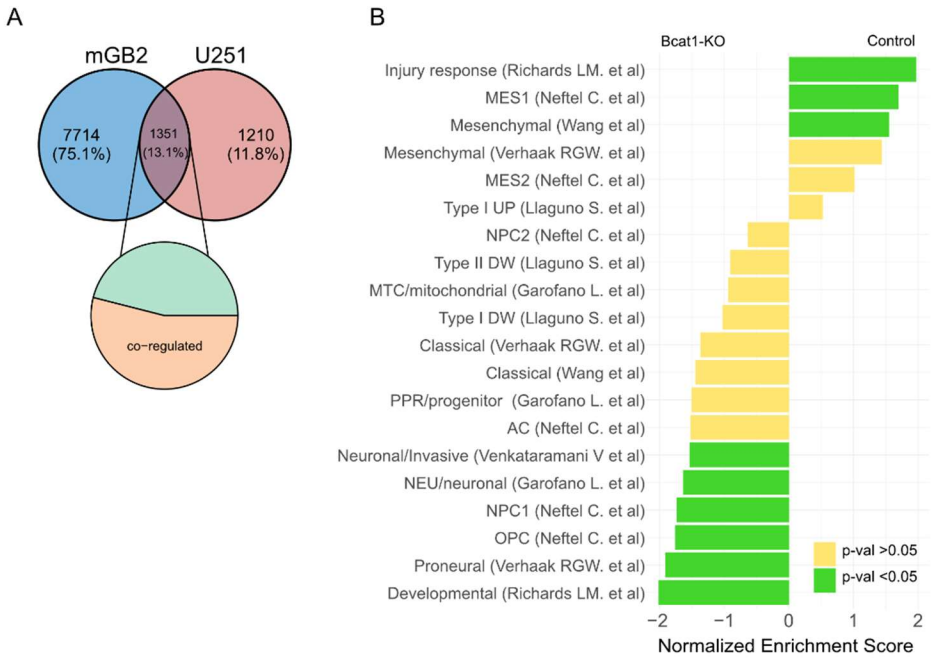

Figure 21 Gene co-regulation in U251 and mGB2 BCAT1-KO cells. A) Venn diagram of the number of significantly regulated genes in mGB2 and U251 cells upon BCAT1-KO. A pie chart showing the proportion of genes co-regulated (in the same direction) between the control and BCAT1-KO cells of the two cell lines. B) pre-ranked GSEA using average logFC of control vs BCAT1-KO U251 and mGB2 cells against the glioblastoma molecular signature geneset. Genesets enriched in BCAT1-KO cells are shown as negative NES enrichment, and the ones enriched in the control cells as positive NES enrichment. Statistically significant enrichment (p-value <0.05) is shown in green and non-significant (p-value>0.05) in yellow.

Upon closer inspection of the co-regulated genes amongst those upregulated in the BCAT1-KO U251 and mGB2 cells, I observed that the highest average regulation accounted for genes commonly described as neuronal or NSC markers and associated with neurodevelopmental processes (Table 16)

Table 16 LogFC values of neuronal-related genes significantly overexpressed in mGB2 and U251 BCAT1-KO cells. The minus sign indicates overexpression of in the BCAT1-KO cells

Gene Symbol	logFC mGB2	LogFC U251
CNTN1	-7.9	-9.3
ADGRL3	-5.9	-7.9
KCNK13	-6.5	-7.2
BRINP2	-7.5	-5.7
OLIG1	-2.0	-10.5
GRIA4	-9.1	-2.6
ERBB4	-6.9	-4.0
OLIG2	-1.1	-9.3
GRIK2	-2.5	-6.2

These data further validate the hypothesis of BCAT1 expression being crucial for retaining the mesenchymal characteristics of glioblastoma by regulating the expression of neuronal-development and differentiation-associated genes in both mouse and human glioblastoma cell lines.

4.2.5. *In vitro* differentiation of mGB2 cells results in a stronger phenotype in the Bcat1-KO cells on the morphological and expressional levels

The bioinformatics analysis indicated a tendency towards a neuronal and developmental expressional shift in Bcat1-KO cells, in both human and mouse glioblastoma cells. I wanted to explore experimentally whether this expressional shift results in observable growth differences of the cells. These experiments were performed partially by Nathalie Wilke under my supervision.

The mGB2 cells are maintained in a stem cell state and can differentiate further upon stimulation. I cultured the cells on a basal membrane matrix in either stem cell (SC) conditions or with the addition of 5% Fetal Calf Serum (FCS) as a differentiation-inducing agent. Once differentiated, the control cells kept growing tightly packed with a rounded flat morphology and minimal cell extensions (Figure 22A). However, the Bcat1-KO cells showed a highly elongated cellular morphology with pronounced cell extensions and an obvious arrest in growth (Figure 22A). These observations could be further confirmed through immunofluorescent staining of the differentiated cells with Tubb3 (a neuronal marker) (Figure 22B).

Next, we performed real-time quantitative PCR (RT-qPCRs) probing the expression of known differentiation markers of neuronal and glial lineages such as Gfap, Tubb3, Map2, S100b, Cspg4 and Aqp4 (Figure 22C and 22D). Upon FCS culturing, the expression of Gfap and Tubb3 significantly increased, confirming the successful differentiation of the cells (Figure 22C). Interestingly, under SC conditions, the expression of Aqp4, S100b Map2 and Cspg4 was already significantly higher in the Bcat1-KO than in control cells (Figure 22D), validating our previous observations of a more differentiated state of these cells. Furthermore, in FCS conditions, the expression of the markers Map2, Aqp4 and S100b increased in both, but was strikingly higher in the differentiated Bcat1-KO than control cells.

This data, together with the morphological observations indicates that the Bcat1-KO cells are more prone to differentiation and show a much more differentiated phenotype already at baseline.

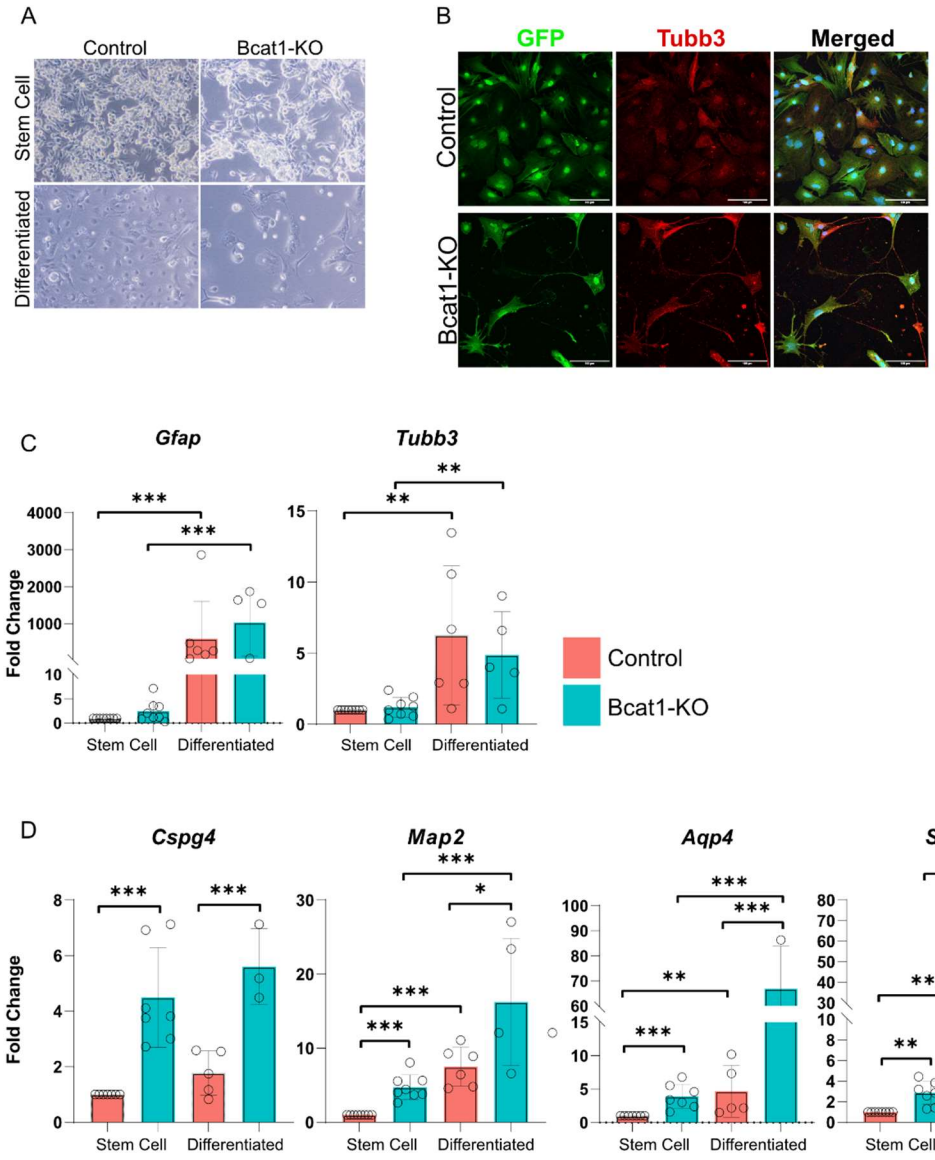

*Figure 22 mGB2 cell differentiation in vitro. A) Brightfield microscopic images of control and Bcat1-KO mGB2 cells cultured on a basal membrane matrix for 5 days either in stem cell conditions or with the addition of 5% FCS (Differentiated). B) Confocal imaging of differentiated control and Bcat1-KO mGB2 cells using GFP as the cell marker (green) and immunofluorescently stained Tubb3 (red). Scale bar = 100µm. C) RT-qPCR analysis of Gfap and Tubb3 expression in control (red) and Bcat1-KO cells (blue) in stem cell conditions or with FCS (Differentiated). The expression was normalized to the control stem cell condition and Tbp expression was used as a housekeeper gene. D) RT-qPCR analysis of Cspg4, Map2, Aqp4 and S100b expression in control (red) and Bcat1-KO cells (blue) in stem cell conditions or with FCS (Differentiated). The expression was normalized to the control stem cell condition and Tbp expression was used as a housekeeper gene. Statistical analysis for C and D was performed using a one-way ANOVA test and Tukey post-hoc testing (n>3). Error bars represent standard deviation Only statistically significant comparisons are marked: * – $p \leqslant 0.05$, ** – $p \leqslant 0.01$, *** – $p \leqslant 0.001$*

4.2.6. Bcat1-KO mGB2 cells show a significant decrease in proliferation upon differentiation which cannot be fully rescued through reintroducing stem cell growth factors

After observing the apparent growth arrest of the Bcat1-KO cells upon differentiation (Figure 23A), I proceeded to investigate cell proliferation under differentiating conditions.

Using Ki67 as a marker of cycling cells, I performed immunofluorescent stainings of the mGB2 control and Bcat1-KO cells under stem cell conditions or differentiated (Figure 23A). As expected, a large majority of both control and Bcat1-KO cells were $Ki67^+$ in stem cell conditions (Figure 23B). Upon differentiation, the number of $Ki67^+$ cells was reduced in both control and Bcat1-KO samples compared to SC condition, however the proportion of $Ki67^+$ cells was significantly lower in Bcat1-KO cells compared to control (on average 41% and 22% $Ki67^+$ cells, respectively, Figure 23B).

To further assess cell proliferation rate, we performed a Click-iT EdU proliferation assay using flow cytometry. Control and Bcat1-KO cells were kept under stem cell conditions or differentiated before treatment with EdU (Figure 23C). Consistent with the Ki67 data, differentiation resulted in a reduced proportion of EdU^+ cells, but this reduction was significantly stronger in the Bcat1-KO cells (from 57% to 40% in control and 56% to 8% in Bcat1-KO cells on average, Figure 23C). Next, I first treated the cells as above, removed the FCS and replaced it with stem cell medium for 3 additional days. Interestingly, the differentiated control cells completely recovered their proliferative capacity on day 2, whereas the Bcat1-KO cells showed only slight recovery after 3 days. (25% EdU^+ cells on day 3 of recovery versus the original 56%, Figure 23C). The recovery was also evident on the morphological level. The control cells reverted to a stem cell-type morphology upon removal of FCS (small and round loosely attached cells, Figure 23D), whereas the morphology of Bcat1-KO cells remained mostly indicative of differentiation (elongated flat morphology with long cellular extensions, Figure 23D).

Glioblastoma cells are known to switch to a more differentiated state during development and invasion of the tumor, with the ability to dedifferentiate towards mesenchymal features (Venkataramani et al. 2022). This data shows that this ability seems to be lost or severely hampered upon the knockout of Bcat1.

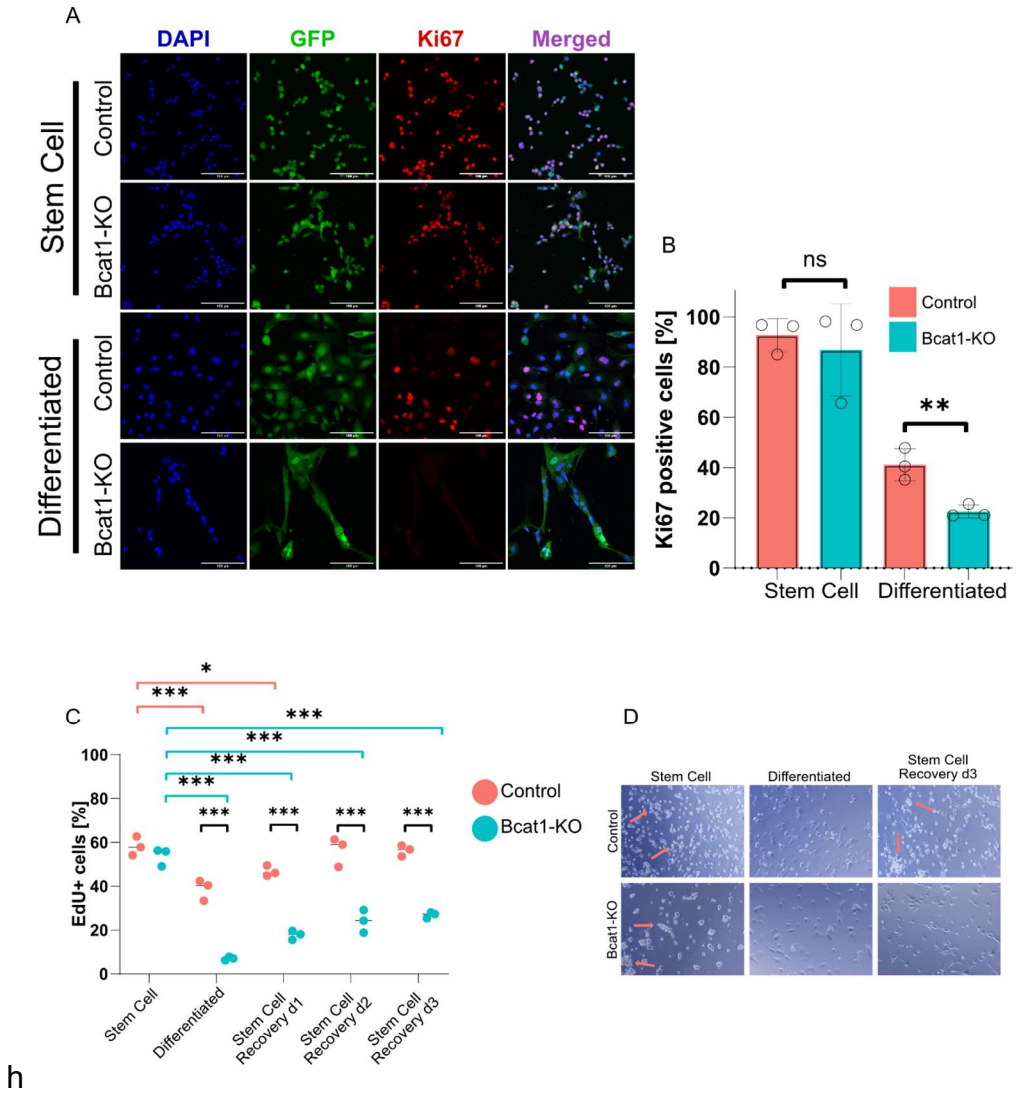

*Figure 23 mGB2 control and Bcat1-KO cell proliferation upon differentiation and recovery. A) Confocal microscopy images of control and Bcat1-KO mGB2 cells in stem cell or differentiated conditions. Cells were visualized using endogenous GFP expression (green) and the nucleus with the DNA dye DAPI (blue). Ki67 was immunolabeled and visualized using the Alexa Fluor 647-conjugated secondary antibody (red). Scale bar = 100µm. B) Ki67⁺ cell quantification. The y-axis shows the percentage of positive control (red) and Bcat1-KO (blue) cells in respect to all DAPI stained nuclei (n=3, with more than 50 cells quantified per condition in every experimental replicate). Error bars represent standard deviation of the replicates, and the statistics was performed using an unpaired students t-test in the marked comparisons. C) EdU incorporation in control (red) and Bcat1-KO (blue) cells. EdU⁺ cells were quantified as a percentage of total single cells using FACS. Statistical significance was determined using a two-way ANOVA with post-hoc multiple testing. Only statistically significant comparisons are denoted with stars. D) Representative light microscopy images of cultured mGB2 control and Bcat1-KO cells in stem cell condition, as differentiated or 3 days after the withdrawal of FCS. Red arrows point to stem cell morphology. ns – non-significant, * – $p \leqslant 0.05$, ** – $p \leqslant 0.01$, *** – $p \leqslant 0.001$.*

4.2.7. Bcat1-KO cells fail to develop into tumors in a syngeneic mouse glioblastoma model

The data so far indicates a strong tendency of Bcat1-KO cells towards differentiation. To further test this hypothesis, I used the same mGB2 cell line in a syngeneic (BL6) mouse model. To assess potential clonal effects related to the CRISPR/Cas9 knockout, I injected 3 mice each with 2 different control and Bcat1-KO mGB2 clones (Figure24 A). Both control clones reached termination criteria, however, out of the 6 mice transplanted with mGB2 Bcat1-KO cells, only one developed a measurable tumor, reaching termination criteria 99 days after the injection (Figure 24B).

Since no obvious clonal effects were observed, I randomly picked one control and one Bcat1-KO clone and proceeded with the transplantation of 8 mice per group with a higher cell number. Tumor growth was followed using *in vivo* bioluminescent imaging (IVIS) (Figure 24C). Mice with control tumors showed a steady tumor growth over time following initial tumor detection (Figure 24D), with only one mouse showing no tumor growth, likely due to technical failure of the transplantation (Figure 24E, red). On the other hand, all of the mice injected with Bcat1-KO mGB2 cells failed to develop detectable tumors even after more than a 100 days post-injection (Figure 24D and 24E, blue).

These initial mouse experiments showed that Bcat1 knockout severely impacts tumor growth *in vivo*.

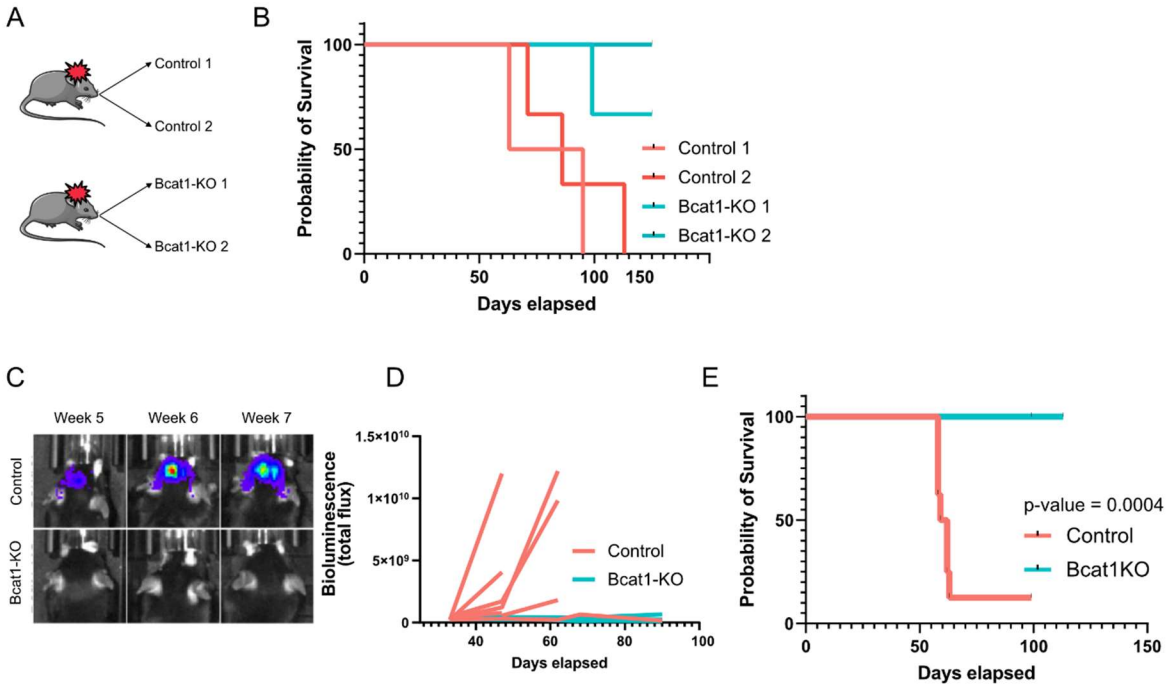

Figure 24 Orthotopic, syngeneic mouse glioblastoma model using control and Bcat1-KO cells. A) A schematic representation of the initial experimental design. Clone 1 and 2 and Bcat1-KO 1 and 2 refer to two different CRISPR clones of the mGB2 control and Bcat1-KO cells. B) Survival plot of mice transplanted with tumor cells according to the scheme in A) (n (control 1)=2, n(control 2)=3, n(Bcat1-KO 1)=3, n(Bcat1-KO 2)=3). C) Representative IVIS tumor measurement in one control and 1 Bact1-KO mouse over the period of 3 weeks. D) Total luminescent flux quantification of IVIS measurements during tumor growth of control (red, n=8) and Bact1-KO (blue, n=8) mGB2 tumors. E) Survival Kaplan-Meier survival analysis of control (red, n=8) and Bcat1-KO (blue, n=8) mGB2-bearing mice (p-value = 0.0004).

4.2.8. mGB2 Bcat1-KO cells retain the ability to engraft *in vivo* but fail to form proliferative tumors and show highly differentiated morphological features

Next, I aimed to investigate the reason behind the lack of Bcat1-KO tumor growth. First, I confirmed that the Bcat1-KO tumor cells retain the ability to engraft. To do this, I sacrificed the mice 100-130 days post-injection with Bcat1-KO cells and examined the brains using a stereotactic microscope for GFP expression. Surprisingly, in all of the brains checked (n>3) I was able to detect a GFP signal matching the approximate coordinates of the tumor injection (Figure 25A, red arrows).

To examine the Bcat1-KO tumor residuals more closely, I dissected the GFP positive regions of the brain and used immunofluorescent staining of GFP to visualize the tumor cells using confocal microscopy. The Bcat1-KO GFP^+ cells were found only in very small regions of the brains of the injected mice (usually less than $1mm^2$ surface per section) (Figure 25C). Furthermore, the morphological features were indicative of cell differentiation characterized by elongated large cells with one or multiple long cell protrusions reminiscent of neuronal extensions (Figure 25C, lower and right-most panels). In control tumors, the GFP^+ cells covered a large part of each coronal section, with cellular morphology reminiscent of human glioblastoma: small, tightly packed, round tumor cells (Figure 25B). A slightly varying tumor cell morphology could be observed in the region of the *corpus callosum*; however, this was previously reported to be due to the migration along the corresponding nerve fibers (Figure 25B, lower right panel).

The detection of mGB2 Bcat1-KO cells in the mouse brains more than 100 days following transplantation indicates that the failure to form outgrown tumors is not due to a lack of engraftment but might be explained by the differentiation phenotype described here.

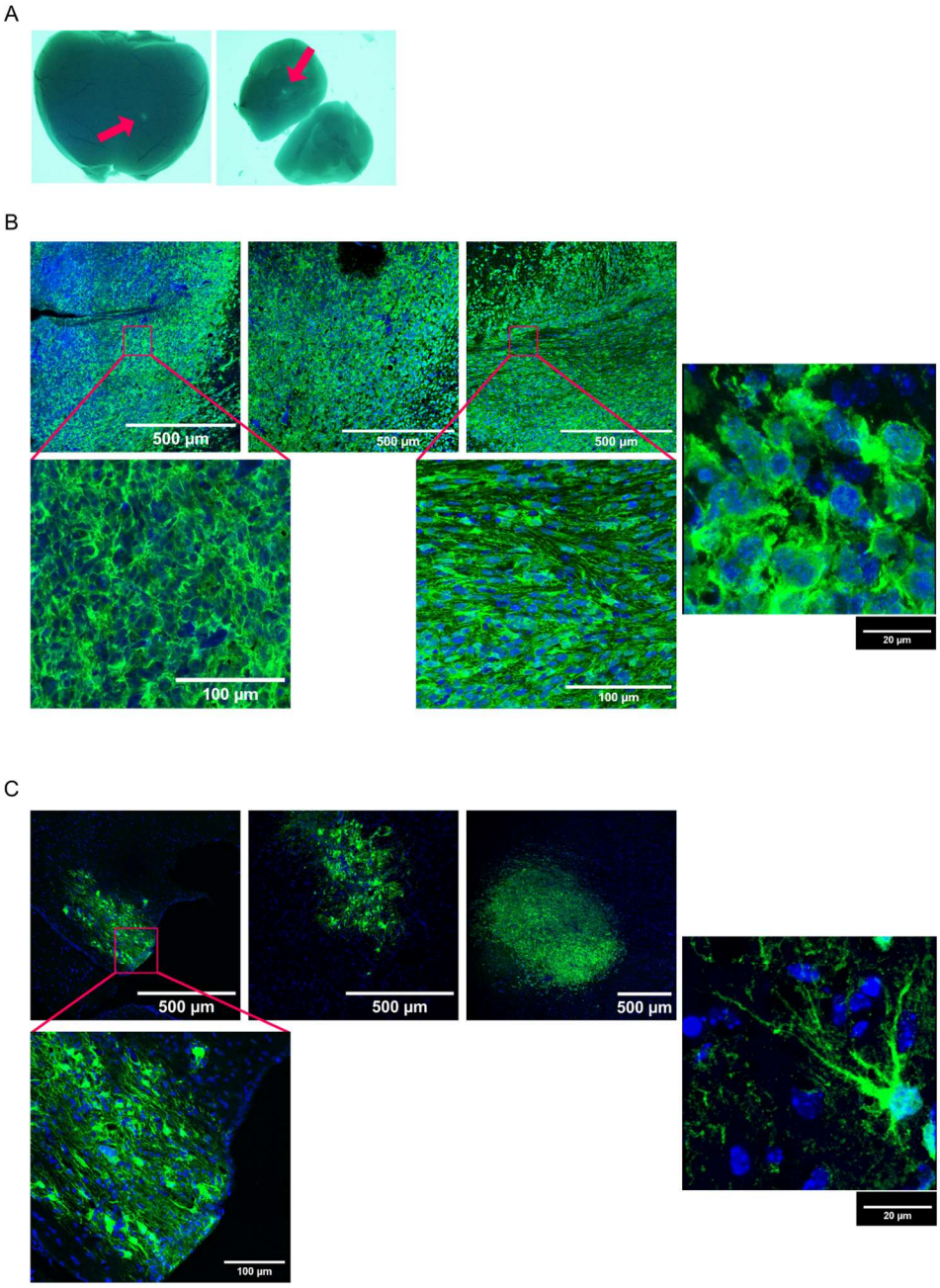

Figure 25 Syngeneic mouse mGB2 glioblastoma model tumor immunofluorescent analysis. A) mGB2 Bcat1-KO-injected brains visualized 100-130 days post injection under the fluorescent stereotactic microscope. Red arrows point to GFP positive areas of the brain indicating tumor cells. B) Confocal images of 3 immunofluorescently labeled control and C) Bcat1-KO tumors or tumor residuals. Anti-GFP antibody was used to immunolabel GFP expressed in tumor cells (green) and DAPI for labeling nuclei (blue). Upper panels of B) and C) represent tile scan images of control and Bcat1-KO GFP⁺ cells (scale bar 500um) and the lower panels are representative zoom-ins o he tumors (scale bar 100um). The right most panel in B) and C) represent closeup images of representative cellular morphology of control and Bcat1-KO cells, respectively (scale bar 20um).

4.2.9. mGB2 Bcat1-KO cells can form tumors in immunocompromised NSG mice but with a significant delay and an obvious differentiated phenotype

The findings so far indicate that Bcat1-KO cells have a strong tendency to differentiate and have a reduced proliferation capacity both *in vivo* and *in vitro* under differentiating conditions.

Next, I wanted to explore whether the impact on tumor growth was due to the inherent differentiation phenotype of the Bcat1-KO cells or if the cells of the immune microenvironment could also play a role in limiting tumor growth. To do this I performed tumor transplantations in immunodeficient NOD/SCID gamma (NSG) mice which lack innate and adaptive immune cells.

In this setup, even though the control cells showed a much faster growth rate, tumor growth could also be detected in mice injected with Bcat1-KO cells after a significant delay (42- and 96-day average survival, respectively) (Figure 26A). To visualize the tumor growth patterns of the control and Bcat1-KO tumors, I performed immunofluorescent GFP labeling of the tumors and imaged whole coronal sections using the Axioscan slide scanner. The images clearly show a typical poorly differentiated phenotype of the control cells (Figure 26B), whereas mouse brains bearing Bcat1-KO tumors present as highly migratory and highly differentiated cells with the morphological features matching those found previously in BL6 mice (Figure 26C). Interestingly, throughout the coronal sections of the Bcat1-KO tumors, small undifferentiated regions could be observed which were not previously identified in BL6 mice (Figure 26C, red arrows).

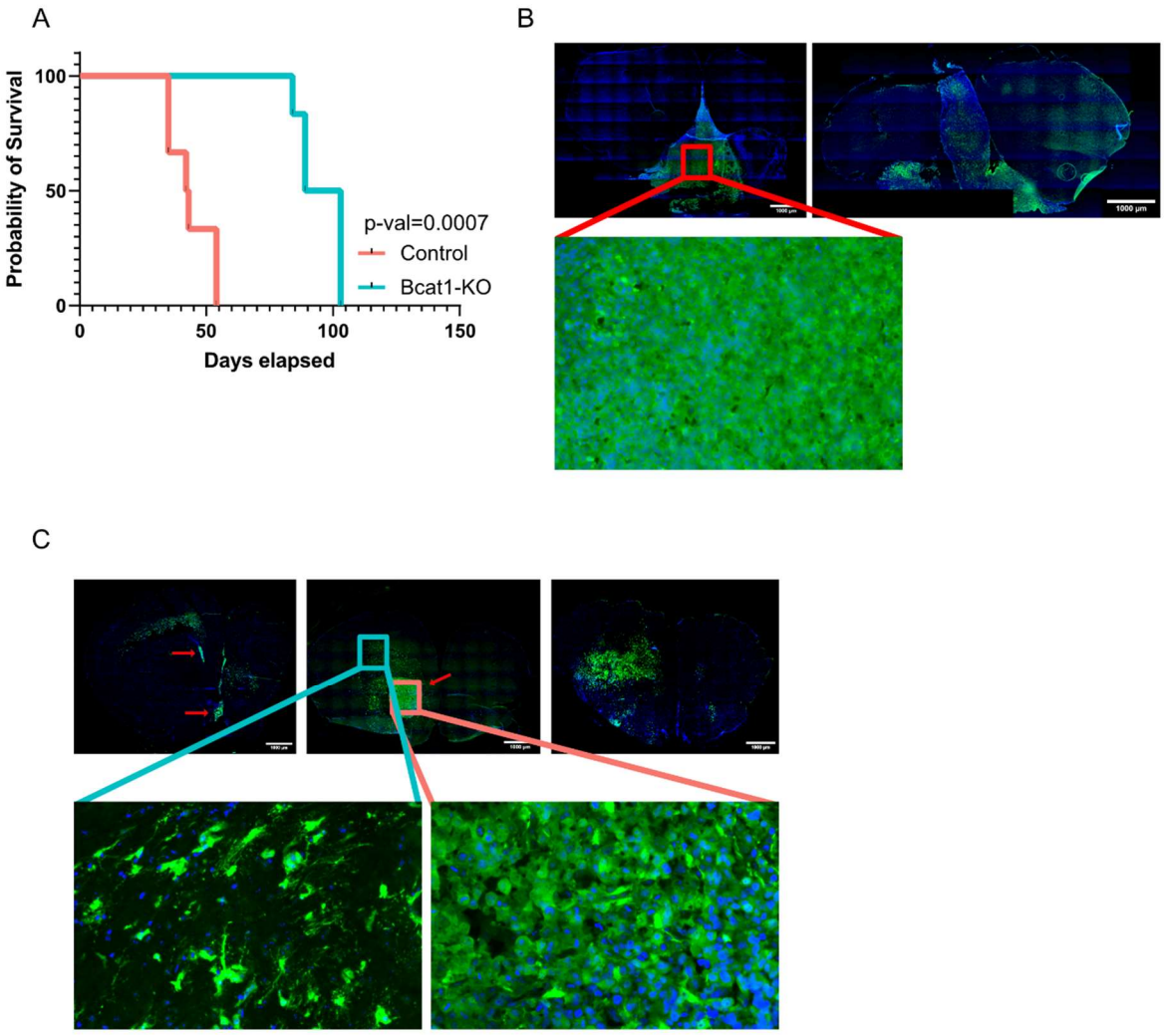

Figure 26 mGB2 cell growth in the NSG mouse model. A) Survival curve representing the survival of NSG mice injected with control (red) or Bcat1-KO (blue) tumor cells. B) Representative whole coronal section imaging of GFP immunolabeled (green) control tumors with whole section overview (top) and a representative zoom-in (lower). DNA was labeled with DAPI (blue). Scale bar is equivalent to 1000um. C) Representative whole coronal section imaging of GFP immunolabeled (green) Bcat1-KO tumors with whole section overview (top) and representative zoom-ins of undifferentiated (red) or differentiated (blue) regions (lower). Red arrows point to undifferentiated regions of the Bcat1-KO tumors. DNA was labeled with DAPI (blue). Scale bar is equivalent to 1000um.

To show that the morphologically distinct, differentiated phenotype is also associated with a reduced proliferative capacity, I analyzed Ki67 positivity in control and Bcat1-KO tumors (Figure 27A). These experiments were partly performed by Nathalie Wilke under my supervision. Based on cellular morphology, we quantified the portion of $Ki67^+$ cells in differentiated and undifferentiated regions of the Bcat1-KO tumors and the control tumors (Figure 27B and 27C). The results clearly show a significant reduction of the portion of $Ki67^+$ cells in the differentiated regions of the Bcat1-KO tumors in comparison to both control cells and Bcat1-KO undifferentiated regions.

These experiments performed in the NSG mouse model provide further confirmation of the differentiation phenotype in Bcat1-KO glioblastoma cells. Even though it is clear that the immune system has an important role in completely abrogating Bcat1-KO tumor growth, the marked increase in survival time of the NSG mice bearing Bcat1-KO tumors further highlights the importance of the differentiation phenotype in mouse survival.

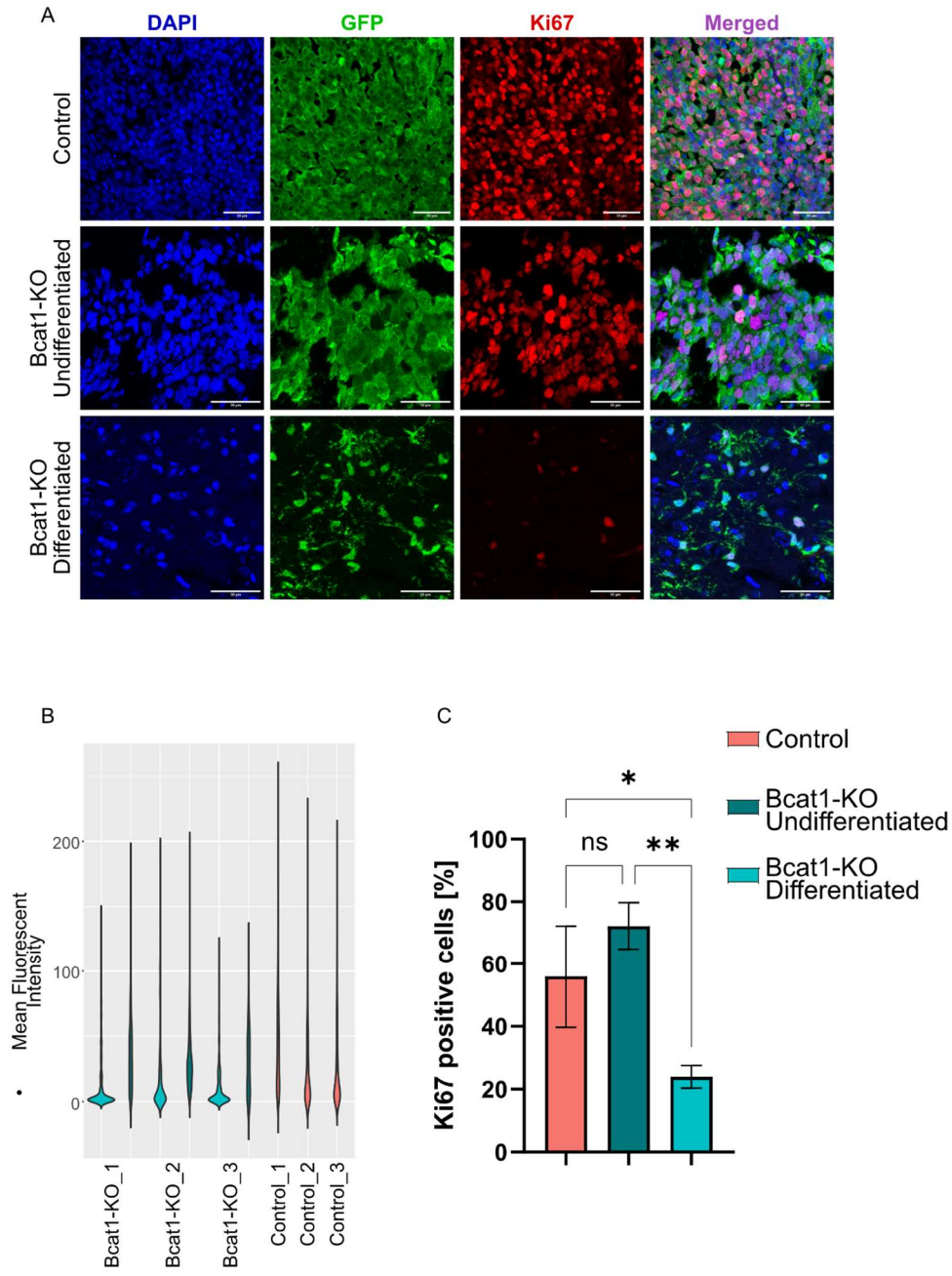

Figure 27 Ki67 expression in control and undifferentiated and differentiated regions of Bcat1-KO tumors. A) Representative confocal microscopy images of mGB2 control, Bcat1-KO Undifferentiated and Differentiated tumors immunolabeled with GFP (green) and Ki67 (red). DAPI was used for nuclear staining. Scale bars represent 50um. B) Violin plot of Ki67 mean fluorescence intensity per nucleus in control cells (red), undifferentiated Bcat1-KO cells (dark blue) and differentiated Bcat1-KO cells (light blue) in 3 mice per group. C) Quantification of the number of Ki67⁺ cells in each of the groups represented as average of the three mice quantified. Significance was determined with a one-way ANOVA test followed by Tukey multiple comparison testing. Error bars represent standard deviation.

4.2.10. Changes in DNA methylation can account for the expressional changes and the differentiation phenotype between control and Bcat1-KO mGB2 cells

When performing its enzymatic function of transamination, BCAT1 exhausts cellular αKG and produces glutamate. αKG is a known epigenetic regulator as it is necessary for the function of TETs which demethylate DNA. As BCAT1 has previously been implicated in regulating DNA methylation (Raffel et al. 2017), I explored the methylation profiles of the control and Bcat1-KO mGB2 cells to determine whether this could explain the observed differentiation phenotypes.

I examined DNA methylation patterns of control and Bcat1-KO mGB2 cells using a CpG array. PCA clearly showed a distinct methylation profile of the two lines (Figure 28A, Principal Component 1) with only small sample-based variation (Figure 28A, Principal Component 2). Within the significantly differentially methylated sites, I could observe an overall increased methylation of CpG sites in the control cells (Figure 28B). In further analysis, I focused on differentially methylated CpG islands only.

Next, I compared the differential expression of genes between the control and Bcat1-KO (see section 4.2.3) and the methylation status of CpG islands associated with those genes. I found a highly significant negative correlation of expression and methylation (Figure 28C, R=-0.36, p-value<0.01 – Spearman ranked correlation test) strongly implicating DNA methylation as a major regulatory mechanism behind the Bcat1-KO induced expressional differences.

To see whether methylation-based regulation can account for the suppression of differentiation-related genes in control cells, I used differentially methylated CpG islands to perform a robust rank aggregation analysis (Ren and Kuan 2019) (Figure 28D). The results show a strong enrichment of genes characterizing neuronal glioblastoma subtypes differentially methylated only in the control cells. Similarly, a metylGSA (Ren and Kuan 2019) showed a highly significant enrichment of neural and glial differentiation signatures associated with genes hypermethylated in control cells (Figure 28E).

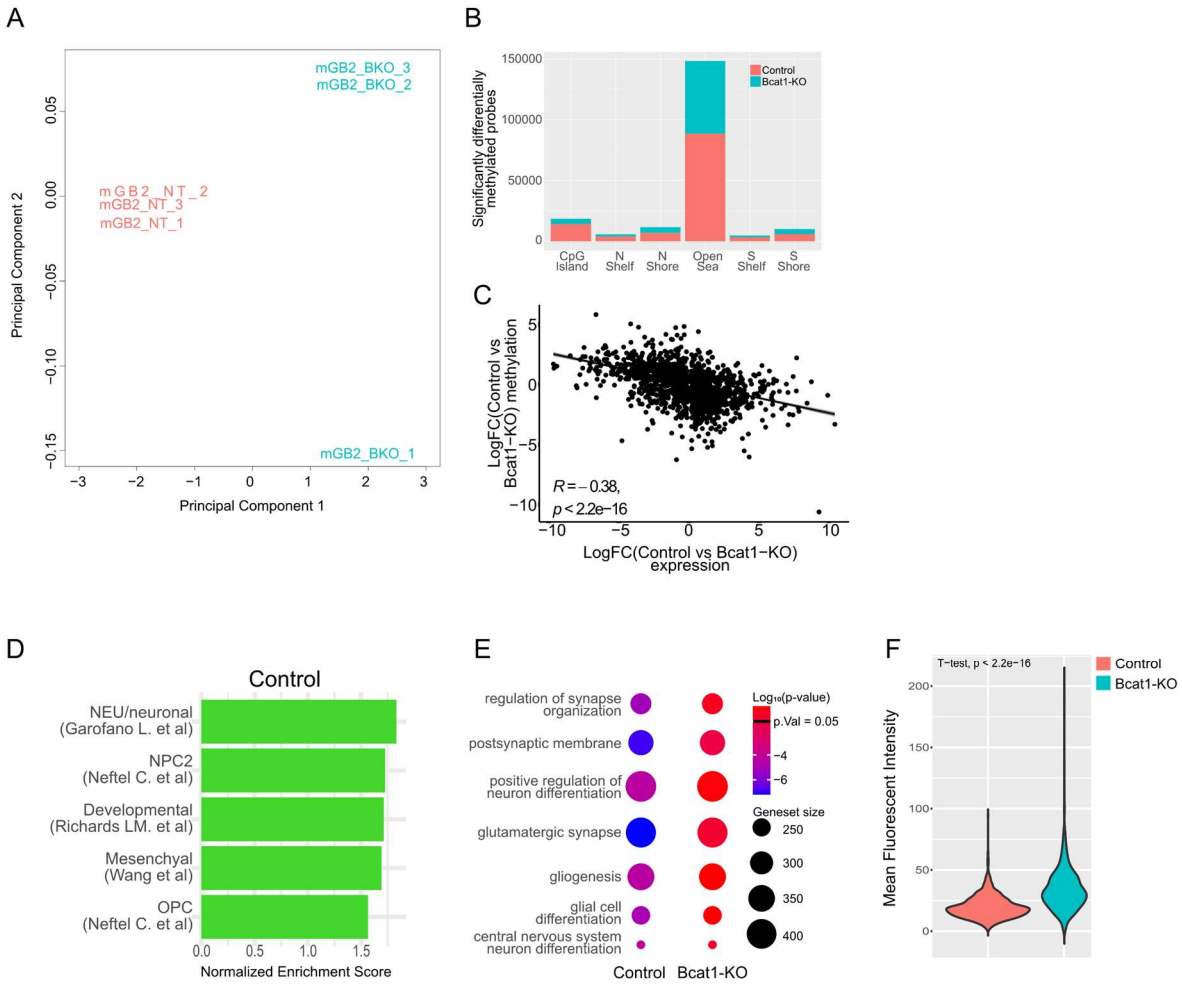

Figure 28 DNA methylation analysis of control and Bcat1-KO mGB2 cells. A) MDS analysis of top 500 differentially methylated sites in the control (NT, red) and Bcat1-KO (BKO, blue) replicates. B) Quantification of significantly differentially regulated sites between the control (red) and Bcat1-KO (blue) in CpG islands or the surrounding regions. C) Correlation analysis of differential gene expression (x-axis) and differential CpG island methylation (y-axis) between control and Bcat1-KO cells. Statistical analysis was performed using spearman's ranked correlation test due to a lack of normality in the distribution of values (R=-0.36, p-value<0.01). D) Robust rank aggregation analysis of differentially methylated sites using the glioblastoma molecular subtype signature. Only significantly enriched signatures (p < 0.05) are shown. E) methylGSA analysis of differentially methylated CpGs in control and Bcat1-KO cells using gene ontology terms. Color scale represents log10(p-value) of each enrichment and the dot size is proportional to the size of the geneset. F) Quantification of 5-hydoxymethylcitosyne immunofluorescence (mean fluorescent intensity) of the nuclei of differentiated mGB2 control (red) and Bcat1-KO (blue) cells. Statistical analysis was performed using a student's t-test (n>500 nuclei per condition). The experiment was repeated independently with the same outcome.

Finally, when examining individual differentially methylated genes, I observed many of the previously mentioned overexpressed differentiation genes in Bcat1-KO cells methylated in the control cells, which likely accounts for their transcriptional repression (Table 17)

Table 17 Differential expression and methylation of selected genes in the control vs Bcat1-KO mGB2 comparison.

Gene Symbol	logFC mGB2 (expression)	LogFC mGB2 (methylation)
NTRK2	-9.7	1.7
ASTN1	-9.6	1.3
GRIK3	-8.5	2.4
BRINP2	-7.5	3.1
ERBB4	-6.9	1.9
BDNF	-6.3	1.5
NEUROD1	-5.3	1.4

These results clearly point towards DNA methylation as a major regulatory mechanism of gene expression upon Bcat1-KO. The loss of methylation of CpG islands associated with differentiation genes in the Bcat1-KO cells could explain their tendency towards differentiation *in vitro* and *in vivo* described previously.

4.3. The role of Bcat1 expression on maintaining an immunosuppressive tumor microenvironment

In the previous section, I have shown that Bcat1 is necessary for maintaining the poorly undifferentiated cellular state typical of aggressive mesenchymal glioblastomas both in human and mouse glioblastoma cells. However, the Bcat1-KO induced differentiation was not sufficient to completely abrogate tumor growth in immunocompromised NSG mice as it did in the BL6 mouse model. This indicates that in addition to the differentiation phenotype, the immune system also plays a role in suppressing tumor outgrowth.

In this section, I will be focusing on the role of the glioblastoma microenvironment and the impact of Bcat1 expression on the shaping of the TME.

4.3.1. Knockout of Bcat1 is not sufficient to completely abrogate tumor growth in a T-cell deficient mouse model

To better delineate which cells of the immune compartment, contribute to the suppression of Bcat1-KO tumor growth, we repeated the experiment using a Rag2-KO mouse line deficient in functional T-cells while retaining seemingly normal myeloid function. We observed that the mGB2 cells in Rag2-KO mice behaved similarly to those in NSG mice. Namely, the Bcat1-KO tumors grew significantly slower than the controls, but ultimately formed substantial tumors, and the mice reached termination criteria (Figure 29A)

With this experiment I identified the T-cells as a crucial immune population necessary for completely preventing Bcat1-KO tumor growth, while again stressing the importance of the differentiation phenotype in a new mouse line.

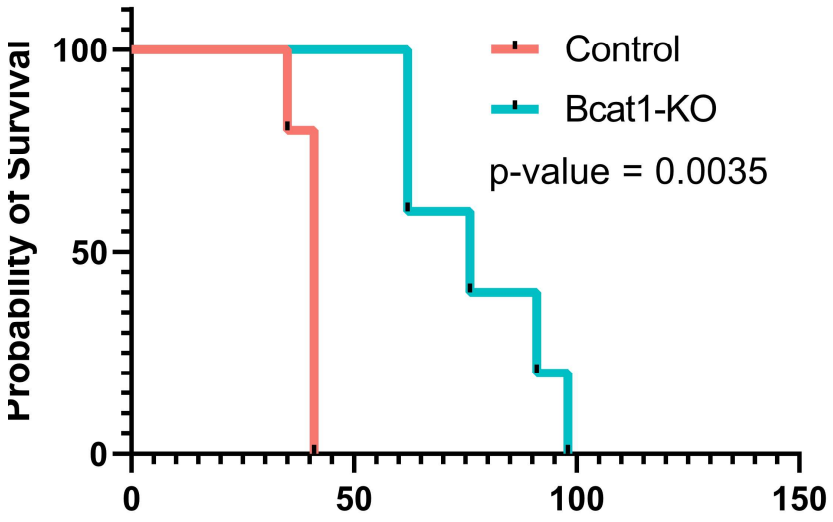

Figure 29 mGB2 glioblastoma model in Rag2-KO mice. A) Kaplan-Meier survival analysis of Rag2KO mice injected with control (n=5, red) and Bcat1.KO (n=5, blue) mGB2 cells.

4.3.2. mGB2 tumors show modified myeloid morphology and a higher abundance of tumor-infiltrating myeloid cells both during early development and at a later time point

Aiming to understand more about the role of the tumor immune microenvironment, I examined the tumor infiltrative myeloid cells in immunocompetent BL6 mice injected with control and Bcat1-KO cells. To get an earlier insight of tumor development, I sacrificed mice 4 weeks post-injection. At this timepoint, the control tumors could be detected via IVIS but were not yet large enough to cause any symptoms (data not shown). I Immunolabeled sagittal brain sections against Iba1, a myeloid marker, and GFP as a tumor cell marker and analyzed the stainings using Axioscan slide scanner (Figure 30).

At this early time point, the striking difference in size between control and Bcat1-KO was evident. Furthermore, the previously observed differentiated morphology of the Bcat1-KO was already detectable (Figure 30A and 30B, upper panel). Through the Iba1 staining, I could observe differences in myeloid morphology. control tumors showed typical GAM morphology (Kvisten et al. 2019) characterized as round, evenly dispersed cells, whereas the Bcat1-KO tumors contained rectified myeloid cells which seemed to be considerably more abundant as well (Figure 30A and 30B, Iba1-red). Quantification of $Iba1^{+}$ cells per nucleus in the tumor region confirmed this observation (Figure 30C).

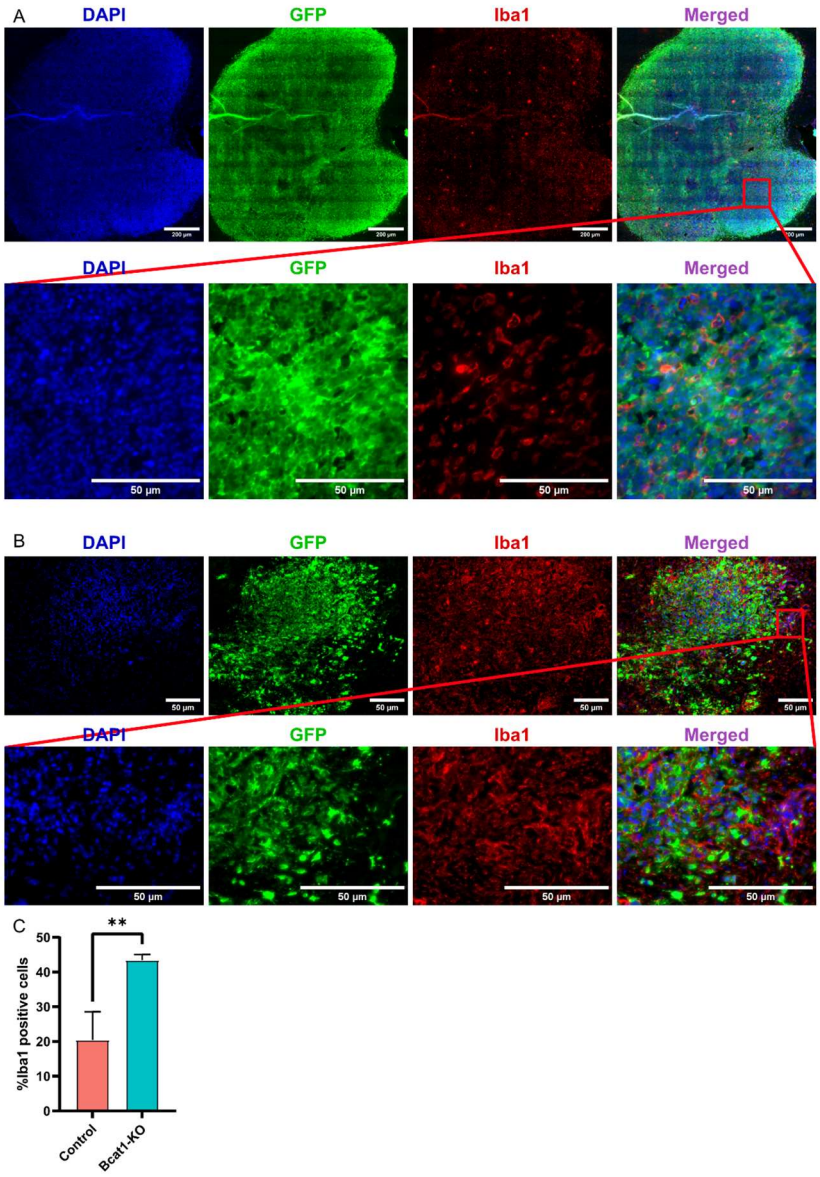

Figure 30 mGB2 control and Bcat1-KO tumor myeloid compartment immunofluorescent imaging. A) A representative control tumor at 4 weeks of development after being detectable with IVIS. The tumor was stained with anti-Iba1 marking myeloid cells (red), anti-GFP marking tumor cells (green) and DAPI was used as a DNA marker. Whole tumor overview is shown in the upper panel and a zoom-in in the lower panel (scale bars 200um and 50um, respectively). B) A representative Bcat1-KO tumor at 4 weeks of development. The tumor was stained with anti-Iba1 marking myeloid cells (red), anti-GFP marking tumor cells (green) and DAPI was used as a DNA marker. Whole tumor overview is shown in the upper panel and a zoom-in in the lower panel (scale bars 50um). C) Quantification of mean Iba1 positive cells as a percentage of detected nuclei in the control (red) and Bcat1-KO (blue) mouse tumors (n=3 per group). The quantification was performed using QuPath. Error bars show standard deviation. Statistical comparison was done using an unpaired, two-tailed student's t-test.

Then, I proceeded to investigate the myeloid environment of the end point control tumors and late stage Bcat1-KO tumor residuals. Figure 31 shows a representative control and Bcat1-KO tumor. Like the early time point, the Iba1$^+$ cells in control tumors showed typical round myeloid morphology of glioblastoma (Figure 31A). On the other hand, the Bcat1-KO tumor residuals showed an abundant and a very rectified Iba1$^+$ cell population, highly outnumbering the tumor cells themselves (Figure 31B). Due to the high density and complex morphology, the quantification of Iba1$^+$ cells could not be performed; however, the observations were made in 3 mice per group with a similar pattern.

These findings indicate that Bcat1 expression in tumor cells affects the myeloid immune microenvironment. Bcat1-KO promotes infiltration of myeloid cells into the tumor and induces morphological changes, which are often associated with myeloid polarization state.

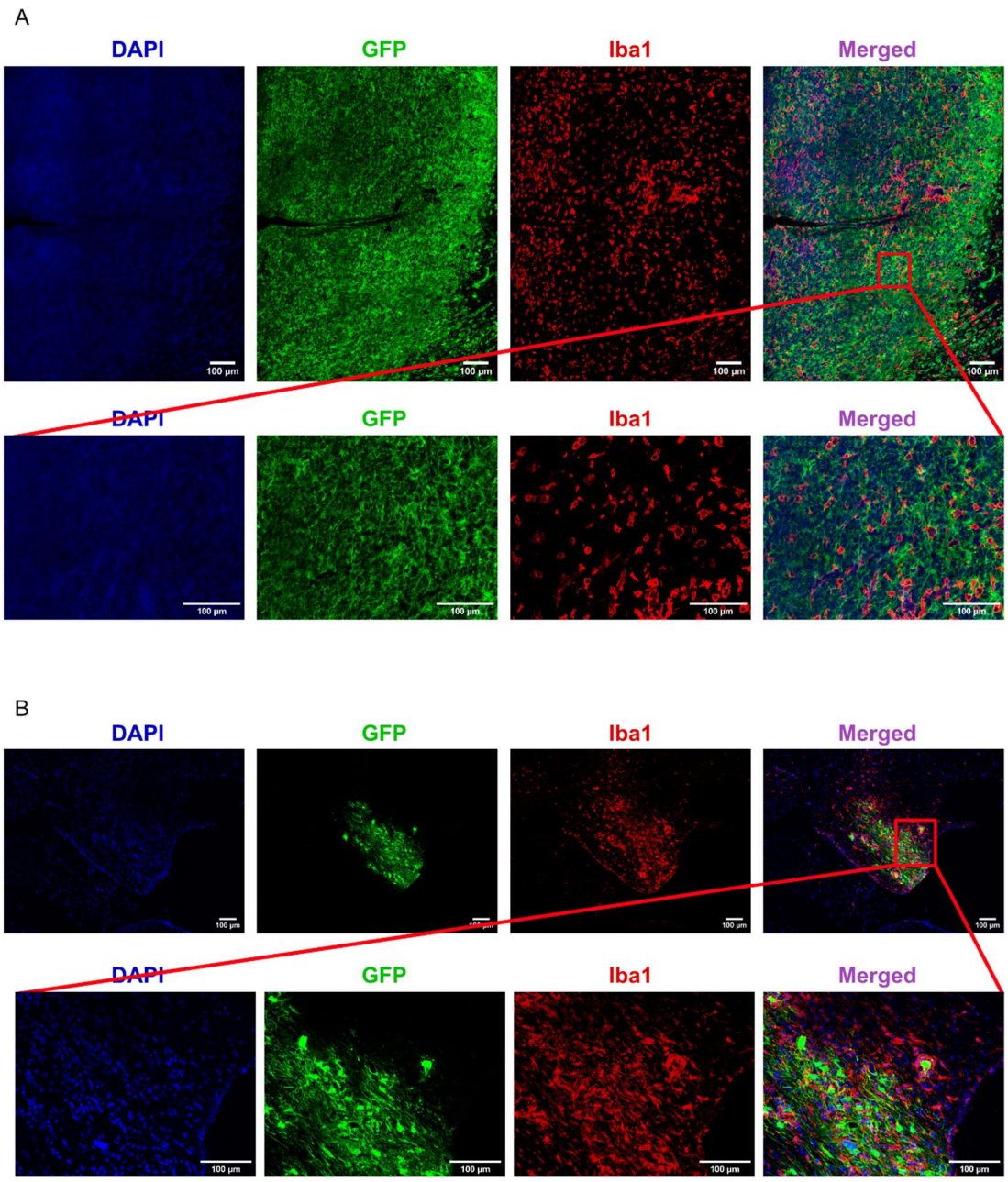

Figure 31 mGB2 control and Bcat1-KO tumor myeloid compartment immunofluorescent confocal imaging. A) A representative control tumor at end point. The tumor was stained with anti-Iba1 marking myeloid cells (red), anti-GFP marking tumor cells (green) and DAPI was used as a DNA marker. Tile scan overview is shown in the upper panel and a zoom-in in the lower panel (scale bars 100um). B) A representative Bcat1-KO tumor residual. The tumor was stained with anti-Iba1 marking myeloid cells (red), anti-GFP marking tumor cells (green) and DAPI was used as a DNA marker. Whole tumor tile scan is shown in the upper panel and a zoom-in in the lower panel (scale bars 100um).

4.3.3. Both control and Bcat1-KO tumors show T-cell infiltration during early development which is lost at late-stage tumor growth in control but not Bcat1-KO tumors

$CD8^+$ T-cells are the main effector cells regulating tumor growth and are heavily influenced by the tumor myeloid microenvironment. Having shown that the T-call compartment is important for limiting tumor growth using the NSG and Rag2-KO models, I explored the tumor effector T-cell population ($CD8^+$ T-cells) in the immunocompetent BL6 mice.

At an early stage (4 weeks post-injection), infiltrating $CD8^+$T cells were detectable in both control (Figure 32A) and Bcat1-KO tumors (Figure 32B). Although Bcat1-KO seemed to have an overall higher $CD8^+$ infiltration, there was also a high inter-tumor variation within the imaged tumors (Figure 32C).

Interestingly, at a late time point the difference in $CD8^+$ cells became more evident. The control tumors showed minimal $CD8^+$ T-cell infiltration (Figure 32D). while the number of $CD8^+$ cells remained high (relative to the tumor cells) in Bcat1-KO tumors (Figure 32E).

In summary, I showed that the infiltration of $Iba1^+$ and $CD8^+$ cells is enhanced and sustained in Bcat1-KO tumors. These results demonstrate that the tumor immune microenvironment is altered in the Bcat1-KO tumors and suggest that Bcat1-expressing tumors are immunosuppressive

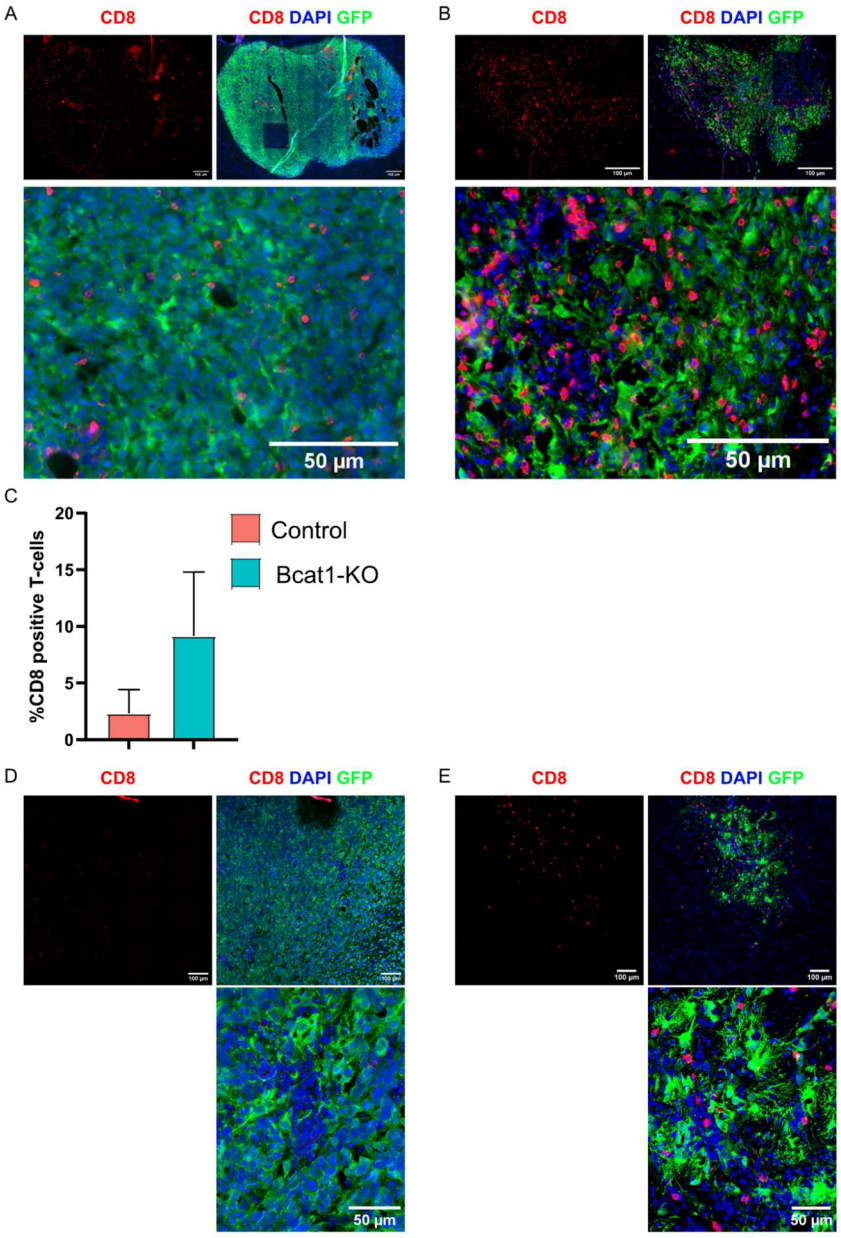

Figure 32 control and Bcat1-KO tumor T-cell immunofluorescent imaging. A) Whole slide immunofluorescent imaging of early time point control and B) Bcat1-KO tumor with anti-CD8 (red) and anti-GFP (green) immunolabeling. Lower panels in A) and B) are zoomed in regions of the respective tumors. Scale bars are 100um and 50um for the whole tumor imaging and the zoomed in segments, respectively. C) Quantification of mean CD8⁺ cells in comparison to all quantified DAPI signals in control (red, n=3) and Bcat1-KO (blue, n=2) mice. Error bars represent standard deviation. D) Confocal tile-scan imaging of control and E) Bcat1-KO tumors at a late time point. Immunolabeling with anti-CD8 (red) and anti-GFP (green). DAPI (blue) was used to stain the nuclei. Lower images in D) and E) represent higher magnification of each of the tumors. Scale bars are 100um and 50um for the tile scan and zoomed in images, respectively.

4.3.4. CIBERSORTx analysis of the TCGA samples shows the same pattern of immune cell infiltration as the mouse tumors

After observing the differences in immune cell infiltration in the mouse mGB2 tumors, I wanted to validate these results in the tumor TCGA-GBM dataset.

To do this, I used the normalized gene expression values of the 141 glioblastoma TCGA samples (see section 4.2.1) for a CIBERSORTx analysis (Newman et al. 2019) using a gene expression matrix of cell signatures derived from 19 single cell sequenced glioblastomas (Mehani et al. 2022). After correlating the individual cell types sores with the normalized BCAT1 expression in all of the samples, I observed a strong negative correlation of BCAT1 expression with the macrophage (Figure 33A) and CD8 T – cell scores (Figure 33B).

Furthermore, I compared the cell type scores of the 20 $BCAT1^{H}$ and $BCAT1^{L}$ samples analyzed in section 4.2.1. The malignancy score was significantly upregulated in the $BCAT1^{H}$ samples (Figure 33C). Consistent with the observed correlations, I found that both the macrophage and the $CD8^{+}$ T cell scores were significantly higher in the $BCAT1^{low}$ samples (Figure 33D and 33E, respectively).

These results match our observations of BCTA1-dependent alterations of the immune TME in the *in vivo* mGB2 model in a human dataset.

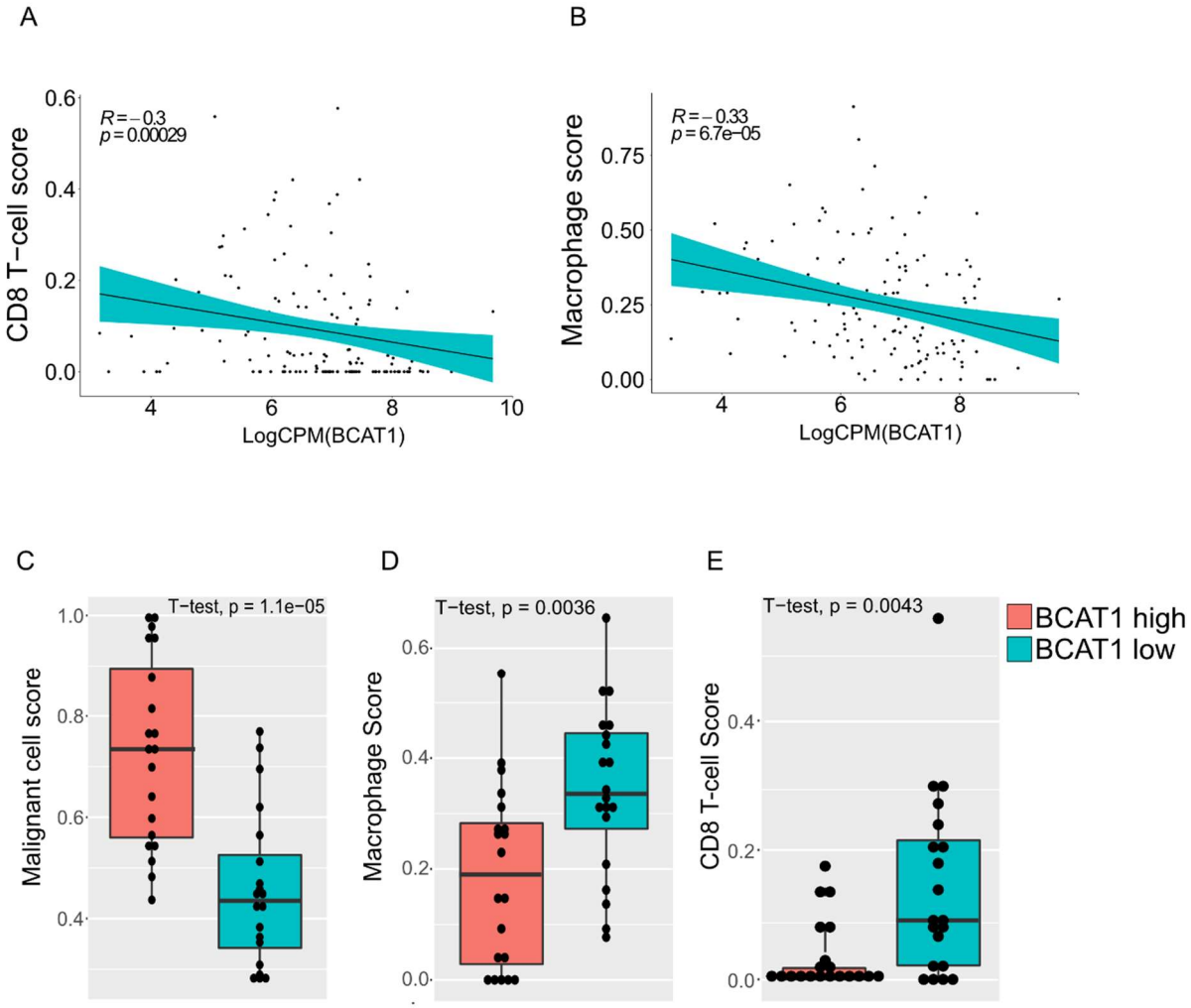

Figure 33 CIBERSORTx cell type scores of the TCGA-GBM samples. A) logCPM values of BCAT1 expression correlated with individual patient CD8 T-cell scores and B) macrophage scores according to the CIBERSORTx analysis. The correlation was performed using the Spearman ranked correlation analysis, with the p-values and R values stated in respective graphs. C) Comparison of Malignant D) macrophage and E) CD8 T – cell scores between the $BCAT1^{H}$ (red) and $BCAT1^{L}$ (blue) groups. Statistical analysis was performed using an unpaired, two-tailed student's t-test. Whiskers represent 1.5 IQR.

4.3.5. Macrophages differentiated in U251 conditioned medium show distinct morphology and immunosuppressive marker expression

To study the influence of BCAT1 expression on the differentiation and polarization of GAMs in more detail, I decided to use an *in vitro* macrophage differentiation model. Using medium conditioned by U251 control and BCAT1-KO cells (control-TCM and KO-TCM) I differentiated peripheral blood monocytes *in vitro* with the addition of low concentration of recombinant M-CSF (Macrophage Colony-Stimulating Factor). I could observe clear differences in morphology with the KO-TCM macrophages showing morphology reminiscent of the Controls (non-conditioned medium), whereas the control-TCM macrophages displayed an elongated morphology previously described *in vitro* as alternative M2 activation (McWhorter et al. 2013; Benner et al. 2019) (Figure 33A).

Next, I performed RNA sequencing on macrophages derived from 4 blood donors. An MDS analysis showed that the effects of the treatment overcome the individual variation of the donors (Figure 33B). Among differentially expressed genes, I observed markers often associated with immunosuppression and TAMs overexpressed in the control-TCM macrophages, and genes associated with antigen-presenting cells (APC) in KO-TCM macrophages (Figure 33C). These findings were further confirmed using a pre-ranked GSEA analysis with gene expression signatures of microglial cells (Patir et al. 2019) and monocyte-derived macrophages and dendritic cells (Tang-Huau et al. 2018). Namely, control-TCM macrophages showed a high enrichment of the microglial signature, likely due to differentiation in glioblastoma conditioned medium, and monocyte-derived macrophage signature (Figure 33D, red). In contrast, the KO-TCM macrophages showed an enrichment in the signature of monocyte-derived dendritic cells, as suggested by individual marker expression (Figure 33D, blue).

Finally, I tested the functional characteristics of the macrophages using a phagocytosis assay. In brief, macrophages were cultured with dead *E. Coli* particles marked with AF488, after which the non-engulfed particles were quenched, and the macrophages fixed and analyzed using confocal microscopy (Figure 34E). I found that the control-TCM macrophages showed a much higher phagocytic capacity than the KO-TCM ones (Figure 34F), consistent once again with a more immunosuppressive phenotype (Schulz et al. 2019).

Collectively, these findings suggest that the factors secreted by the U251 cells lacking BACT1 expression are unable to induce the tumor-associated-like immunosuppressive polarization of macrophages *in vitro*.

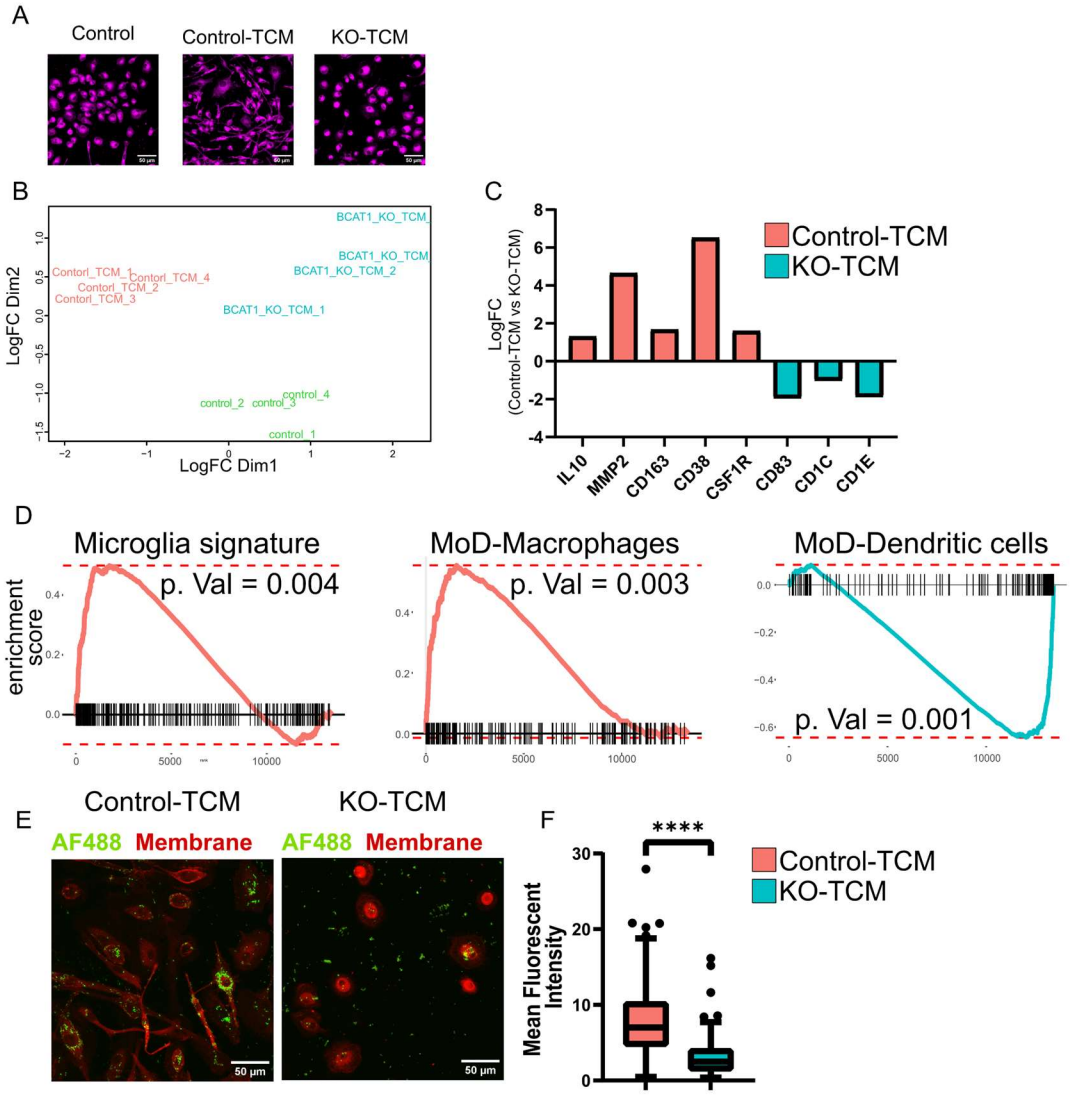

Figure 34 In vitro differentiation of PBMCs in tumor conditioned medium. A) morphological features of macrophages differentiated in non-conditioned medium (control), control U251 conditioned medium (control-TCM) and BCAT1-KO U251 conditioned medium (KO-TCM). Membranes were stained with the DeepRed membraned dye. Scale bar represents 50um. B) MDS plot based on 500 most variable genes of the control (green), control-TCM (red) and KO-TCM (blue) macrophages. C) log-fold-change (lofFC) values of selected marker genes overexpressed in either control-TCM (red) or KO-TCM (blue) macrophages. D) pre-ranked GSEA analysis using gene set signatures describing microglia (left), monocyte-derived macrophages (MoD-Macrophages, middle) and monocyte-derived dendritic cells (MoD-Dendritic cells, right) in control-TCM (red) and KO-TCM (blue) macrophages; p-values o each enrichment are denoted in the corresponding plot. E) Representative confocal images of control-TCM and KO-TCM macrophages stained with the DeppRed dye (red) with phagocytic particles labeled with AF488 (green). Scale bar represents 50um. F) Quantification of mean fluorescent intensity of phagocytic particles per cell of control-TCM (red) and KO-TCM (blue) macrophages. Results are presented as Tukey plots. The experiment was repeated twice each time quantifying more than 100 cells per condition. Statistical significance was determined using an unpaired, two-tailed student's t-test

5. Discussion

BCAT1 expression has been reported as a driving or prognostic factor in many cancer entities including, but not limited to, glioblastoma, lung cancer, breast cancer, AML and CML (Tönjes et al. 2013; Thewes et al. 2017; Y. Wang et al. 2019; Raffel et al. 2017; Hattori et al. 2017). As it is mainly expressed during embryonic development and shows very limited expression in adult tissues other than cancer (Benvenisty et al. 1992), BCAT1 is a prime candidate for selectively targeting cancer cells in new therapeutic approaches. To do so effectively, it is necessary to understand the underlying mechanisms behind its oncogenic potential. Different mechanisms have been proposed for this, mostly revolving around the metabolic function of BCAT1 and its influence on BCAA, glutamate and α-KG intracellular levels and secretion (Tönjes et al. 2013; Thewes et al. 2017; Y. Wang et al. 2019; Raffel et al. 2017, 1; Go et al. 2022, 1; Silva et al. 2017). Recent findings regarding the redox potential of the BCAT1 CXXC motif provided a novel mechanism of BACT1 action through modulating tumor cell redox signaling (Hillier et al. 2022; Francois et al. 2022).

In this thesis, I presented experiments aimed at understanding the role of BCAT1 in mitosis and in glioblastoma cell differentiation and the tumor-microenvironment crosstalk.

5.1. BCAT1 interacts with the components of the mitotic machinery and promotes the activity of key mitotic kinases

In recent years, many metabolic enzymes have been described as having moonlighting functions beyond the well-known canonical one. For example, the glycolytic enzyme phosphofructokinase (PFK) was found to have an additional function promoting YAP/TAZ (Yes-associated protein/ transcriptional co-activator with PDZ binding motif) signaling (Enzo et al. 2015); Glyceraldehyde 3-phosphate dehydrogenase (GAPDH) was described to translocate to the nucleus where it can modify nuclear proteins and alter transcription (Hara et al. 2005; Kornberg et al. 2010). With this in mind, and after the discovery of L. Francois that BCAT1 localizes not only in the nucleus of interphase cells but also at the mitotic spindle and the midbody during cell mitosis in multiple cancer and non-transformed cell lines (Francois et al. 2022) we explored the potential novel functions of BCAT1 contributing to mitosis.

BCAT1 was previously shown to be post-translationally modified through S-nitrosylation, S-glutathionylation (Forshaw and Conway 2019), oxidation (Myra Elizabeth Conway 2021) and phosphorylation (Harris et al. 2020; Shafei et al. 2020). These studies have additionally hypothesized a model of BCAT1 interaction with different proteins through a novel oxidoreductase chaperone activity (Hillier et al. 2022). Interestingly, in our phosphoproteomics dataset of the U251 and LN229 glioblastoma cell lines, we could not detect any phosphopeptides attributed to BCAT1 despite its reported phosphorylation through protein kinase C (PKC) (Harris et al. 2020) and proposed phosphorylation by other kinases (Shafei et al. 2020). Because of this, we focused our efforts on the interactions of BCAT1 with mitotic proteins and kinases regulating mitosis. After analyzing the proteins co-immunoprecipitated with BCAT1 in mitosis, I could confirm the interaction with many of the major constituents of the mitotic spindle and the kinetochore. These findings were further validated through Western blotting by L. Francois (Francois et al. 2022). In line with this, BCAT1-KO induced mitotic aberrations in multiple cell lines, proving that it is not only co-localizing with the mitotic components, but also crucial for their proper functioning.

To gain a more mechanistic insight into the role of BCAT1 in mitosis I analyzed the phosphoproteome of mitotic control and BCAT1-KO cells. Interestingly, there were few changes to the phosphorylation status of the key mitotic kinases such as TTK, AURKA and AURKB. However, the downstream targets of these kinases showed markedly reduced phosphorylation in BCAT1-KO cells.

The role of reactive oxygen species (ROS) and redox modifications of proteins in mitosis is not very well understood. Some studies have reported dynamic changes or ROS throughout the cell cycle which could influence mitotic progression (Patterson et al. 2019). This, together with the fact that kinases such as EGFR (Paulsen et al. 2011), phosphatases such as PTEN (Lee et al. 2002) and mitotic regulators such as CDC25 and AURKA (Savitsky and Finkel 2002; Lim et al. 2020) are regulated through oxidation, prompted us to explore the CXXC-dependent redox role of BCAT1. Using an overexpression-rescue system, L. Francois not only confirmed the reduced activity of the mitotic kinase TTK that was suggested in the phosphoproteome analysis, but additionally showed a mislocalization of AURKB in a CXXC-motif dependent fashion. These findings could explain its reduced activity observed in my analysis, despite the seemingly unaltered phosphorylation (Francois et al. 2022). As AURKB localization is closely related to its function in maintaining the proper spindle assembly checkpoint (Liang et al. 2020)

Interestingly, one of the first papers on the function of BCAT1 in yeast described it as a regulator of the cell cycle G1/S phase (Schuldiner et al. 1996). However, its role in the regulation of the

G1/S transition could be related to the metabolic function of BCAT1 wherein the BCAAs regulate major cellular pathways such as mTOR (Luo et al. 2021; Meijer et al. 2015; Shu et al. 2021). In this thesis and in (Francois et al. 2022) we describe a novel function of BCAT1 in maintaining mitotic fidelity through the proper functioning and localization of key SAC kinases TTK and AURKB via the CXXC motif.

5.2. BCAT1 expression maintains the plasticity of human and mouse glioblastoma cells

Glioblastomas are generally poorly differentiated tumors characterized by high intratumoral heterogeneity and cellular plasticity (Friedmann-Morvinski 2014). Under the assumption that these features contribute to the aggressiveness of glioblastoma and its overall resistance to treatments, researches have made multiple attempts to induce cellular differentiation of glioblastoma cells which would in turn slow down or stop their growth entirely (Park et al. 2017; Cheng et al. 2019; Guichet et al. 2013). Unfortunately, this line of research proved unfruitful as true terminal differentiation could not be reached without exogeneous gene overexpression (Carén et al. 2015). Namely, glioblastoma cells could revert to a poorly differentiated proliferative state upon the removal of differentiation cues *in vitro*. In fact, cells not only have the ability to differentiate, but to use this in order to propagate migration and tumor growth as differentiated fractions of cells within the tumors have been shown to promote tumor growth (Uneda et al. 2021). Furthermore, glioblastoma cells have been shown to appropriate neuronal features including synaptic signaling when migrating throughout the brain, while retaining the ability to form typical tumor masses once the migration is complete (Venkataramani et al. 2022).

Notably, different approaches relying on directly overexpressing transcription regulators of neuronal fate did show promising terminal differentiation features of glioblastoma cells. For example, the overexpression of ASCL1 (Achaete-Scute Family bHLH Transcription Factor 2 and 1) in glioblastoma cells could promote their differentiation and reduce tumorigenicity (Azzarelli et al. 2022; Cheng et al. 2019; Park et al. 2017, 2; X. Wang et al. 2021). Similarly, the overexpression of NEUROD1 induced cell death and differentiation (Guichet et al. 2013; X. Wang et al. 2021). Even though these results show a promising phenotype, they are all based on an overexpression of genes that can otherwise severely impact non-tumor cells, reducing the applicability of this method *in vivo* (Matsuda et al. 2019, 1; Rao et al. 2021, 1).

In the experiments presented in this thesis, I was able to confirm the cellular plasticity of the mouse glioblastoma model mGB2, which although showing an initial ability to differentiate, did revert back to a proliferative poorly differentiated state after the removal of extrinsic cues, as reported previously (Carén et al. 2015). However, I also showed that in the lack of Bcat1 expression, this ability was severely hampered *in vitro*. Interestingly, the mouse glioblastoma stem cells showed an increased expression of many neuronal and glial differentiation marker genes even in the stem cell-propagating conditions, including the major fate regulators mentioned previously: NeudoD1 and Ascl1. This data shows that depleting Bcat1 expression could achieve similar effects to those observed with the ectopic overexpression of these transcription factors.

Using expressional signatures derived from many glioblastoma studies based on either bulk sequencing or single cell sequencing characterization (Verhaak et al. 2010; Q. Wang et al. 2017; Neftel et al. 2019; S. R. Alcantara Llaguno et al. 2015; Garofano et al. 2021; Venkataramani et al. 2022) I was able to associate the Bcat1-KO cells with the more differentiated, neuronal glioblastoma signatures, as well as developmental and migratory neuronal ones mentioned previously (Venkataramani et al. 2022). This was further consolidated by the *in* vivo experiments in which I observed highly differentiated features of Bcat1-KO cells and could show either complete lack of tumor growth or severe delay in BL6 and NSG mice, respectively. I compared how the lack of BCAT1 expression influences the human glioblastoma cell line U251. Notably, this cell line is cultured under differentiating conditions (10% FCS), however, the knockout cells nevertheless showed a similar pattern of differentiation as the mouse mGB2 cells, even including a high number of co-regulated genes between the cell lines. Furthermore, I could show that low expression of BCAT1 in sequenced patient tumors is also associated with a more differentiated and less mesenchymal features of the tumors, proving that our mouse and human *in vivo* and *in vitro* data has translational relevance.

DNA methylation has been shown to be involved in glioblastoma development and tumorigenicity (Klughammer et al. 2018). Usually, it has been described as factor in the development of IDH-mutant gliomas, as the oncometabolite produced by mutant IDH, 2-HG, directly competes with α-KG and causes an overall increased methylation of the genome due to the reduced activity of TET enzymes. Interestingly, inhibiting the mutated enzyme and thus decreasing the levels of DNA methylation of IDH^{MUT} gliomas was shown to decrease tumorigenicity and induce differentiation of the tumor cells (Pusch et al. 2017; Turcan et al. 2013). It is worth mentioning here that IDH^{MUT} gliomas do have a favorable outcome in comparison to the IDH^{WT} glioblastomas (Unruh et al. 2019), but this could be due to a different overall etiology of these two tumor types. These findings,

together with the previously suggested role of BCAT1 in restricting cellular α-KG and causing DNA hypermethylation in AML (Raffel et al. 2017) led me to explore the DNA methylation status of the mGB2 mouse glioblastoma stem cells. Consistent with the proposed function, Bcat1-KO mGB2 cells showed an overall reduction of DNA methylation which correlated highly with the expressional differences between the cells. Moreover, methylation potentially regulates the expression of differentiation genes such as NeuroD1 and Ascl1 as they (among others) show a hypermethylation in the control cells. Collectively, this data is consistent with published and proposed mechanisms and suggest that BCAT1 could be a promising target for future exploration of the induction of glioblastoma differentiation.

5.3. BCAT1 expression modifies the glioblastoma immune microenvironment

BCAT1 was previously shown to be relevant for glioblastoma progression and proliferation (Tönjes et al. 2013). Tönjes et al proposed a glutamate dependent mechanism of BCAT1 in glioblastoma and showed a slower progression of Bcat1-KO glioblastoma cells transplanted in immunodeficient mice. However, the exact mechanism behind this observation *in vivo* as well as the detailed characterization of the tumors remained to be elucidated. In my thesis work, I used different mouse strains to delineate between the effects of BCAT1-induced differentiation and any potential influence of BCAT1 expression in the tumor cells on the cells of the immune microenvironment

Glioblastoma is generally characterized as an immune “cold” tumor entity referring to the low infiltration of lymphoid cells, and in particular $CD8^+$ T-cells (Singh et al. 2021). On the other hand, the tumors are rich in myeloid cells originating from the brain’s endogenous microglial population or circulating blood monocytes (Kvisten et al. 2019). These myeloid cells are, however, greatly contributing to the immunosuppressive nature of the tumors, preventing T-cell infiltration and/or activation. Some of these effects have been attributed to the secretion of immunosuppressive cytokines such as interleukin-10 (IL-10) (Ravi et al. 2022). Consistent with this work, I have found a substantial myeloid infiltration in the mouse mGB2 tumors when injected intracranially into immunocompetent BL6 mice, with a very characteristic glioma-associated macrophage morphological features (Kvisten et al. 2019). Interestingly, I have found that the myeloid infiltration of the mBG2 Bcat1-KO tumors is even more pronounced, however, their morphological features are more resembling dendritic cells (D’Agostino et al. 2012) than glioma associated-

macrophages. This suggests an alternate function. Furthermore, when I visualized the $CD8^+$ T-cells of the tumors, even though I could observe T-cell infiltration in both control and Bcat1-KO tumors at an early time point, at a late stage of tumor development I could detect a substantial T-cell infiltration only in the Bcat1-KO tumors. It is worth noting that the early T cell infiltration into the control tumors could be an artifact of the brain injury induced during intracranial cell transplantation (Daglas et al. 2019). The observations of the different immune infiltration between the tumors were further strengthened by the fact that Bcat1-KO formed tumors in the NSG and Rag2-KO but not the BL6 mouse models. These results clearly indicate an important role of the immune system in regulating the growth of the Bcat1-KO tumors, although it should be emphasized that the tumor growth of the Bcat1-KO cells in both immunocompromised models was significantly slower than of the control tumors. Furthermore, these results indicate a crucial importance of the T-cell compartment, even though it is very likely that the activity of the T-cells is directly promoted or at least not inhibited by the altered myeloid cells of the Bcat1-KO tumors.

Beyond looking at just the mouse model, the wide availability of glioblastoma single-cell sequencing datasets allows for a more detailed look into the immune scores of bulk-sequenced tumors through deconvolution and software such as CIBERSORTx (Mehani et al. 2022). Utilizing this, I explored the cell scores of the macrophage and CD8 T-cells in the $BACT1^{high}$ and $BCAT1^{low}$ TCGA tumors and observed a higher score for both populations in the $BCAT1^{low}$ samples, consistent with the mouse data. Furthermore, *in vitro* macrophage experiments using the conditioned medium of the U251 cells confirmed an antigen-presenting-like phenotype of the cells differentiated in the KO-TCM. This was in contrast to the expected and previously described tumor-associated macrophage phenotype acquired with differentiation in control-TCM (Benner et al. 2019).

Collectively, these findings suggest that BCAT1 expression in glioblastoma cells influences the tumor microenvironment and in particular the composition and activation of the immune cells. Even though my previous experiments show a strong effect of Bcat1 on cellular plasticity and differentiation of glioblastoma, it is clear that the immune component is necessary to completely abrogate tumor growth of the Bcat1-KO glioblastoma cells.

5.4. Conclusions

In the work presented in this thesis I focused on the 1) novel role of BCAT1 in regulating the fidelity of cellular mitosis, 2) its function in maintaining the plasticity of glioblastoma cells and 3) how its expression influences the glioblastoma microenvironment. Through unbiased phosphoproteomic and proteomic approaches I could show that BCAT1 interacts with many components of the mitotic machinery and influences the efficiency of key SAC kinases TTK and AURKB in two glioblastoma cell lines. These findings were further confirmed in different *in vitro*, *in situ* and *in vivo* systems together with L. Francois (Francois et al. 2022).

Using a mouse stem cell glioblastoma model, I was able to show that cellular plasticity is reduced, and differentiation potential increased with the knockout of Bcat1, even without the presence of exogenous differentiation drivers. These findings were consistent in an *in vivo* setting in different mouse strains and were consistent with TCGA human tumor data and a human glioblastoma cell line.

Finally, using different immunodeficient mouse models, I showed that even though Bcat1-mediated differentiation has a prominent effect on tumor growth it is not the only relevant factor, and that a functional immune system is required to completely abrogate tumors. This was likely possible due to a lack of immunosuppressive signaling originating from the Bcat1-KO tumor cells.

Taken together, the data presented here propose a novel role of BCAT1 in glioblastoma consolidating it as a potential target in future glioblastoma treatment efforts.

5.5. Outlook

In this thesis, I have addressed in detail the phenotypical changes occurring upon the knockout of BCAT1 or its reduced expression. Even though these changes are consistent in both human samples and human and mouse glioblastoma cell lines, a lot remains to be discovered regarding the underlying mechanism.

The data show an impact of BCAT1 on DNA methylation, however, whether this effect is dependent on a specific DNA demethylase, i.e., TET1, 2 or 3, or whether it is a broad mechanism solely dependent on the availability of αKG in the nucleus in general remains to be determined. To do so, experiments involving the selective knockdown of the TET enzymes in glioblastoma cells will be able to show the exact mechanism and further expand the potential of using BCAT1 in differentiation-based therapeutic approaches.

Beyond the mechanistic investigation, much more remains to be elucidated regarding the role of BCAT1 in maintaining the immunosuppressive properties of glioblastoma. Future efforts to expand on this topic will include advanced sequencing and imaging techniques. Even though it is likely that the differentiation of glioblastoma cells resulting from the knockout of BCAT1 is related to the lack of immunosuppression, expressional characterization of the altered myeloid microenvironment utilizing a broad approach such as single cell transcriptomics or a more targeted one such as multiplexed RNA-FISH can identify factors directly responsible for this phenotype. Once discovered, these factors or the mechanisms can be further exploited for targeting downstream of BCAT1.

Finally, after detailed examinations of the mechanistic basis of the effect of BCAT1 in glioblastoma, we would like to focus our attention on exploiting this enzyme in the treatment of the disease. Even though, as mentioned before, BCAT1 expression is tissue and developmentally restricted, potential inhibitors working in ranges optimal for patient treatment are difficult to achieve due to their affinity towards unspecifically inhibiting BCAT2. High-throughput screening strategies for finding BCAT1-specific inhibitors, followed by chemical studies for optimizing its blood-brain barrier permeability represent the final challenge of the pre-clinical study part of the role of BCAT1 in glioblastoma.

6. Publications

1. Liliana Francois*, **Pavle Boskovic***, Julian Knerr, Wei He, Gianluca Sigismondo, Carsten Schwan, Tushar H. More, Magdalena Schlotter, Jeroen Krijgsveld, Karsten Hiller, Robert Grosse, Peter Lichter, Bernhard Radlwimmer.

   BCAT1 redox function maintains mitotic fidelity. Cell Reports, 2022.

2. Ivanova, E. L., Costa, B., Eisemann, T., Lohr, S., **Boskovic, P**., Eichwald, V., Meckler, J., Jugold, M., Orian-Rousseau, V., Peterziel, H., & Angel, P.

   CD44 expressed by myeloid cells promotes glioma invasion. Frontiers in oncology, 2022.

3. Casati, B., Verdi, J. P., Hempelmann, A., Kittel, M., Klaebisch, A. G., Meister, B., Welker, S., Asthana, S., Di Giorgio, S., **Boskovic, P**., Man, K. H., Schopp, M., Ginno, P. A., Radlwimmer, B., Stebbins, C. E., Miethke, T., Papavasiliou, F. N., & Pecori, R.

   Rapid, adaptable and sensitive Cas13-based COVID-19 diagnostics using ADESSO. Nature communications, 2022.

4. Costa, B., Fletcher, M., **Boskovic, P**., Ivanova, E. L., Eisemann, T., Lohr, S., Bunse, L., Löwer, M., Burchard, S., Korshunov, A., Coltella, N., Cusimano, M., Naldini, L., Liu, H. K., Platten, M., Radlwimmer, B., Angel, P., & Peterziel, H.

   A Set of Cell Lines Derived from a Genetic Murine Glioblastoma Model Recapitulates Molecular and Morphological Characteristics of Human Tumors. Cancers, 2021

7. References

Abdelfattah, Nourhan, Parveen Kumar, Caiyi Wang, Jia-Shiun Leu, William F. Flynn, Ruli Gao, David S. Baskin, et al. 2022. “Single-Cell Analysis of Human Glioma and Immune Cells Identifies S100A4 as an Immunotherapy Target.” *Nature Communications* 13 (1): 767. https://doi.org/10.1038/s41467-022-28372-y.

Abrieu, A., L. Magnaghi-Jaulin, J. A. Kahana, M. Peter, A. Castro, S. Vigneron, T. Lorca, D. W. Cleveland, and J. C. Labbé. 2001. “Mps1 Is a Kinetochore-Associated Kinase Essential for the Vertebrate Mitotic Checkpoint.” *Cell* 106 (1): 83–93. https://doi.org/10.1016/s0092-8674(01)00410-x.

Alcantara Llaguno, Sheila, Jian Chen, Chang-Hyuk Kwon, Erica L. Jackson, Yanjiao Li, Dennis K. Burns, Arturo Alvarez-Buylla, and Luis F. Parada. 2009. “Malignant Astrocytomas Originate from Neural Stem/Progenitor Cells in a Somatic Tumor Suppressor Mouse Model.” *Cancer Cell* 15 (1): 45–56. https://doi.org/10.1016/j.ccr.2008.12.006.

Alcantara Llaguno, Sheila R., Zilai Wang, Daochun Sun, Jian Chen, Jing Xu, Euiseok Kim, Kimmo J. Hatanpaa, et al. 2015. “Adult Lineage-Restricted CNS Progenitors Specify Distinct Glioblastoma Subtypes.” *Cancer Cell* 28 (4): 429–40. https://doi.org/10.1016/j.ccell.2015.09.007.

Alcasabas, Annette A., Alexander J. Osborn, Jeff Bachant, Fenghua Hu, Petra J. H. Werler, Kristine Bousset, Kanji Furuya, John F. X. Diffley, Antony M. Carr, and Stephen J. Elledge. 2001. “Mrc1 Transduces Signals of DNA Replication Stress to Activate Rad53.” *Nature Cell Biology* 3 (11): 958–65. https://doi.org/10.1038/ncb1101-958.

Aryee, Martin J., Andrew E. Jaffe, Hector Corrada-Bravo, Christine Ladd-Acosta, Andrew P. Feinberg, Kasper D. Hansen, and Rafael A. Irizarry. 2014. “Minfi: A Flexible and Comprehensive Bioconductor Package for the Analysis of Infinium DNA Methylation Microarrays.” *Bioinformatics* 30 (10): 1363–69. https://doi.org/10.1093/bioinformatics/btu049.

Azzarelli, Roberta, Aoibheann McNally, Claudia Dell’Amico, Marco Onorati, Benjamin Simons, and Anna Philpott. 2022. “ASCL1 Phosphorylation and ID2 Upregulation Are Roadblocks to Glioblastoma Stem Cell Differentiation.” *Scientific Reports* 12 (1): 2341. https://doi.org/10.1038/s41598-022-06248-x.

Baghban, Roghayyeh, Leila Roshangar, Rana Jahanban-Esfahlan, Khaled Seidi, Abbas Ebrahimi-Kalan, Mehdi Jaymand, Saeed Kolahian, Tahereh Javaheri, and Peyman Zare. 2020. "Tumor Microenvironment Complexity and Therapeutic Implications at a Glance." *Cell Communication and Signaling* 18 (1): 59. https://doi.org/10.1186/s12964-020-0530-4.

Barr, Francis A., and Ulrike Gruneberg. 2007. "Cytokinesis: Placing and Making the Final Cut." *Cell* 131 (5): 847–60. https://doi.org/10.1016/j.cell.2007.11.011.

Bayraktar, Gonca, PingAn Yuanxiang, Alessandro D. Confettura, Guilherme M. Gomes, Syed A. Raza, Oliver Stork, Shoji Tajima, et al. 2020. "Synaptic Control of DNA Methylation Involves Activity-Dependent Degradation of DNMT3A1 in the Nucleus." *Neuropsychopharmacology* 45 (12): 2120–30. https://doi.org/10.1038/s41386-020-0780-2.

Benner, Brooke, Luke Scarberry, Lorena P. Suarez-Kelly, Megan C. Duggan, Amanda R. Campbell, Emily Smith, Gabriella Lapurga, et al. 2019. "Generation of Monocyte-Derived Tumor-Associated Macrophages Using Tumor-Conditioned Media Provides a Novel Method to Study Tumor-Associated Macrophages in Vitro." *Journal for ImmunoTherapy of Cancer* 7 (1): 140. https://doi.org/10.1186/s40425-019-0622-0.

Benvenisty, N., A. Leder, A. Kuo, and P. Leder. 1992. "An Embryonically Expressed Gene Is a Target for C-Myc Regulation via the c-Myc-Binding Sequence." *Genes & Development* 6 (12b): 2513–23. https://doi.org/10.1101/gad.6.12b.2513.

Binnewies, Mikhail, Edward W. Roberts, Kelly Kersten, Vincent Chan, Douglas F. Fearon, Miriam Merad, Lisa M. Coussens, et al. 2018. "Understanding the Tumor Immune Microenvironment (TIME) for Effective Therapy." *Nature Medicine* 24 (5): 541–50. https://doi.org/10.1038/s41591-018-0014-x.

Bird, Adrian P, and Alan P Wolffe. 1999. "Methylation-Induced Repression— Belts, Braces, and Chromatin." *Cell* 99 (5): 451–54. https://doi.org/10.1016/S0092-8674(00)81532-9.

Borah, Naheed Arfin, Swatishree Sradhanjali, Manas Ranjan Barik, Atimukta Jha, Devjyoti Tripathy, Swathi Kaliki, Suryasnata Rath, et al. 2021. "Aurora Kinase B Expression, Its Regulation and Therapeutic Targeting in Human Retinoblastoma." *Investigative Ophthalmology & Visual Science* 62 (3): 16. https://doi.org/10.1167/iovs.62.3.16.

Brandao, Mayra, Thomas Simon, Giles Critchley, and Georgios Giamas. 2019. "Astrocytes, the Rising Stars of the Glioblastoma Microenvironment." *Glia* 67 (5): 779–90. https://doi.org/10.1002/glia.23520.

Brandenburg, Susan, Annett Müller, Kati Turkowski, Yordan T. Radev, Sergej Rot, Christin Schmidt, Alexander D. Bungert, et al. 2016. “Resident Microglia Rather than Peripheral Macrophages Promote Vascularization in Brain Tumors and Are Source of Alternative Pro-Angiogenic Factors.” *Acta Neuropathologica* 131 (3): 365–78. https://doi.org/10.1007/s00401-015-1529-6.

Brat, Daniel J., Kenneth Aldape, Howard Colman, Eric C. Holland, David N. Louis, Robert B. Jenkins, B. K. Kleinschmidt-DeMasters, et al. 2018. “CIMPACT-NOW Update 3: Recommended Diagnostic Criteria for ‘Diffuse Astrocytic Glioma, IDH-Wildtype, with Molecular Features of Glioblastoma, WHO Grade IV.’” *Acta Neuropathologica* 136 (5): 805–10. https://doi.org/10.1007/s00401-018-1913-0.

Bray, Julie K., Meelad M. Dawlaty, Amit Verma, and Anirban Maitra. 2021. “Roles and Regulations of TET Enzymes in Solid Tumors.” *Trends in Cancer* 7 (7): 635–46. https://doi.org/10.1016/j.trecan.2020.12.011.

Carén, Helena, Stefan H. Stricker, Harry Bulstrode, Sladjana Gagrica, Ewan Johnstone, Thomas E. Bartlett, Andrew Feber, et al. 2015. “Glioblastoma Stem Cells Respond to Differentiation Cues but Fail to Undergo Commitment and Terminal Cell-Cycle Arrest.” *Stem Cell Reports* 5 (5): 829–42. https://doi.org/10.1016/j.stemcr.2015.09.014.

Chen, Shaohui, Bohan Chen, Guangsong Su, Jun Chen, Dianhao Guo, Qingqing Yin, Wenbin Wang, et al. 2020. “Branched-Chain Amino Acid Aminotransferase-1 Regulates Self-Renewal and Pluripotency of Mouse Embryonic Stem Cells through Ras Signaling.” *Stem Cell Research* 49 (December): 102097. https://doi.org/10.1016/j.scr.2020.102097.

Cheng, Xueyan, Zijian Tan, Xiao Huang, Yimin Yuan, Shangyao Qin, Yakun Gu, Dan Wang, Cheng He, and Zhida Su. 2019. “Inhibition of Glioma Development by ASCL1-Mediated Direct Neuronal Reprogramming.” *Cells* 8 (6): 571. https://doi.org/10.3390/cells8060571.

Coniglio, Salvatore J., Eliseo Eugenin, Kostantin Dobrenis, E. Richard Stanley, Brian L. West, Marc H. Symons, and Jeffrey E. Segall. 2012. “Microglial Stimulation of Glioblastoma Invasion Involves Epidermal Growth Factor Receptor (EGFR) and Colony Stimulating Factor 1 Receptor (CSF-1R) Signaling.” *Molecular Medicine (Cambridge, Mass.)* 18 (May): 519–27. https://doi.org/10.2119/molmed.2011.00217.

Conway, Myra E., Steven J. Coles, Mohammad M. Islam, and Susan M. Hutson. 2008. “Regulatory Control of Human Cytosolic Branched-Chain Aminotransferase by Oxidation and S-

Glutathionylation and Its Interactions with Redox Sensitive Neuronal Proteins." *Biochemistry* 47 (19): 5465–79. https://doi.org/10.1021/bi800303h.

Conway, Myra Elizabeth. 2021. "Emerging Moonlighting Functions of the Branched-Chain Aminotransferase Proteins." *Antioxidants & Redox Signaling*, April. https://doi.org/10.1089/ars.2020.8118.

Cooper, Geoffrey M. 2000. "The Nucleus during Mitosis." *The Cell: A Molecular Approach. 2nd Edition*. https://www.ncbi.nlm.nih.gov/books/NBK9890/.

Costa, Barbara, Michael N. C. Fletcher, Pavle Boskovic, Ekaterina L. Ivanova, Tanja Eisemann, Sabrina Lohr, Lukas Bunse, et al. 2021. "A Set of Cell Lines Derived from a Genetic Murine Glioblastoma Model Recapitulates Molecular and Morphological Characteristics of Human Tumors." *Cancers* 13 (2): 230. https://doi.org/10.3390/cancers13020230.

Couturier, Charles P., Shamini Ayyadhury, Phuong U. Le, Javad Nadaf, Jean Monlong, Gabriele Riva, Redouane Allache, et al. 2020. "Single-Cell RNA-Seq Reveals That Glioblastoma Recapitulates a Normal Neurodevelopmental Hierarchy." *Nature Communications* 11 (1): 3406. https://doi.org/10.1038/s41467-020-17186-5.

D. B., D. 1930. "Degeneration and Regeneration of the Nervous System." *Nature* 125 (3146): 230–31. https://doi.org/10.1038/125230a0.

Daglas, Maria, Dominik F. Draxler, Heidi Ho, Fiona McCutcheon, Adam Galle, Amanda E. Au, Pia Larsson, et al. 2019. "Activated CD8+ T Cells Cause Long-Term Neurological Impairment after Traumatic Brain Injury in Mice." *Cell Reports* 29 (5): 1178-1191.e6. https://doi.org/10.1016/j.celrep.2019.09.046.

D'Agostino, Paul M., Andres Gottfried-Blackmore, Niroshana Anandasabapathy, and Karen Bulloch. 2012. "Brain Dendritic Cells: Biology and Pathology." *Acta Neuropathologica* 124 (5): 599–614. https://doi.org/10.1007/s00401-012-1018-0.

De Palma, Michele, Daniela Biziato, and Tatiana V. Petrova. 2017. "Microenvironmental Regulation of Tumour Angiogenesis." *Nature Reviews Cancer* 17 (8): 457–74. https://doi.org/10.1038/nrc.2017.51.

Dhanani, Zameer N., Gagandeep Mann, and Olasunkanmi A. J. Adegoke. 2019. "Depletion of Branched-chain Aminotransferase 2 (BCAT2) Enzyme Impairs Myoblast Survival and Myotube Formation." *Physiological Reports* 7 (23): e14299. https://doi.org/10.14814/phy2.14299.

Doetsch, F., I. Caillé, D. A. Lim, J. M. García-Verdugo, and A. Alvarez-Buylla. 1999. “Subventricular Zone Astrocytes Are Neural Stem Cells in the Adult Mammalian Brain.” *Cell* 97 (6): 703–16. https://doi.org/10.1016/s0092-8674(00)80783-7.

“Dynamic Documents with R and Knitr.” n.d. Routledge & CRC Press. Accessed October 13, 2022. https://www.routledge.com/Dynamic-Documents-with-R-and-knitr/Xie/p/book/9781498716963.

Enzo, Elena, Giulia Santinon, Arianna Pocaterra, Mariaceleste Aragona, Silvia Bresolin, Mattia Forcato, Daniela Grifoni, et al. 2015. “Aerobic Glycolysis Tunes YAP/TAZ Transcriptional Activity.” *The EMBO Journal* 34 (10): 1349–70. https://doi.org/10.15252/embj.201490379.

Esteller, M., J. Garcia-Foncillas, E. Andion, S. N. Goodman, O. F. Hidalgo, V. Vanaclocha, S. B. Baylin, and J. G. Herman. 2000. “Inactivation of the DNA-Repair Gene MGMT and the Clinical Response of Gliomas to Alkylating Agents.” *The New England Journal of Medicine* 343 (19): 1350–54. https://doi.org/10.1056/NEJM200011093431901.

Evan, Gerard I., Andrew H. Wyllie, Christopher S. Gilbert, Trevor D. Littlewood, Hartmut Land, Mary Brooks, Catherine M. Waters, Linda Z. Penn, and David C. Hancock. 1992. “Induction of Apoptosis in Fibroblasts by C-Myc Protein.” *Cell* 69 (1): 119–28. https://doi.org/10.1016/0092-8674(92)90123-T.

Fang, Xiaoguang, Zhi Huang, Kui Zhai, Qian Huang, Weiwei Tao, Leo Kim, Qiulian Wu, et al. 2021. “Inhibiting DNA-PK Induces Glioma Stem Cell Differentiation and Sensitizes Glioblastoma to Radiation in Mice.” *Science Translational Medicine* 13 (600): eabc7275. https://doi.org/10.1126/scitranslmed.abc7275.

Farc, Ovidiu, and Victor Cristea. 2021. “An Overview of the Tumor Microenvironment, from Cells to Complex Networks (Review).” *Experimental and Therapeutic Medicine* 21 (1): 1–1. https://doi.org/10.3892/etm.2020.9528.

Farhood, Bagher, Masoud Najafi, and Keywan Mortezaee. 2019. “CD8+ Cytotoxic T Lymphocytes in Cancer Immunotherapy: A Review.” *Journal of Cellular Physiology* 234 (6): 8509–21. https://doi.org/10.1002/jcp.27782.

Feng, Xi, Frank Szulzewsky, Alexan Yerevanian, Zhihong Chen, David Heinzmann, Rikke Darling Rasmussen, Virginia Alvarez-Garcia, et al. 2015. “Loss of CX3CR1 Increases Accumulation of Inflammatory Monocytes and Promotes Gliomagenesis.” *Oncotarget* 6 (17): 15077–94. https://doi.org/10.18632/oncotarget.3730.

Ferrucci, Veronica, and Massimo Zollo. 2016. “Glioblastoma Stem Cells Differentiation through Epigenetic Modulation Is Driven by MiR-296-5p/HMGA1/Sox2 Axis.” *Translational Cancer Research* 5 (4). https://doi.org/10.21037/tcr.2016.10.88.

Fomenko, Dmitri E., and Vadim N. Gladyshev. 2003. “Identity and Functions of CxxC-Derived Motifs.” *Biochemistry* 42 (38): 11214–25. https://doi.org/10.1021/bi034459s.

Forshaw, Thomas E., and Myra E. Conway. 2019. “Detection of S-Nitrosation and S-Glutathionylation of the Human Branched-Chain Aminotransferase Proteins.” In *Redox-Mediated Signal Transduction: Methods and Protocols*, edited by John T. Hancock and Myra E. Conway, 71–84. Methods in Molecular Biology. New York, NY: Springer US. https://doi.org/10.1007/978-1-4939-9463-2_6.

Francois, Liliana, Pavle Boskovic, Julian Knerr, Wei He, Gianluca Sigismondo, Carsten Schwan, Tushar H. More, et al. 2022. “BCAT1 Redox Function Maintains Mitotic Fidelity.” *Cell Reports* 41 (3). https://doi.org/10.1016/j.celrep.2022.111524.

Friedmann-Morvinski, Dinorah. 2014. “Glioblastoma Heterogeneity and Cancer Cell Plasticity.” *Critical Reviews in Oncogenesis* 19 (5): 327–36. https://doi.org/10.1615/critrevoncog.2014011777.

Gage, F. H. 2000. “Mammalian Neural Stem Cells.” *Science (New York, N.Y.)* 287 (5457): 1433–38. https://doi.org/10.1126/science.287.5457.1433.

Galvao, Rui Pedro, Anita Kasina, Robert S. McNeill, Jordan E. Harbin, Oded Foreman, Roel G. W. Verhaak, Akiko Nishiyama, C. Ryan Miller, and Hui Zong. 2014. “Transformation of Quiescent Adult Oligodendrocyte Precursor Cells into Malignant Glioma through a Multistep Reactivation Process.” *Proceedings of the National Academy of Sciences* 111 (40). https://doi.org/10.1073/pnas.1414389111.

García, María G., Antonella Carella, Rocío G. Urdinguio, Gustavo F. Bayón, Virginia Lopez, Juan Ramón Tejedor, Marta I. Sierra, et al. 2018. “Epigenetic Dysregulation of TET2 in Human Glioblastoma.” *Oncotarget* 9 (40): 25922–34. https://doi.org/10.18632/oncotarget.25406.

Garnier, Delphine, Ophélie Renoult, Marie-Clotilde Alves-Guerra, François Paris, and Claire Pecqueur. 2019. “Glioblastoma Stem-Like Cells, Metabolic Strategy to Kill a Challenging Target.” *Frontiers in Oncology* 9. https://www.frontiersin.org/articles/10.3389/fonc.2019.00118.

Garofano, Luciano, Simona Migliozzi, Young Taek Oh, Fulvio D'Angelo, Ryan D. Najac, Aram Ko, Brulinda Frangaj, et al. 2021. "Pathway-Based Classification of Glioblastoma Uncovers a Mitochondrial Subtype with Therapeutic Vulnerabilities." *Nature Cancer* 2 (2): 141–56. https://doi.org/10.1038/s43018-020-00159-4.

Gilbert, Mark R., Meihua Wang, Kenneth D. Aldape, Roger Stupp, Monika E. Hegi, Kurt A. Jaeckle, Terri S. Armstrong, et al. 2013. "Dose-Dense Temozolomide for Newly Diagnosed Glioblastoma: A Randomized Phase III Clinical Trial." *Journal of Clinical Oncology: Official Journal of the American Society of Clinical Oncology* 31 (32): 4085–91. https://doi.org/10.1200/JCO.2013.49.6968.

Ginhoux, Florent, Melanie Greter, Marylene Leboeuf, Sayan Nandi, Peter See, Solen Gokhan, Mark F. Mehler, et al. 2010. "Fate Mapping Analysis Reveals That Adult Microglia Derive from Primitive Macrophages." *Science (New York, N.Y.)* 330 (6005): 841–45. https://doi.org/10.1126/science.1194637.

Go, Miyeon, Eunji Shin, Seo Young Jang, Miso Nam, Geum-Sook Hwang, and Soo Young Lee. 2022. "BCAT1 Promotes Osteoclast Maturation by Regulating Branched-Chain Amino Acid Metabolism." *Experimental & Molecular Medicine* 54 (6): 825–33. https://doi.org/10.1038/s12276-022-00775-3.

Goll, Mary Grace, and Timothy H. Bestor. 2005. "Eukaryotic Cytosine Methyltransferases." *Annual Review of Biochemistry* 74: 481–514. https://doi.org/10.1146/annurev.biochem.74.010904.153721.

Gould, Kathleen L., and Paul Nurse. 1989. "Tyrosine Phosphorylation of the Fission Yeast Cdc2+ Protein Kinase Regulates Entry into Mitosis." *Nature* 342 (6245): 39–45. https://doi.org/10.1038/342039a0.

Guichet, Pierre-Olivier, Ivan Bieche, Marisa Teigell, Ché Serguera, Bernard Rothhut, Valérie Rigau, Frédérique Scamps, et al. 2013. "Cell Death and Neuronal Differentiation of Glioblastoma Stem-like Cells Induced by Neurogenic Transcription Factors." *Glia* 61 (2): 225–39. https://doi.org/10.1002/glia.22429.

Hack, Michael A., Armen Saghatelyan, Antoine de Chevigny, Alexander Pfeifer, Ruth Ashery-Padan, Pierre-Marie Lledo, and Magdalena Götz. 2005. "Neuronal Fate Determinants of Adult Olfactory Bulb Neurogenesis." *Nature Neuroscience* 8 (7): 865–72. https://doi.org/10.1038/nn1479.

Hall, T. R., R. Wallin, G. D. Reinhart, and S. M. Hutson. 1993. “Branched Chain Aminotransferase Isoenzymes. Purification and Characterization of the Rat Brain Isoenzyme.” *Journal of Biological Chemistry* 268 (5): 3092–98. https://doi.org/10.1016/S0021-9258(18)53663-2.

Hambardzumyan, Dolores, David H. Gutmann, and Helmut Kettenmann. 2016. “The Role of Microglia and Macrophages in Glioma Maintenance and Progression.” *Nature Neuroscience* 19 (1): 20–27. https://doi.org/10.1038/nn.4185.

Han, Sue, Yang Liu, Sabrina J. Cai, Mingyu Qian, Jianyi Ding, Mioara Larion, Mark R. Gilbert, and Chunzhang Yang. 2020. “IDH Mutation in Glioma: Molecular Mechanisms and Potential Therapeutic Targets.” *British Journal of Cancer* 122 (11): 1580–89. https://doi.org/10.1038/s41416-020-0814-x.

Hara, Makoto R., Nishant Agrawal, Sangwon F. Kim, Matthew B. Cascio, Masahiro Fujimuro, Yuji Ozeki, Masaaki Takahashi, et al. 2005. “S-Nitrosylated GAPDH Initiates Apoptotic Cell Death by Nuclear Translocation Following Siah1 Binding.” *Nature Cell Biology* 7 (7): 665–74. https://doi.org/10.1038/ncb1268.

Harris, M., M. El Hindy, M. Usmari-Moraes, F. Hudd, M. Shafei, M. Dong, M. Hezwani, et al. 2020. “BCAT-Induced Autophagy Regulates Aβ Load through an Interdependence of Redox State and PKC Phosphorylation-Implications in Alzheimer’s Disease.” *Free Radical Biology and Medicine* 152 (May): 755–66. https://doi.org/10.1016/j.freeradbiomed.2020.01.019.

Hattori, Ayuna, Makoto Tsunoda, Takaaki Konuma, Masayuki Kobayashi, Tamas Nagy, John Glushka, Fariba Tayyari, et al. 2017. “Cancer Progression by Reprogrammed BCAA Metabolism in Myeloid Leukaemia.” *Nature* 545 (7655): 500–504. https://doi.org/10.1038/nature22314.

Henrik Heiland, Dieter, Vidhya M. Ravi, Simon P. Behringer, Jan Hendrik Frenking, Julian Wurm, Kevin Joseph, Nicklas W. C. Garrelfs, et al. 2019. “Tumor-Associated Reactive Astrocytes Aid the Evolution of Immunosuppressive Environment in Glioblastoma.” *Nature Communications* 10 (1): 2541. https://doi.org/10.1038/s41467-019-10493-6.

Hillier, James, Gemma J. Allcott, Laura A. Guest, Wayne Heaselgrave, Alex Tonks, Myra E. Conway, Amy L. Cherry, and Steven J. Coles. 2022. “The BCAT1 CXXC Motif Provides Protection against ROS in Acute Myeloid Leukaemia Cells.” *Antioxidants* 11 (4): 683. https://doi.org/10.3390/antiox11040683.

Huang, Yubin, Zhen Xu, Shanshan Xiong, Fangfang Sun, Guangrong Qin, Guanglei Hu, Jingjing Wang, et al. 2018. “Repopulated Microglia Are Solely Derived from the Proliferation of Residual

Microglia after Acute Depletion." *Nature Neuroscience* 21 (4): 530–40. https://doi.org/10.1038/s41593-018-0090-8.

Huber, Wolfgang, Anja von Heydebreck, Holger Sültmann, Annemarie Poustka, and Martin Vingron. 2002. "Variance Stabilization Applied to Microarray Data Calibration and to the Quantification of Differential Expression." *Bioinformatics* 18 (suppl_1): S96–104. https://doi.org/10.1093/bioinformatics/18.suppl_1.S96.

Hudson, Damien F., Kathryn M. Marshall, and William C. Earnshaw. 2009. "Condensin: Architect of Mitotic Chromosomes." *Chromosome Research: An International Journal on the Molecular, Supramolecular and Evolutionary Aspects of Chromosome Biology* 17 (2): 131–44. https://doi.org/10.1007/s10577-008-9009-7.

Hull, Jonathon, Maya El Hindy, Patrick G. Kehoe, Katy Chalmers, Seth Love, and Myra E. Conway. 2012. "Distribution of the Branched Chain Aminotransferase Proteins in the Human Brain and Their Role in Glutamate Regulation." *Journal of Neurochemistry* 123 (6): 997–1009. https://doi.org/10.1111/jnc.12044.

Hull, Jonathon, Vinood B. Patel, Susan M. Hutson, and Myra E. Conway. 2015. "New Insights into the Role of the Branched-Chain Aminotransferase Proteins in the Human Brain." *Journal of Neuroscience Research* 93 (7): 987–98. https://doi.org/10.1002/jnr.23558.

J, Bertran-Alamillo, Cattan V, Schoumacher M, Codony-Servat J, Giménez-Capitán A, Cantero F, Burbridge M, et al. 2019. "AURKB as a Target in Non-Small Cell Lung Cancer with Acquired Resistance to Anti-EGFR Therapy." *Nature Communications* 10 (1). https://doi.org/10.1038/s41467-019-09734-5.

Jin, Ming-Zhu, and Wei-Lin Jin. 2020. "The Updated Landscape of Tumor Microenvironment and Drug Repurposing." *Signal Transduction and Targeted Therapy* 5 (1): 1–16. https://doi.org/10.1038/s41392-020-00280-x.

Kallio, Marko J., Mark L. McCleland, P. Todd Stukenberg, and Gary J. Gorbsky. 2002. "Inhibition of Aurora B Kinase Blocks Chromosome Segregation, Overrides the Spindle Checkpoint, and Perturbs Microtubule Dynamics in Mitosis." *Current Biology: CB* 12 (11): 900–905. https://doi.org/10.1016/s0960-9822(02)00887-4.

Kapoor, Tarun M. 2017. "Metaphase Spindle Assembly." *Biology* 6 (1): 8. https://doi.org/10.3390/biology6010008.

Kim, Hani Jieun, Taiyun Kim, Nolan J. Hoffman, Di Xiao, David E. James, Sean J. Humphrey, and Pengyi Yang. 2021. “PhosR Enables Processing and Functional Analysis of Phosphoproteomic Data.” *Cell Reports* 34 (8): 108771. https://doi.org/10.1016/j.celrep.2021.108771.

Klughammer, Johanna, Barbara Kiesel, Thomas Roetzer, Nikolaus Fortelny, Amelie Nemc, Karl-Heinz Nenning, Julia Furtner, et al. 2018. “The DNA Methylation Landscape of Glioblastoma Disease Progression Shows Extensive Heterogeneity in Time and Space.” *Nature Medicine* 24 (10): 1611–24. https://doi.org/10.1038/s41591-018-0156-x.

Ko, Jeong-Hun, Antoni Olona, Adonia E. Papathanassiu, Norzawani Buang, Kwon-Sik Park, Ana S. H. Costa, Claudio Mauro, Christian Frezza, and Jacques Behmoaras. 2020. “BCAT1 Affects Mitochondrial Metabolism Independently of Leucine Transamination in Activated Human Macrophages.” *Journal of Cell Science* 133 (22): jcs247957. https://doi.org/10.1242/jcs.247957.

Körber, Verena, Jing Yang, Pankaj Barah, Yonghe Wu, Damian Stichel, Zuguang Gu, Michael Nai Chung Fletcher, et al. 2019. “Evolutionary Trajectories of IDHWT Glioblastomas Reveal a Common Path of Early Tumorigenesis Instigated Years Ahead of Initial Diagnosis.” *Cancer Cell* 35 (4): 692-704.e12. https://doi.org/10.1016/j.ccell.2019.02.007.

Kornberg, Michael D., Nilkantha Sen, Makoto R. Hara, Krishna R. Juluri, Judy Van K. Nguyen, Adele M. Snowman, Lindsey Law, Lynda D. Hester, and Solomon H. Snyder. 2010. “GAPDH Mediates Nitrosylation of Nuclear Proteins.” *Nature Cell Biology* 12 (11): 1094–1100. https://doi.org/10.1038/ncb2114.

Korotkevich, Gennady, Vladimir Sukhov, Nikolay Budin, Boris Shpak, Maxim N. Artyomov, and Alexey Sergushichev. 2021. “Fast Gene Set Enrichment Analysis.” bioRxiv. https://doi.org/10.1101/060012.

Koshy, Matthew, John L. Villano, Therese A. Dolecek, Andrew Howard, Usama Mahmood, Steven J. Chmura, Ralph R. Weichselbaum, and Bridget J. McCarthy. 2012. “Improved Survival Time Trends for Glioblastoma Using the SEER 17 Population-Based Registries.” *Journal of Neuro-Oncology* 107 (1): 207–12. https://doi.org/10.1007/s11060-011-0738-7.

Krug, Karsten, Philipp Mertins, Bin Zhang, Peter Hornbeck, Rajesh Raju, Rushdy Ahmad, Matthew Szucs, et al. 2019a. “A Curated Resource for Phosphosite-Specific Signature Analysis *[S].” *Molecular & Cellular Proteomics* 18 (3): 576–93. https://doi.org/10.1074/mcp.TIR118.000943.

———. 2019b. “A Curated Resource for Phosphosite-Specific Signature Analysis*[S].” *Molecular & Cellular Proteomics* 18 (3): 576–93. https://doi.org/10.1074/mcp.TIR118.000943.

Kuhn, H. G., H. Dickinson-Anson, and F. H. Gage. 1996. “Neurogenesis in the Dentate Gyrus of the Adult Rat: Age-Related Decrease of Neuronal Progenitor Proliferation.” *The Journal of Neuroscience: The Official Journal of the Society for Neuroscience* 16 (6): 2027–33.

Kvisten, Magnus, Vilde E. Mikkelsen, Anne Line Stensjøen, Ole Solheim, Johannes Van Der Want, and Sverre H. Torp. 2019. “Microglia and Macrophages in Human Glioblastomas: A Morphological and Immunohistochemical Study.” *Molecular and Clinical Oncology* 11 (1): 31–36. https://doi.org/10.3892/mco.2019.1856.

Lecona, Emilio, and Oscar Fernandez-Capetillo. 2018. “Targeting ATR in Cancer.” *Nature Reviews. Cancer* 18 (9): 586–95. https://doi.org/10.1038/s41568-018-0034-3.

Lee, Seung-Rock, Kap-Seok Yang, Jaeyul Kwon, Chunghee Lee, Woojin Jeong, and Sue Goo Rhee. 2002. “Reversible Inactivation of the Tumor Suppressor PTEN by H2O2*.” *Journal of Biological Chemistry* 277 (23): 20336–42. https://doi.org/10.1074/jbc.M111899200.

Liang, Cai, Zhenlei Zhang, Qinfu Chen, Haiyan Yan, Miao Zhang, Linli Zhou, Junfen Xu, Weiguo Lu, and Fangwei Wang. 2020. “Centromere-Localized Aurora B Kinase Is Required for the Fidelity of Chromosome Segregation.” *The Journal of Cell Biology* 219 (2): e201907092. https://doi.org/10.1083/jcb.201907092.

Liberzon, Arthur, Chet Birger, Helga Thorvaldsdóttir, Mahmoud Ghandi, Jill P. Mesirov, and Pablo Tamayo. 2015. “The Molecular Signatures Database (MSigDB) Hallmark Gene Set Collection.” *Cell Systems* 1 (6): 417–25. https://doi.org/10.1016/j.cels.2015.12.004.

Lim, Daniel C., Vladimir Joukov, T. Justin Rettenmaier, Akiko Kumagai, William G. Dunphy, James A. Wells, and Michael B. Yaffe. 2020. “Redox Priming Promotes Aurora A Activation during Mitosis.” *Science Signaling* 13 (641): eabb6707. https://doi.org/10.1126/scisignal.abb6707.

Liu, Xing, Jun Ying, Xifeng Wang, Qingcui Zheng, Tiancheng Zhao, Sungtae Yoon, Wen Yu, Danying Yang, Yang Fang, and Fuzhou Hua. 2021. “Astrocytes in Neural Circuits: Key Factors in Synaptic Regulation and Potential Targets for Neurodevelopmental Disorders.” *Frontiers in Molecular Neuroscience* 14. https://www.frontiersin.org/articles/10.3389/fnmol.2021.729273.

Lopes-Coelho, Filipa, Filipa Martins, Sofia A. Pereira, and Jacinta Serpa. 2021. “Anti-Angiogenic Therapy: Current Challenges and Future Perspectives.” *International Journal of Molecular Sciences* 22 (7): 3765. https://doi.org/10.3390/ijms22073765.

Louis, David N, Arie Perry, Pieter Wesseling, Daniel J Brat, Ian A Cree, Dominique Figarella-Branger, Cynthia Hawkins, et al. 2021. “The 2021 WHO Classification of Tumors of the Central Nervous System: A Summary.” *Neuro-Oncology* 23 (8): 1231–51. https://doi.org/10.1093/neuonc/noab106.

Love, Michael I., Wolfgang Huber, and Simon Anders. 2014. “Moderated Estimation of Fold Change and Dispersion for RNA-Seq Data with DESeq2.” *Genome Biology* 15 (12): 550. https://doi.org/10.1186/s13059-014-0550-8.

Luo, Lifang, Wenjing Sun, Weijian Zhu, Shuhan Li, Wenqi Zhang, Xiaohui Xu, Daoquan Fang, Tan Hooi Min Grahn, Lei Jiang, and Yihu Zheng. 2021. “BCAT1 Decreases the Sensitivity of Cancer Cells to Cisplatin by Regulating MTOR-Mediated Autophagy via Branched-Chain Amino Acid Metabolism.” *Cell Death & Disease* 12 (2): 1–13. https://doi.org/10.1038/s41419-021-03456-7.

Ma, Dengke K., Michael A. Bonaguidi, Guo-li Ming, and Hongjun Song. 2009. “Adult Neural Stem Cells in the Mammalian Central Nervous System.” *Cell Research* 19 (6): 672–82. https://doi.org/10.1038/cr.2009.56.

Ma, Dengke K., Guo-Li Ming, and Hongjun Song. 2005. “Glial Influences on Neural Stem Cell Development: Cellular Niches for Adult Neurogenesis.” *Current Opinion in Neurobiology* 15 (5): 514–20. https://doi.org/10.1016/j.conb.2005.08.003.

Mantovani, Alberto, Silvano Sozzani, Massimo Locati, Paola Allavena, and Antonio Sica. 2002. “Macrophage Polarization: Tumor-Associated Macrophages as a Paradigm for Polarized M2 Mononuclear Phagocytes.” *Trends in Immunology* 23 (11): 549–55. https://doi.org/10.1016/s1471-4906(02)02302-5.

Markovic, D. S., K. Vinnakota, S. Chirasani, M. Synowitz, H. Raguet, K. Stock, M. Sliwa, et al. 2009. “Gliomas Induce and Exploit Microglial MT1-MMP Expression for Tumor Expansion.” *Proceedings of the National Academy of Sciences of the United States of America* 106 (30): 12530–35. https://doi.org/10.1073/pnas.0804273106.

Matson, Jacob P., and Jeanette G. Cook. 2017. “Cell Cycle Proliferation Decisions: The Impact of Single Cell Analyses.” *The FEBS Journal* 284 (3): 362–75. https://doi.org/10.1111/febs.13898.

Matsuda, Taito, Takashi Irie, Shutaro Katsurabayashi, Yoshinori Hayashi, Tatsuya Nagai, Nobuhiko Hamazaki, Aliya Mari D. Adefuin, et al. 2019. “Pioneer Factor NeuroD1 Rearranges Transcriptional and Epigenetic Profiles to Execute Microglia-Neuron Conversion.” *Neuron* 101 (3): 472-485.e7. https://doi.org/10.1016/j.neuron.2018.12.010.

Matthews, Helen K., Cosetta Bertoli, and Robertus A. M. de Bruin. 2022. “Cell Cycle Control in Cancer.” *Nature Reviews Molecular Cell Biology* 23 (1): 74–88. https://doi.org/10.1038/s41580-021-00404-3.

McIntosh, J. Richard. 2016. “Mitosis.” *Cold Spring Harbor Perspectives in Biology* 8 (9): a023218. https://doi.org/10.1101/cshperspect.a023218.

McWhorter, Frances Y., Tingting Wang, Phoebe Nguyen, Thanh Chung, and Wendy F. Liu. 2013. “Modulation of Macrophage Phenotype by Cell Shape.” *Proceedings of the National Academy of Sciences* 110 (43): 17253–58. https://doi.org/10.1073/pnas.1308887110.

Medikonda, Ravi, Gavin Dunn, Maryam Rahman, Peter Fecci, and Michael Lim. 2021. “A Review of Glioblastoma Immunotherapy.” *Journal of Neuro-Oncology* 151 (1): 41–53. https://doi.org/10.1007/s11060-020-03448-1.

Mehani, Bharati, Saleembhasha Asanigari, Hye-Jung Chung, Karen Dazelle, Arashdeep Singh, Sridhar Hannenhalli, and Kenneth Aldape. 2022. “Immune Cell Gene Expression Signatures in Diffuse Glioma Are Associated with IDH Mutation Status, Patient Outcome and Malignant Cell State, and Highlight the Importance of Specific Cell Subsets in Glioma Biology.” *Acta Neuropathologica Communications* 10 (1): 19. https://doi.org/10.1186/s40478-022-01323-w.

Meijer, Alfred J., Séverine Lorin, Edward F. Blommaart, and Patrice Codogno. 2015. “Regulation of Autophagy by Amino Acids and MTOR-Dependent Signal Transduction.” *Amino Acids* 47 (10): 2037–63. https://doi.org/10.1007/s00726-014-1765-4.

Melhem, Jawad M., Jay Detsky, Mary Jane Lim-Fat, and James R. Perry. 2022. “Updates in IDH-Wildtype Glioblastoma.” *Neurotherapeutics*, May, 1–19. https://doi.org/10.1007/s13311-022-01251-6.

Merkle, Florian T., Zaman Mirzadeh, and Arturo Alvarez-Buylla. 2007. “Mosaic Organization of Neural Stem Cells in the Adult Brain.” *Science (New York, N.Y.)* 317 (5836): 381–84. https://doi.org/10.1126/science.1144914.

Ming, Guo-li, and Hongjun Song. 2005. “Adult Neurogenesis in the Mammalian Central Nervous System.” *Annual Review of Neuroscience* 28: 223–50. https://doi.org/10.1146/annurev.neuro.28.051804.101459.

Molinaro, Annette M., Shawn Hervey-Jumper, Ramin A. Morshed, Jacob Young, Seunggu J. Han, Pranathi Chunduru, Yalan Zhang, et al. 2020. “Association of Maximal Extent of Resection of Contrast-Enhanced and Non–Contrast-Enhanced Tumor With Survival Within Molecular Subgroups of Patients With Newly Diagnosed Glioblastoma.” *JAMA Oncology* 6 (4): 495–503. https://doi.org/10.1001/jamaoncol.2019.6143.

Morantz, R. A., G. W. Wood, M. Foster, M. Clark, and K. Gollahon. 1979. “Macrophages in Experimental and Human Brain Tumors. Part 2: Studies of the Macrophage Content of Human Brain Tumors.” *Journal of Neurosurgery* 50 (3): 305–11. https://doi.org/10.3171/jns.1979.50.3.0305.

Morrow, Christopher J., Anthony Tighe, Victoria L. Johnson, Maria I. F. Scott, Claire Ditchfield, and Stephen S. Taylor. 2005. “Bub1 and Aurora B Cooperate to Maintain BubR1-Mediated Inhibition of APC/CCdc20.” *Journal of Cell Science* 118 (Pt 16): 3639–52. https://doi.org/10.1242/jcs.02487.

Müller, Annett, Susan Brandenburg, Kati Turkowski, Susanne Müller, and Peter Vajkoczy. 2015. “Resident Microglia, and Not Peripheral Macrophages, Are the Main Source of Brain Tumor Mononuclear Cells.” *International Journal of Cancer* 137 (2): 278–88. https://doi.org/10.1002/ijc.29379.

Müller, Tim, Marco Gessi, Anke Waha, Lukas Jan Isselstein, Daniel Luxen, Dorothee Freihoff, Johannes Freihoff, et al. 2012. “Nuclear Exclusion of TET1 Is Associated with Loss of 5-Hydroxymethylcytosine in IDH1 Wild-Type Gliomas.” *The American Journal of Pathology* 181 (2): 675–83. https://doi.org/10.1016/j.ajpath.2012.04.017.

Murata-Hori, Maki, Masaaki Tatsuka, and Yu-Li Wang. 2002. “Probing the Dynamics and Functions of Aurora B Kinase in Living Cells during Mitosis and Cytokinesis.” *Molecular Biology of the Cell* 13 (4): 1099–1108. https://doi.org/10.1091/mbc.01-09-0467.

Musacchio, Andrea, and Kevin G. Hardwick. 2002. “The Spindle Checkpoint: Structural Insights into Dynamic Signalling.” *Nature Reviews Molecular Cell Biology* 3 (10): 731–41. https://doi.org/10.1038/nrm929.

Nakajima, Hideaki, and Hiroyoshi Kunimoto. 2014. “TET2 as an Epigenetic Master Regulator for Normal and Malignant Hematopoiesis.” *Cancer Science* 105 (9): 1093–99. https://doi.org/10.1111/cas.12484.

Narasimha, Anil M, Manuel Kaulich, Gary S Shapiro, Yoon J Choi, Piotr Sicinski, and Steven F Dowdy. 2014. “Cyclin D Activates the Rb Tumor Suppressor by Mono-Phosphorylation.” Edited by Roger Davis. *ELife* 3 (May): e02872. https://doi.org/10.7554/eLife.02872.

Neftel, Cyril, Julie Laffy, Mariella G. Filbin, Toshiro Hara, Marni E. Shore, Gilbert J. Rahme, Alyssa R. Richman, et al. 2019. “An Integrative Model of Cellular States, Plasticity, and Genetics for Glioblastoma.” *Cell* 178 (4): 835-849.e21. https://doi.org/10.1016/j.cell.2019.06.024.

Newman, Aaron M., Chloé B. Steen, Chih Long Liu, Andrew J. Gentles, Aadel A. Chaudhuri, Florian Scherer, Michael S. Khodadoust, et al. 2019. “Determining Cell Type Abundance and Expression from Bulk Tissues with Digital Cytometry.” *Nature Biotechnology* 37 (7): 773–82. https://doi.org/10.1038/s41587-019-0114-2.

Nobusawa, Sumihito, Takuya Watanabe, Paul Kleihues, and Hiroko Ohgaki. 2009. “IDH1 Mutations as Molecular Signature and Predictive Factor of Secondary Glioblastomas.” *Clinical Cancer Research: An Official Journal of the American Association for Cancer Research* 15 (19): 6002–7. https://doi.org/10.1158/1078-0432.CCR-09-0715.

Noy, Roy, and Jeffrey W. Pollard. 2014. “Tumor-Associated Macrophages: From Mechanisms to Therapy.” *Immunity* 41 (1): 49–61. https://doi.org/10.1016/j.immuni.2014.06.010.

Nurcombe, V., M. D. Ford, J. A. Wildschut, and P. F. Bartlett. 1993. “Developmental Regulation of Neural Response to FGF-1 and FGF-2 by Heparan Sulfate Proteoglycan.” *Science (New York, N.Y.)* 260 (5104): 103–6. https://doi.org/10.1126/science.7682010.

Nurse, Paul. 2000. “A Long Twentieth Century of the Cell Cycle and Beyond.” *Cell* 100 (1): 71–78. https://doi.org/10.1016/S0092-8674(00)81684-0.

Ostrom, Quinn T., David J. Cote, Mustafa Ascha, Carol Kruchko, and Jill S. Barnholtz-Sloan. 2018. “Adult Glioma Incidence and Survival by Race or Ethnicity in the United States From 2000 to 2014.” *JAMA Oncology* 4 (9): 1254–62. https://doi.org/10.1001/jamaoncol.2018.1789.

Ostrom, Quinn T., Haley Gittleman, Paul Farah, Annie Ondracek, Yanwen Chen, Yingli Wolinsky, Nancy E. Stroup, Carol Kruchko, and Jill S. Barnholtz-Sloan. 2013. “CBTRUS Statistical Report:

Primary Brain and Central Nervous System Tumors Diagnosed in the United States in 2006-2010." *Neuro-Oncology* 15 Suppl 2 (November): ii1-56. https://doi.org/10.1093/neuonc/not151.

Park, Nicole I., Paul Guilhamon, Kinjal Desai, Rochelle F. McAdam, Ellen Langille, Madlen O'Connor, Xiaoyang Lan, et al. 2017. "ASCL1 Reorganizes Chromatin to Direct Neuronal Fate and Suppress Tumorigenicity of Glioblastoma Stem Cells." *Cell Stem Cell* 21 (2): 209-224.e7. https://doi.org/10.1016/j.stem.2017.06.004.

Parney, Ian F., James S. Waldron, and Andrew T. Parsa. 2009. "Flow Cytometry and in Vitro Analysis of Human Glioma-Associated Macrophages. Laboratory Investigation." *Journal of Neurosurgery* 110 (3): 572–82. https://doi.org/10.3171/2008.7.JNS08475.

Pastor, William A., L. Aravind, and Anjana Rao. 2013. "TETonic Shift: Biological Roles of TET Proteins in DNA Demethylation and Transcription." *Nature Reviews Molecular Cell Biology* 14 (6): 341–56. https://doi.org/10.1038/nrm3589.

Pataskar, Abhijeet, Johannes Jung, Pawel Smialowski, Florian Noack, Federico Calegari, Tobias Straub, and Vijay K Tiwari. 2016. "NeuroD1 Reprograms Chromatin and Transcription Factor Landscapes to Induce the Neuronal Program." *The EMBO Journal* 35 (1): 24–45. https://doi.org/10.15252/embj.201591206.

Patir, Anirudh, Barbara Shih, Barry W. McColl, and Tom C. Freeman. 2019. "A Core Transcriptional Signature of Human Microglia: Derivation and Utility in Describing Region-Dependent Alterations Associated with Alzheimer's Disease." *Glia* 67 (7): 1240–53. https://doi.org/10.1002/glia.23572.

Patterson, Jesse C., Brian A. Joughin, Bert van de Kooij, Daniel C. Lim, Douglas A. Lauffenburger, and Michael B. Yaffe. 2019. "ROS and Oxidative Stress Are Elevated in Mitosis during Asynchronous Cell Cycle Progression and Are Exacerbated by Mitotic Arrest." *Cell Systems* 8 (2): 163-167.e2. https://doi.org/10.1016/j.cels.2019.01.005.

Paulsen, Candice E., Thu H. Truong, Francisco J. Garcia, Arne Homann, Vinayak Gupta, Stephen E. Leonard, and Kate S. Carroll. 2011. "Peroxide-Dependent Sulfenylation of the EGFR Catalytic Site Enhances Kinase Activity." *Nature Chemical Biology* 8 (1): 57–64. https://doi.org/10.1038/nchembio.736.

Peereboom, David M., Dale R. Shepard, Manmeet S. Ahluwalia, Cathy J. Brewer, Neeraj Agarwal, Glen H. J. Stevens, John H. Suh, et al. 2010. "Phase II Trial of Erlotinib with

Temozolomide and Radiation in Patients with Newly Diagnosed Glioblastoma Multiforme." *Journal of Neuro-Oncology* 98 (1): 93–99. https://doi.org/10.1007/s11060-009-0067-2.

Perez-Catalan, Nelson A., Chris Q. Doe, and Sarah D. Ackerman. 2021. "The Role of Astrocyte-mediated Plasticity in Neural Circuit Development and Function." *Neural Development* 16 (1): 1. https://doi.org/10.1186/s13064-020-00151-9.

Peters, Jan-Michael. 2006. "The Anaphase Promoting Complex/Cyclosome: A Machine Designed to Destroy." *Nature Reviews Molecular Cell Biology* 7 (9): 644–56. https://doi.org/10.1038/nrm1988.

Peters, Timothy J, Michael J Buckley, Yunshun Chen, Gordon K Smyth, Christopher C Goodnow, and Susan J Clark. 2021. "Calling Differentially Methylated Regions from Whole Genome Bisulphite Sequencing with DMRcate." *Nucleic Acids Research* 49 (19): e109. https://doi.org/10.1093/nar/gkab637.

Phillips, Heidi S., Samir Kharbanda, Ruihuan Chen, William F. Forrest, Robert H. Soriano, Thomas D. Wu, Anjan Misra, et al. 2006. "Molecular Subclasses of High-Grade Glioma Predict Prognosis, Delineate a Pattern of Disease Progression, and Resemble Stages in Neurogenesis." *Cancer Cell* 9 (3): 157–73. https://doi.org/10.1016/j.ccr.2006.02.019.

Phipson, Belinda, Jovana Maksimovic, and Alicia Oshlack. 2016. "MissMethyl: An R Package for Analyzing Data from Illumina's HumanMethylation450 Platform." *Bioinformatics (Oxford, England)* 32 (2): 286–88. https://doi.org/10.1093/bioinformatics/btv560.

Pollack, Ian F., Regina I. Jakacki, Susan M. Blaney, Michael L. Hancock, Mark W. Kieran, Peter Phillips, Larry E. Kun, et al. 2007. "Phase I Trial of Imatinib in Children with Newly Diagnosed Brainstem and Recurrent Malignant Gliomas: A Pediatric Brain Tumor Consortium Report." *Neuro-Oncology* 9 (2): 145–60. https://doi.org/10.1215/15228517-2006-031.

Pusch, Stefan, Sonja Krausert, Viktoria Fischer, Jörg Balss, Martina Ott, Daniel Schrimpf, David Capper, et al. 2017. "Pan-Mutant IDH1 Inhibitor BAY 1436032 for Effective Treatment of IDH1 Mutant Astrocytoma in Vivo." *Acta Neuropathologica* 133 (4): 629–44. https://doi.org/10.1007/s00401-017-1677-y.

Raffel, Simon, Mattia Falcone, Niclas Kneisel, Jenny Hansson, Wei Wang, Christoph Lutz, Lars Bullinger, et al. 2017. "BCAT1 Restricts AKG Levels in AML Stem Cells Leading to IDHmut-like DNA Hypermethylation." *Nature* 551 (7680): 384–88. https://doi.org/10.1038/nature24294.

Rao, Yanxia, Siling Du, Baozhi Yang, Yuqing Wang, Yuxin Li, Ruofan Li, Tian Zhou, et al. 2021. “NeuroD1 Induces Microglial Apoptosis and Cannot Induce Microglia-to-Neuron Cross-Lineage Reprogramming.” *Neuron* 109 (24): 4094-4108.e5. https://doi.org/10.1016/j.neuron.2021.11.008.

Raskov, Hans, Adile Orhan, Jan Pravsgaard Christensen, and Ismail Gögenur. 2021. “Cytotoxic CD8+ T Cells in Cancer and Cancer Immunotherapy.” *British Journal of Cancer* 124 (2): 359–67. https://doi.org/10.1038/s41416-020-01048-4.

Ravi, Vidhya M., Nicolas Neidert, Paulina Will, Kevin Joseph, Julian P. Maier, Jan Kückelhaus, Lea Vollmer, et al. 2022. “T-Cell Dysfunction in the Glioblastoma Microenvironment Is Mediated by Myeloid Cells Releasing Interleukin-10.” *Nature Communications* 13 (1): 925. https://doi.org/10.1038/s41467-022-28523-1.

Ren, Xu, and Pei Fen Kuan. 2019. “MethylGSA: A Bioconductor Package and Shiny App for DNA Methylation Data Length Bias Adjustment in Gene Set Testing.” *Bioinformatics* 35 (11): 1958–59. https://doi.org/10.1093/bioinformatics/bty892.

Richards, Laura M., Owen K. N. Whitley, Graham MacLeod, Florence M. G. Cavalli, Fiona J. Coutinho, Julia E. Jaramillo, Nataliia Svergun, et al. 2021. “Gradient of Developmental and Injury Response Transcriptional States Defines Functional Vulnerabilities Underpinning Glioblastoma Heterogeneity.” *Nature Cancer* 2 (2): 157–73. https://doi.org/10.1038/s43018-020-00154-9.

Ritchie, Matthew E., Belinda Phipson, Di Wu, Yifang Hu, Charity W. Law, Wei Shi, and Gordon K. Smyth. 2015. “Limma Powers Differential Expression Analyses for RNA-Sequencing and Microarray Studies.” *Nucleic Acids Research* 43 (7): e47. https://doi.org/10.1093/nar/gkv007.

Rossi, M. L., J. T. Hughes, M. M. Esiri, H. B. Coakham, and D. B. Brownell. 1987. “Immunohistological Study of Mononuclear Cell Infiltrate in Malignant Gliomas.” *Acta Neuropathologica* 74 (3): 269–77. https://doi.org/10.1007/BF00688191.

Rubin, Seth M., Julien Sage, and Jan M. Skotheim. 2020. “Integrating Old and New Paradigms of G1/S Control.” *Molecular Cell* 80 (2): 183–92. https://doi.org/10.1016/j.molcel.2020.08.020.

Sahai, Erik, Igor Astsaturov, Edna Cukierman, David G. DeNardo, Mikala Egeblad, Ronald M. Evans, Douglas Fearon, et al. 2020. “A Framework for Advancing Our Understanding of Cancer-Associated Fibroblasts.” *Nature Reviews Cancer* 20 (3): 174–86. https://doi.org/10.1038/s41568-019-0238-1.

Sanchez-Vega, Francisco, Marco Mina, Joshua Armenia, Walid K. Chatila, Augustin Luna, Konnor C. La, Sofia Dimitriadoy, et al. 2018. “Oncogenic Signaling Pathways in The Cancer Genome Atlas.” *Cell* 173 (2): 321-337.e10. https://doi.org/10.1016/j.cell.2018.03.035.

Santaguida, Stefano, and Andrea Musacchio. 2009. “The Life and Miracles of Kinetochores.” *The EMBO Journal* 28 (17): 2511–31. https://doi.org/10.1038/emboj.2009.173.

Savitsky, Pavel A., and Toren Finkel. 2002. “Redox Regulation of Cdc25C*.” *Journal of Biological Chemistry* 277 (23): 20535–40. https://doi.org/10.1074/jbc.M201589200.

Schafer, K. A. 1998. “The Cell Cycle: A Review.” *Veterinary Pathology* 35 (6): 461–78. https://doi.org/10.1177/030098589803500601.

Schiweck, Juliane, Kai Murk, Julia Ledderose, Agnieszka Münster-Wandowski, Marta Ornaghi, Imre Vida, and Britta J. Eickholt. 2021. “Drebrin Controls Scar Formation and Astrocyte Reactivity upon Traumatic Brain Injury by Regulating Membrane Trafficking.” *Nature Communications* 12 (1): 1490. https://doi.org/10.1038/s41467-021-21662-x.

Scholey, Jonathan M., Ingrid Brust-Mascher, and Alex Mogilner. 2003. “Cell Division.” *Nature* 422 (6933): 746–52. https://doi.org/10.1038/nature01599.

Schuldiner, O, A Eden, T Ben-Yosef, O Yanuka, G Simchen, and N Benvenisty. 1996. “ECA39, a Conserved Gene Regulated by c-Myc in Mice, Is Involved in G1/S Cell Cycle Regulation in Yeast.” *Proceedings of the National Academy of Sciences of the United States of America* 93 (14): 7143–48.

Schulz, Daniel, Yannik Severin, Vito Riccardo Tomaso Zanotelli, and Bernd Bodenmiller. 2019. “In-Depth Characterization of Monocyte-Derived Macrophages Using a Mass Cytometry-Based Phagocytosis Assay.” *Scientific Reports* 9 (1): 1925. https://doi.org/10.1038/s41598-018-38127-9.

Segurado, Mónica, and José Antonio Tercero. 2009. “The S-Phase Checkpoint: Targeting the Replication Fork.” *Biology of the Cell* 101 (11): 617–27. https://doi.org/10.1042/BC20090053.

Seki, Akiko, Judith A. Coppinger, Chang-Young Jang, John R. Yates, and Guowei Fang. 2008. “Bora and the Kinase Aurora A Cooperatively Activate the Kinase Plk1 and Control Mitotic Entry.” *Science* 320 (5883): 1655–58. https://doi.org/10.1126/science.1157425.

Seri, B., D. G. Herrera, A. Gritti, S. Ferron, L. Collado, A. Vescovi, J. M. Garcia-Verdugo, and Arturo Alvarez-Buylla. 2006. “Composition and Organization of the SCZ: A Large Germinal Layer

Containing Neural Stem Cells in the Adult Mammalian Brain." *Cerebral Cortex (New York, N.Y.: 1991)* 16 Suppl 1 (July): i103-111. https://doi.org/10.1093/cercor/bhk027.

Shafei, Mai Ahmed, Thomas Forshaw, Jasmine Davis, Arwa Flemban, David Qualtrough, Sarah Dean, Claire Perks, Ming Dong, Robert Newman, and Myra Elizabeth Conway. 2020. "BCATc Modulates Crosstalk between the PI3K/Akt and the Ras/ERK Pathway Regulating Proliferation in Triple Negative Breast Cancer." *Oncotarget* 11 (21): 1971–87. https://doi.org/10.18632/oncotarget.27607.

Shu, Xiong, Pan-Pan Zhan, Li-Xin Sun, Long Yu, Jun Liu, Li-Chao Sun, Zhi-Hua Yang, Yu-Liang Ran, and Yue-Min Sun. 2021. "BCAT1 Activates PI3K/AKT/MTOR Pathway and Contributes to the Angiogenesis and Tumorigenicity of Gastric Cancer." *Frontiers in Cell and Developmental Biology* 9. https://www.frontiersin.org/articles/10.3389/fcell.2021.659260.

Silva, Lidia Santos, Gernot Poschet, Yannic Nonnenmacher, Holger M Becker, Sean Sapcariu, Ann-Christin Gaupel, Magdalena Schlotter, et al. 2017. "Branched-Chain Ketoacids Secreted by Glioblastoma Cells via MCT1 Modulate Macrophage Phenotype." *EMBO Reports* 18 (12): 2172–85. https://doi.org/10.15252/embr.201744154.

Singh, Kirit, Kelly M. Hotchkiss, Kisha K. Patel, Daniel S. Wilkinson, Aditya A. Mohan, Sarah L. Cook, and John H. Sampson. 2021. "Enhancing T Cell Chemotaxis and Infiltration in Glioblastoma." *Cancers* 13 (21): 5367. https://doi.org/10.3390/cancers13215367.

Stricker, Stefan H., and Magdalena Götz. 2018. "DNA-Methylation: Master or Slave of Neural Fate Decisions?" *Frontiers in Neuroscience* 12. https://www.frontiersin.org/articles/10.3389/fnins.2018.00005.

Stupp, Roger, Warren P. Mason, Martin J. van den Bent, Michael Weller, Barbara Fisher, Martin J. B. Taphoorn, Karl Belanger, et al. 2005. "Radiotherapy plus Concomitant and Adjuvant Temozolomide for Glioblastoma." *The New England Journal of Medicine* 352 (10): 987–96. https://doi.org/10.1056/NEJMoa043330.

Subramanian, Aravind, Pablo Tamayo, Vamsi K. Mootha, Sayan Mukherjee, Benjamin L. Ebert, Michael A. Gillette, Amanda Paulovich, et al. 2005. "Gene Set Enrichment Analysis: A Knowledge-Based Approach for Interpreting Genome-Wide Expression Profiles." *Proceedings of the National Academy of Sciences* 102 (43): 15545–50. https://doi.org/10.1073/pnas.0506580102.

Sudakin, Valery, Gordon K.T. Chan, and Tim J. Yen. 2001. “Checkpoint Inhibition of the APC/C in HeLa Cells Is Mediated by a Complex of BUBR1, BUB3, CDC20, and MAD2.” *Journal of Cell Biology* 154 (5): 925–36. https://doi.org/10.1083/jcb.200102093.

Sun, Jiaqi, Junzheng Yang, Xiaoli Miao, Horace H. Loh, Duanqing Pei, and Hui Zheng. 2021. “Proteins in DNA Methylation and Their Role in Neural Stem Cell Proliferation and Differentiation.” *Cell Regeneration* 10 (March): 7. https://doi.org/10.1186/s13619-020-00070-4.

Sweatt, Andrew J., Mac Wood, Agus Suryawan, Reidar Wallin, Mark C. Willingham, and Susan M. Hutson. 2004. “Branched-Chain Amino Acid Catabolism: Unique Segregation of Pathway Enzymes in Organ Systems and Peripheral Nerves.” *American Journal of Physiology-Endocrinology and Metabolism* 286 (1): E64–76. https://doi.org/10.1152/ajpendo.00276.2003.

Szulzewsky, Frank, Andreas Pelz, Xi Feng, Michael Synowitz, Darko Markovic, Thomas Langmann, Inge R. Holtman, et al. 2015. “Glioma-Associated Microglia/Macrophages Display an Expression Profile Different from M1 and M2 Polarization and Highly Express Gpnmb and Spp1.” *PloS One* 10 (2): e0116644. https://doi.org/10.1371/journal.pone.0116644.

Takizawa, Takumi, Kinichi Nakashima, Masakazu Namihira, Wataru Ochiai, Atsumi Uemura, Makoto Yanagisawa, Naoyuki Fujita, Mitsuyoshi Nakao, and Tetsuya Taga. 2001. “DNA Methylation Is a Critical Cell-Intrinsic Determinant of Astrocyte Differentiation in the Fetal Brain.” *Developmental Cell* 1 (6): 749–58. https://doi.org/10.1016/S1534-5807(01)00101-0.

Tamimi, Ahmad Faleh, and Malik Juweid. 2017. “Epidemiology and Outcome of Glioblastoma.” In *Glioblastoma*, edited by Steven De Vleeschouwer. Brisbane (AU): Codon Publications. http://www.ncbi.nlm.nih.gov/books/NBK470003/.

Tang-Huau, Tsing-Lee, Paul Gueguen, Christel Goudot, Mélanie Durand, Mylène Bohec, Sylvain Baulande, Benoit Pasquier, Sebastian Amigorena, and Elodie Segura. 2018. “Human in Vivo-Generated Monocyte-Derived Dendritic Cells and Macrophages Cross-Present Antigens through a Vacuolar Pathway.” *Nature Communications* 9 (1): 2570. https://doi.org/10.1038/s41467-018-04985-0.

Thewes, V., R. Simon, M. Hlevnjak, M. Schlotter, P. Schroeter, K. Schmidt, Y. Wu, et al. 2017. “The Branched-Chain Amino Acid Transaminase 1 Sustains Growth of Antiestrogen-Resistant and ERα-Negative Breast Cancer.” *Oncogene* 36 (29): 4124–34. https://doi.org/10.1038/onc.2017.32.

Tönjes, Martje, Sebastian Barbus, Yoon Jung Park, Wei Wang, Magdalena Schlotter, Anders M. Lindroth, Sabrina V. Pleier, et al. 2013. “BCAT1 Promotes Cell Proliferation through Amino Acid Catabolism in Gliomas Carrying Wild-Type IDH1.” *Nature Medicine* 19 (7): 901–8. https://doi.org/10.1038/nm.3217.

Turcan, Sevin, Armida WM Fabius, Alexandra Borodovsky, Alicia Pedraza, Cameron Brennan, Jason Huse, Agnes Viale, Gregory J. Riggins, and Timothy A. Chan. 2013. “Efficient Induction of Differentiation and Growth Inhibition in IDH1 Mutant Glioma Cells by the DNMT Inhibitor Decitabine.” *Oncotarget* 4 (10): 1729–36. https://doi.org/10.18632/oncotarget.1412.

Uneda, Atsuhito, Kazuhiko Kurozumi, Atsushi Fujimura, Kentaro Fujii, Joji Ishida, Yosuke Shimazu, Yoshihiro Otani, et al. 2021. “Differentiated Glioblastoma Cells Accelerate Tumor Progression by Shaping the Tumor Microenvironment via CCN1-Mediated Macrophage Infiltration.” *Acta Neuropathologica Communications* 9 (1): 29. https://doi.org/10.1186/s40478-021-01124-7.

Unruh, Dusten, Makda Zewde, Adam Buss, Michael R. Drumm, Anh N. Tran, Denise M. Scholtens, and Craig Horbinski. 2019. “Methylation and Transcription Patterns Are Distinct in IDH Mutant Gliomas Compared to Other IDH Mutant Cancers.” *Scientific Reports* 9 (1): 8946. https://doi.org/10.1038/s41598-019-45346-1.

Venkataramani, Varun, Dimitar Ivanov Tanev, Christopher Strahle, Alexander Studier-Fischer, Laura Fankhauser, Tobias Kessler, Christoph Körber, et al. 2019. “Glutamatergic Synaptic Input to Glioma Cells Drives Brain Tumour Progression.” *Nature* 573 (7775): 532–38. https://doi.org/10.1038/s41586-019-1564-x.

Venkataramani, Varun, Yvonne Yang, Marc Cicero Schubert, Ekin Reyhan, Svenja Kristin Tetzlaff, Niklas Wißmann, Michael Botz, et al. 2022. “Glioblastoma Hijacks Neuronal Mechanisms for Brain Invasion.” *Cell* 185 (16): 2899-2917.e31. https://doi.org/10.1016/j.cell.2022.06.054.

Venkatesh, Humsa S., Wade Morishita, Anna C. Geraghty, Dana Silverbush, Shawn M. Gillespie, Marlene Arzt, Lydia T. Tam, et al. 2019. “Electrical and Synaptic Integration of Glioma into Neural Circuits.” *Nature* 573 (7775): 539–45. https://doi.org/10.1038/s41586-019-1563-y.

Verhaak, Roel G. W., Katherine A. Hoadley, Elizabeth Purdom, Victoria Wang, Yuan Qi, Matthew D. Wilkerson, C. Ryan Miller, et al. 2010. “Integrated Genomic Analysis Identifies Clinically Relevant Subtypes of Glioblastoma Characterized by Abnormalities in PDGFRA, IDH1, EGFR, and NF1.” *Cancer Cell* 17 (1): 98–110. https://doi.org/10.1016/j.ccr.2009.12.020.

Walczak, Claire E., and Rebecca Heald. 2008. “Chapter Three - Mechanisms of Mitotic Spindle Assembly and Function.” In *International Review of Cytology*, edited by Kwang W. Jeon, 265:111–58. A Survey of Cell Biology. Academic Press. https://doi.org/10.1016/S0074-7696(07)65003-7.

Wang, Hongsheng, Huangao Zhou, Jianing Xu, Yunpeng Lu, Xiaoyun Ji, Yizheng Yao, Hou Chao, et al. 2021. “Different T-Cell Subsets in Glioblastoma Multiforme and Targeted Immunotherapy.” *Cancer Letters* 496 (January): 134–43. https://doi.org/10.1016/j.canlet.2020.09.028.

Wang, Lixia, Jinfang Zhang, Lixin Wan, Xiuxia Zhou, Zhiwei Wang, and Wenyi Wei. 2015. “Targeting Cdc20 as a Novel Cancer Therapeutic Strategy.” *Pharmacology & Therapeutics* 151 (July): 141–51. https://doi.org/10.1016/j.pharmthera.2015.04.002.

Wang, Qianghu, Baoli Hu, Xin Hu, Hoon Kim, Massimo Squatrito, Lisa Scarpace, Ana C. deCarvalho, et al. 2017. “Tumor Evolution of Glioma Intrinsic Gene Expression Subtype Associates with Immunological Changes in the Microenvironment.” *Cancer Cell* 32 (1): 42-56.e6. https://doi.org/10.1016/j.ccell.2017.06.003.

Wang, Xin, Zifei Pei, Aasma Hossain, Yuting Bai, and Gong Chen. 2021. “Transcription Factor-Based Gene Therapy to Treat Glioblastoma through Direct Neuronal Conversion.” *Cancer Biology & Medicine* 18 (3): 860–74. https://doi.org/10.20892/j.issn.2095-3941.2020.0499.

Wang, Yuetong, Jian Zhang, Shengxiang Ren, Dan Sun, Hsin-Yi Huang, Hua Wang, Yujuan Jin, et al. 2019. “Branched-Chain Amino Acid Metabolic Reprogramming Orchestrates Drug Resistance to EGFR Tyrosine Kinase Inhibitors.” *Cell Reports* 28 (2): 512-525.e6. https://doi.org/10.1016/j.celrep.2019.06.026.

Weiss, E., and M. Winey. 1996. “The Saccharomyces Cerevisiae Spindle Pole Body Duplication Gene MPS1 Is Part of a Mitotic Checkpoint.” *The Journal of Cell Biology* 132 (1–2): 111–23. https://doi.org/10.1083/jcb.132.1.111.

Weiss, S., C. Dunne, J. Hewson, C. Wohl, M. Wheatley, A. C. Peterson, and B. A. Reynolds. 1996. “Multipotent CNS Stem Cells Are Present in the Adult Mammalian Spinal Cord and Ventricular Neuroaxis.” *The Journal of Neuroscience: The Official Journal of the Society for Neuroscience* 16 (23): 7599–7609.

Wickham, Hadley. 2009. *Ggplot2*. New York, NY: Springer. https://doi.org/10.1007/978-0-387-98141-3.

Woroniecka, Karolina, and Peter E. Fecci. 2018. “T-Cell Exhaustion in Glioblastoma.” *Oncotarget* 9 (82): 35287. https://doi.org/10.18632/oncotarget.26228.

Xiang, Xiaonan, Jianguo Wang, Di Lu, and Xiao Xu. 2021. “Targeting Tumor-Associated Macrophages to Synergize Tumor Immunotherapy.” *Signal Transduction and Targeted Therapy* 6 (1): 1–12. https://doi.org/10.1038/s41392-021-00484-9.

Xu, Wei, Hui Yang, Ying Liu, Ying Yang, Ping Wang, Se-Hee Kim, Shinsuke Ito, et al. 2011. “Oncometabolite 2-Hydroxyglutarate Is a Competitive Inhibitor of α-Ketoglutarate-Dependent Dioxygenases.” *Cancer Cell* 19 (1): 17–30. https://doi.org/10.1016/j.ccr.2010.12.014.

Yeo, Alan T., Shruti Rawal, Bethany Delcuze, Anthos Christofides, Agata Atayde, Laura Strauss, Leonora Balaj, et al. 2022. “Single-Cell RNA Sequencing Reveals Evolution of Immune Landscape during Glioblastoma Progression.” *Nature Immunology* 23 (6): 971–84. https://doi.org/10.1038/s41590-022-01215-0.

Yılmaz, Serhan, Marzieh Ayati, Daniela Schlatzer, A. Ercüment Çiçek, Mark R. Chance, and Mehmet Koyutürk. 2021. “Robust Inference of Kinase Activity Using Functional Networks.” *Nature Communications* 12 (1): 1177. https://doi.org/10.1038/s41467-021-21211-6.

Young, Matthew D., Matthew J. Wakefield, Gordon K. Smyth, and Alicia Oshlack. 2010. “Gene Ontology Analysis for RNA-Seq: Accounting for Selection Bias.” *Genome Biology* 11 (2): R14. https://doi.org/10.1186/gb-2010-11-2-r14.

Yudkoff, M., Y. Daikhin, I. Nissim, D. Pleasure, J. Stern, and I. Nissim. 1994. “Inhibition of Astrocyte Glutamine Production by Alpha-Ketoisocaproic Acid.” *Journal of Neurochemistry* 63 (4): 1508–15. https://doi.org/10.1046/j.1471-4159.1994.63041508.x.

Yudkoff, M., I. Nissim, Y. Daikhin, Z. P. Lin, D. Nelson, D. Pleasure, and M. Erecinska. 1993. “Brain Glutamate Metabolism: Neuronal-Astroglial Relationships.” *Developmental Neuroscience* 15 (3–5): 343–50. https://doi.org/10.1159/000111354.

Zhu, Ziwen, Abhinav Achreja, Noah Meurs, Olamide Animasahun, Sarah Owen, Anjali Mittal, Pooja Parikh, et al. 2020. “Tumour-Reprogrammed Stromal BCAT1 Fuels Branched-Chain Ketoacid Dependency in Stromal-Rich PDAC Tumours.” *Nature Metabolism* 2 (8): 775–92. https://doi.org/10.1038/s42255-020-0226-5.

8. Supplementary Figures

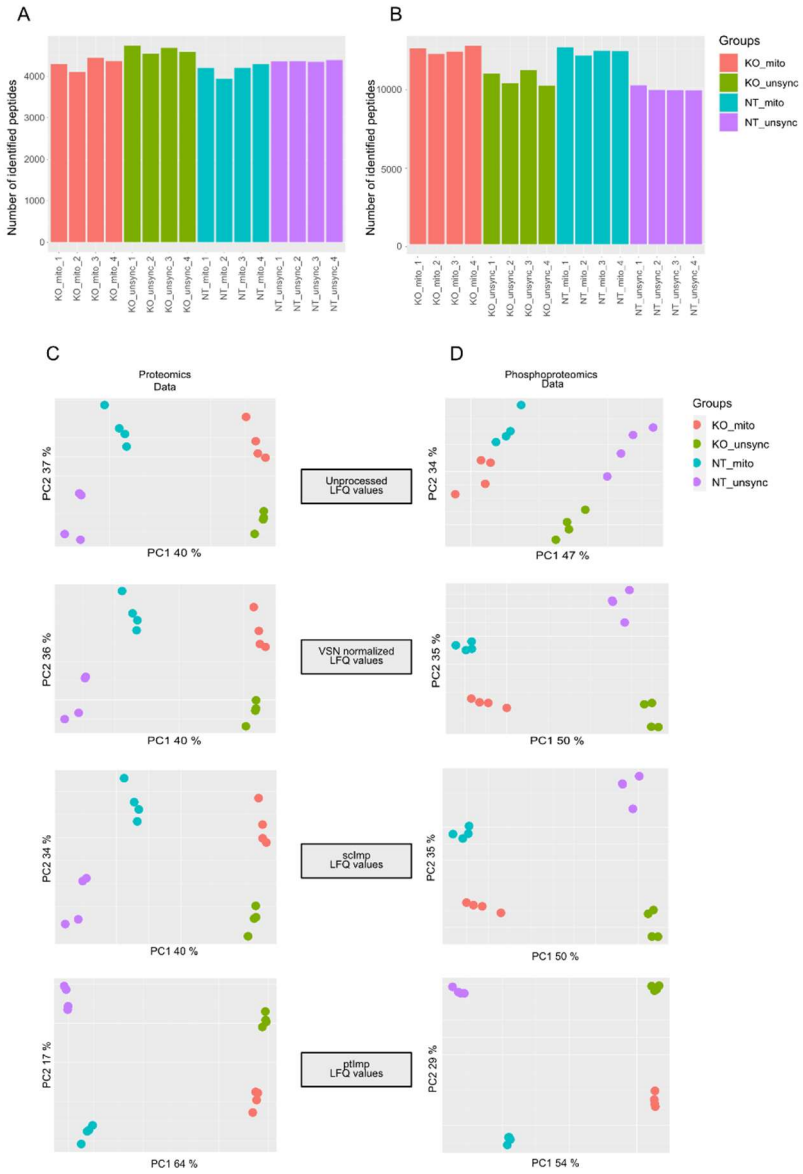

Supplementary Figure 1 Proteomic and phosphoproteomic data preparation of U251 control (NT) and BCAT1-KO (KO) mitotic (mito) and unsynchronized (unsync) samples. A) Number of identified peptides and B) phosphopeptides in the respective samples following stringent filtering for low-detection proteins. C) Principal component analysis of proteomic and D) phosphoproteomic datasets in different stages of data pre-processing: vsn normalization, site- and condition-specific imputation (scImp) and paired tail imputation (ptImp).

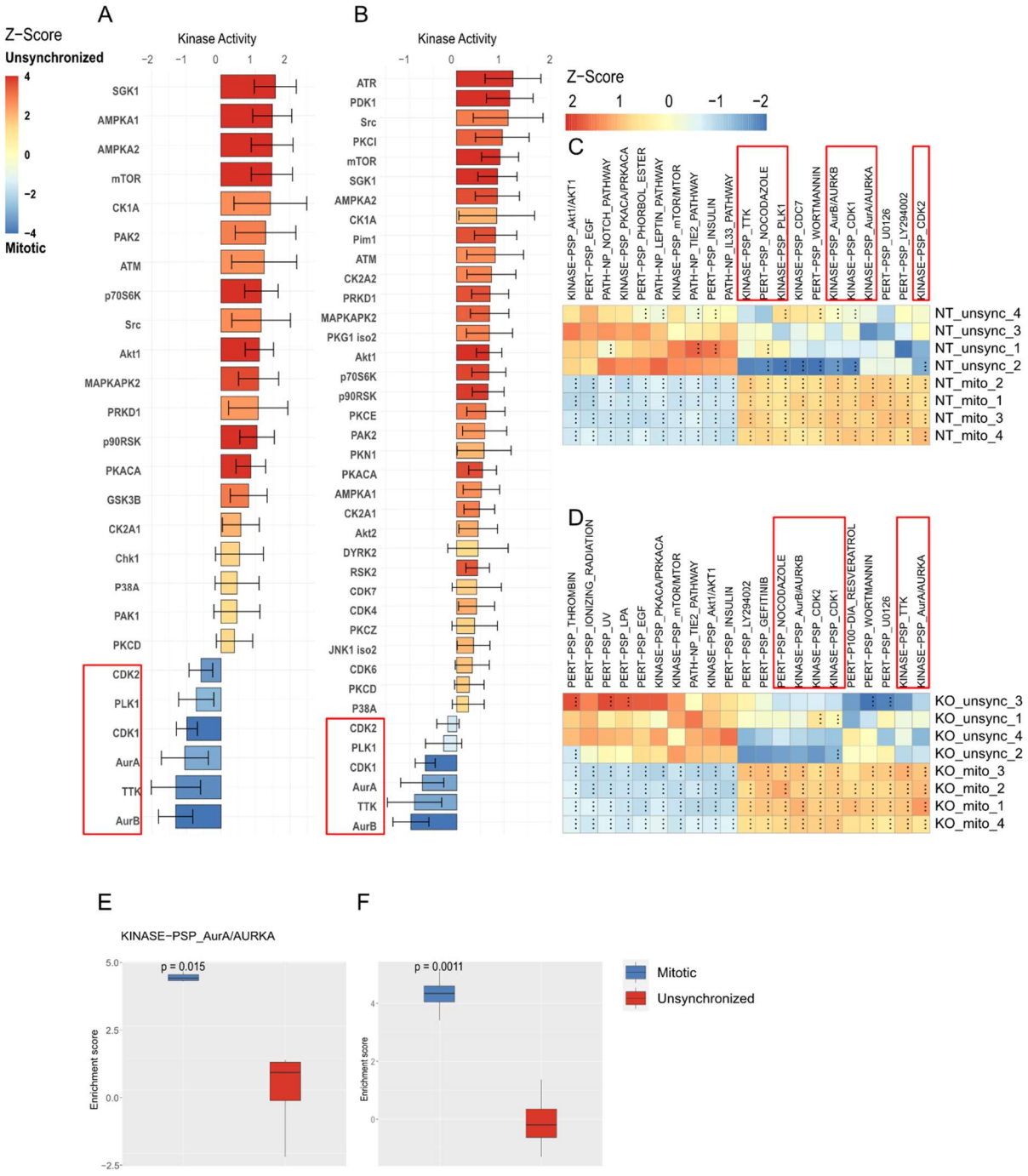

Supplementary Figure 2 RoKAI Kinase Substrate analysis of LN229 mitotic vs unsynchronized A) control and B) BCAT1-KO cells. The x-axis represents kinase activity scores with the positive scores corresponding to kinases with enriched activity in Unsynchronized samples and the negative to the enriched activity of the kinases in the Mitotic samples. The color scale denotes the z-score value

of the inferred kinase activity in red (Unsynchronized) or blue (Mitotic). The graph was produced using the web-based tool http://rokai.io. C) Z-score normalized heat map of signatures positively (red) and negatively (blue) enriched in control(NT) and D) BCAT1-KO (KO) mitotic (mito) and unsynchronized (unsync) LN229 cells, with noticeable mitotic signatures highlighted. E) Tukey plots of average normalized enrichment score (NES) across the 4 mitotic (blue) and unsynchronized (red) samples for the AURKA signaling signature in control and F) BCAT1-KO cells. Statistically significantly enriched signatures (adjusted p-value<0.05) are denoted with "…" in panels C) and D). Statistical significance of the NES difference in panels E) and F) was determined using an unpaired two-tailed student's t-test. Whiskers represent 1.5IQR (Interquartile range)

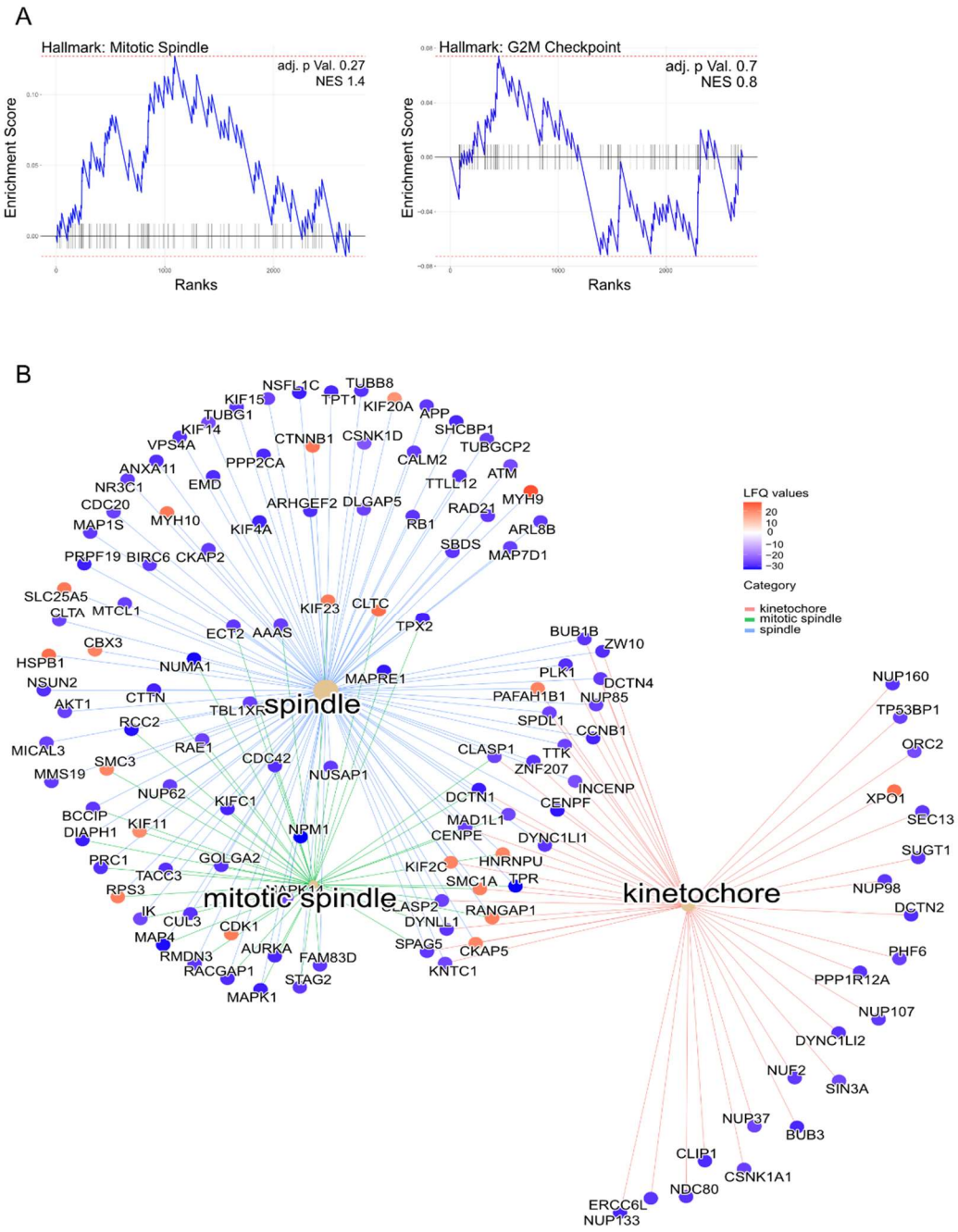

Supplementary Figure 3 HA-CFP co-immunoprecipitation of mitotic proteins in synchronized U251 BCAT1-KO cells. A) pre-Ranked GSEA analysis of proteins detected in the CFP-HA co-IP fraction (positive values) against the non-bound proteins detected in the input (negative values) according to the Hallmark MSigDb signature sets Mitotic spindle (NES=2, adjusted p-value=0.01) and G2M Checkpoint (NES=2.3, adjusted p-value=0.003). B) mitotic spindle and kinetochore protein networks with CFP-HA-bound peptides represented as red and the un-bound proteins identified in the input represented as blue nodes.

9. Acknowledgements

I would like to thank my direct supervisor, Dr Bernhard Radlwimmer for his support during my PhD studies. Through his supervision, not only have I felt supported in my scientific pursuits, from making new cell lines to making new model systems, I have learned to work independently, ask (mostly) relevant questions and design ways of getting relevant answers. Through our discussions and occasional lighthearted disagreements, I have learned more than I could have imagined. Thank you for your (considerable) patience and imperturbability and most importantly for treating me as an equal and my ideas, outrageous or otherwise, as those of a colleague rather than a student.

I would also like to thank Prof Dr Peter Lichter for giving me the opportunity to work on my PhD thesis in his division. I am thankful for all the questions, comments, concerns, and advice that was always spot on.

My gratitude also goes to Prof Dr Mathias Heikenwälder and Prof Dr Karsten Hiller for participating in my Thesis Advisory Committee, offering advice and asking the right questions. I would especially like to thank Prof Dr Peter Angel, with whom I have worked for many years, starting as a master student, where his advice and input allowed me to grow and pursue a PhD in the first place. The impact of his opinions and advice is reflected in the fact that he remained a crucial part of my PhD work, as a TAC member and one of the examiners of this thesis work. I would also like to thank Pro. Dr. Christian Shaaf and Dr Sevin Turcan for agreeing to evaluate this work and be a part of my thesis exam committee.

During my PhD, I have had the amazing opportunity to work with and learn from Liliana Francois. From simple lab questions and method troubleshooting to entertaining and helping execute many of my more ‘eccentric’ ideas, Liliana has been there consistently and with an enthusiasm matching my own. Working with you on 2 manuscripts, your input in my experiments and this thesis has been instrumental for my success in the lab and my development as a scientist.

During my PhD I have had the pleasure of learning that there is more to lab life than simply the science of it all. For this, I would like to thank the members of the B060 division and in particular Mona, Matthew, Nathalie (the best master student a supervisor can hope for), Jasmin and Theresa. For all the coffee breaks, discussions, supportive words, sincere laughs and much, much more.

Finally, I would like to thank my family. My parents, who have raised me to be who I am and do what I love, often having the distinct displeasure of having to deal with the consequences of that choice, but never regretting it. My sister and my brother, through our ups and downs you made life in a small town feel like a never-ending adventure.

None of this would have been possible without my aunt and father. Both supported me every step of the way that they were with me, believed in me long before I did and more than I probably ever could. I am sorry for the loud silences, unsaid goodbyes, and everything that you will not be there to see, but I am forever grateful for every lesson you taught me and every memory you left me.